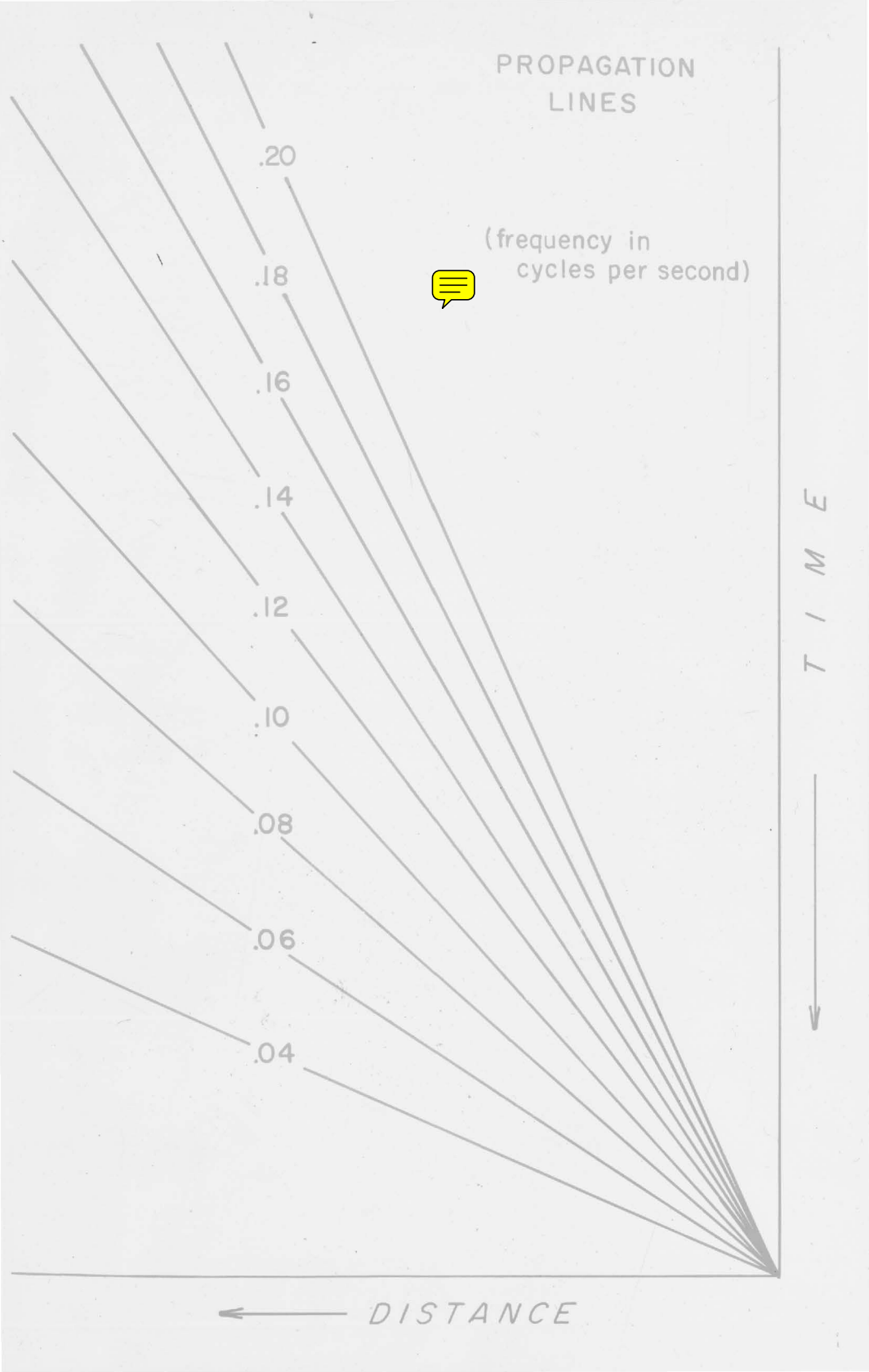
PROPAGATION
LINES
(frequency in
cycles per second)
.20
.18
.16
.14
.12
.10
.08
.06
.04
TIME
DISTANCE

AN ABSTRACT OF THE THESIS OF

David Bruce Enfield (Name) for the Ph. D. (Degree)

in Oceanography (Major) presented on May 25, 1973 (Date)

Title: PREDICTION OF HAZARDOUS COLUMBIA RIVER BAR CONDITIONS

Abstract approved: Redacted for Privacy

William H. Quinn

In this study methods were developed for the prediction of wave conditions that are hazardous to navigation at river entrances, with emphasis on applicability to the Columbia River. There are two basic components to the prediction system: (1) a semi-automated spectral method for forecasting the significant height and average period of waves in deep water, and (2) an index of navigation hazard at river entrances that depends on the significant height and average period in deep water and on the mean current and water depth at the entrance.

The computerized, deep water forecast method is a hybrid scheme that combines the spectral principles of the Pierson-Neumann-James method with the graphical input techniques of Wilson and the fetch limited spectrum of Liu. The significant heights generated by the method are well verified by winter wave measurements at Newport, Oregon.

The hazard index is based on the probability of wave-breaking in water of arbitrary depth and current. The breaking probability is derived under the assumption that wave heights and squared periods are

statistically independent and distributed according to a Rayleigh probability density function. The breaking-wave probability and the hazard index depend on the wave steepness in deep slack water and on the depth (relative to the wave period squared) and current (relative to the period) at the river entrance. The dependence on depth and current is achieved in two ways: (1) the limiting steepness (breaking index) is found as a function of relative depth and relative current, and (2) the wave spectrum in water of arbitrary depth and current is found by transformation of the spectrum in deep slack water. The transformation is performed by requiring that the rate of wave energy propagation remain constant. The hazard index is closely related to the probability of breaking swell. At water depths that are typical of river entrances, the hazard index depends strongly on the significant wave height, mean current and depth, but only weakly on the mean wave period (since the breaking height of swell at such depths is only weakly dependent on period).

Hindcasts of deep water significant wave heights and hazard indices compared reasonably well with measured heights and Columbia River bar closure periods. Forecasts based on accurate prognostic weather charts should provide similar results.

Prediction of Hazardous Columbia River Bar Conditions

by

David Bruce Enfield

A THESIS

submitted to

Oregon State University

In partial fulfillment of
the requirements for the
degree of

Doctor of Philosophy

completed May 25, 1973
commencement June, 1974

APPROVED:

Redacted for Privacy

Assistant Professor of Oceanography

in charge of major

Redacted for Privacy

Dean of the School of Oceanography

Redacted for Privacy

Dean of Graduate School

Date thesis is presented May 25, 1973

Typed by S. Williams and C. Rathbun for David Bruce Enfield

Figures drafted by William E. Gilbert

ACKNOWLEDGEMENTS

I wish to thank my major professor, Dr. William H. Quinn, for his guidance and encouragement during this study. The contributions of Drs. J. Nath and F. Ramsey, which have provided the nucleus for much of the statistical work developed in this thesis, are gratefully acknowledged. I am also indebted to Mr. David Zopf, Mr. Clayton Creech and Mr. Gerald Burdwell for their interest and help in evaluating the operational aspects of the computerized wave forecasting techniques. I wish to express my appreciation to Drs. W. Quinn, J. Nath and V. Neal for their help in reviewing this thesis.

I particularly wish to thank the Columbia River Bar Pilots Association (Astoria, Oregon) for their unselfish cooperation in providing bar closure data and personal interviews. The conscientious work of Mr. Norm Kujala in faithfully taking valuable breaker observations under the most severe weather conditions is also gratefully acknowledged, as well as his liaison with the Coast Guard and the Bar Pilots.

I am grateful to the National Science Foundation for graduate traineeship and assistantship support during the three years of this work. The research itself has been funded by Department of Commerce Contract No. 7-35356, administered under Mr. N. Arthur Pore (Technical Representative, Techniques Development Laboratory, National Weather Service, NOAA).

Finally, I wish to thank my wife, Elena, for her patience and encouragement, and for providing a peaceful, agreeable home environment.

TABLE OF CONTENTS

LIST OF FIGURES

LIST OF TABLES

LIST OF SYMBOLS

Symbols that are frequently used or that may not be defined at every occurrence are listed in order of appearance.

Symbol	Meaning
T	zero upcrossing wave period
L	wave length
H	wave height
C	wave celerity
d	water depth
U	wind speed
ω	angular frequency
σ	standard deviation of the water surface elevation
S	spectral energy density
f	cyclic frequency
$\hat{f}$	cyclic frequency at spectral peak
$\hat{S}$	spectral energy density of spectral peak
M_k	kth moment of the wave spectrum
g	acceleration due to gravity
Γ	gamma function
n,m	spectral form integers
$H_{1/3}, H_s$	significant wave height
$\overline{T}$	average period between zero upcrossings in a wave record
F	fetch length

Symbol	Meaning
X	dimensionless fetch parameter (gF/U^2)
A_I	initial angular spreading factor (start of fetch history, at fetch rear)
A_F	final angular spreading factor (end of fetch history, at fetch front)
A_i	angular spreading factor for the ith frequency component (interpolated from A_I and A_F)
D_i	generation distance associated with the ith frequency component
E_i	energy in the ith frequency band
Δf	band width
C_o	celerity in deep slack water
L_o	wavelength
n	ratio of group velocity to phase velocity
K_s	monochromatic shoaling coefficient
K_{sc}	monochromatic shoaling-current coefficient
S_o	spectral energy density in deep slack water
f_o^{max}	spectral peak frequency in deep slack water
$\tilde{f}$	normalized frequency
$\tilde{S}$	normalized spectral energy density
$\overline{K}$	amplification factor for wave heights (from spectral transformation)
f_{min}	frequency at which spectral density is a relative minimum and beyond which turbulent wave breaking occurs (opposing currents)
H_b	height of breaking waves

Symbol	Meaning
L_b	wavelength of breaking waves
C_b	celerity of breaking waves
$P(A)$	probability that the event "A" occurs
F_H, F_T	cumulative distribution functions for height and period
f_H, f_T	probability density functions for height and periods
η, τ^2	r.m.s. values of height and squared period
h, t	realizations of the random variables for height and period
t_m	most probable period
t_c	cutoff period (below which the period distribution is truncated)
ν	breaking index
P_{bw}	probability that a given wave breaks
f_T^*	probability density function for periods of breaking waves
τ_b^2	r.m.s. squared period of breaking waves
$\overline{T}_o$	average zero upcrossing period in deep slack water
α	hazard index

PREDICTION OF HAZARDOUS COLUMBIA RIVER BAR CONDITIONS

I. INTRODUCTION

Statement of the Problem

The goal of this study is to develop methods for prediction of hazardous bar conditions at the Columbia River mouth sufficiently in advance for advisories to be issued. The methods should permit those with little knowledge of wave forecasting to predict average wave conditions offshore of the river entrance as well as the relative hazard due to high breaking swell over the bar itself.

Justification of the Study

The mouth of the Columbia River is one of the most formidable harbor entrances in the world during periods of heavy sea and swell. As large swell encounter decreasing depths and strong ebb currents they become steeper and break more frequently.

Every year several lives are lost and hundreds of distress calls are handled by the Coast Guard's Columbia River Bar Patrol from Cape Disappointment. Most boating disasters involve small fishing boats and pleasure craft with inexperienced operators, and occur during the good weather months, July and August, when these small boats are particularly active.

The Columbia River entrance is frequently impassable to all vessels during winter months due to high waves created by local storms, or high long period swell arriving from distant storms. The shoal areas to

either side of the bar channel have been called the "Graveyard of the Pacific" due to the large number of ships and men lost on and along them before bar pilot operations were begun. Loss rates of larger ships have been reduced in recent years, since experienced seamen seek the aid of the Columbia River Bar Pilots when conditions are hazardous.

Though the loss of merchant ships is becoming rare, the disruption of shipping during hazardous periods creates costly delays. The fixed operating costs of these vessels are in the approximate range of $3,000 to $3,500 per day ($125 to $140 per hour). Hundreds of ships pass through the entrance each winter, and the bar is impassable for about 300 hours on the average. At present, bar crossing decisions are based on existing reports of conditions. The lack of prior knowledge as to the expected onset of hazardous conditions prevents proper planning of ship arrivals and departures or rerouting to alternate ports.

If reasonably accurate predictions of bar conditions were readily available, the lead time would allow ships to be diverted more frequently to alternate ports. Wood products are the predominant cargo and their availability at several ports gives shipping agents some flexibility in scheduling. Greater efficiency in operational scheduling of longshoremen, pilots, ships' crews, and many other such groups could be achieved, since delays and cancellations could be anticipated and better use made of work and leisure time.

Accurate predictions of wave conditions could materially reduce the toll of lives and small craft not only at the Columbia River mouth but also along the adjoining coasts north and south of there. Advisories issued 12 to 24 hours in advance could prevent many disastrous

fishing and pleasure-boat excursions. Those issued 6 to 12 hours in advance would provide helpful guidance to those engaging in beach and surf zone activities.

Essential Features of the Methods

The prediction method has been simplified to the point that is can readily be applied at the weather forecast office level by meteorologists. The time required to make wave forecasts is reasonably short and the work involved is chiefly limited to the interpretation of meteorological charts. The method of forecasting the offshore (deep water) waves is largely automated and compatible with other weather office work routines.

It is desirable to develop a predictable index of bar hazard which reflects the wave steepness and breaking frequency as well as the dependence on depths and currents. As offshore waves propagate into the bar area their characteristics are modified by interaction with varying depths and strong currents. Shoal areas and ebb currents cause sea and swell to become higher and steeper and to break more frequently.

The methods developed here include a semi-automated method of predicting significant height (the average of the highest one-third of the waves) and the average period of waves in relatively deep water. A hazard index is developed which is related to the frequency of high, breaking swell in the vicinity of the river entrance. This index is dependent on the significant height and average period of waves offshore and on the water depth and current at the entrance. Though the

effects of shoaling and currents are accounted for through this index, it has not been possible to include refraction effects due to a lack of accurate information on bathymetry and current distribution.

The semi-automated forecast method is a hybrid scheme which combines the best features of existing manual forecasting methods with the latest developments in empirical-theoretical wave spectra. Due to the lack of suitable wave observations at the Columbia River entrance, measurements taken at Newport, Oregon (130 nautical miles to the south) are used to verify the method. A warning time of at least 24 hours appears to be feasible at present.

The hazard index is an outgrowth of the statistical probability of wave breaking in water of arbitrary depth and current strength. Index computations are obtained and studied for known periods of bar closure at the Columbia River. (A bar closure is a period during which bar pilots consider conditions to be too hazardous to escort ship traffic.) The tendency for high index values to coincide with bar closures suggests that the index is a potentially useful indicator of hazardous navigation conditions during periods of high swell.

Definitions of Terms

Progressive gravity waves, and primarily those of longer period (swell), are of interest to this study. A convenient way of defining such waves and their characteristics is by their appearance on wave records. A wave may be defined by the recording trace between two successive upcrossings (by the trace) of the mean water level.

The wave period (T) is the time elapsed between two successive

upcrossings.

The wavelength (L) is the horizontal distance between the crests (or troughs) of successive waves.

The wave height (H) is the vertical distance between the maximum and minimum water surface elevations of a wave.

The wave steepness is given by the ratio H/L.

The wave celerity (C) is the speed of movement of some identifiable part of a wave, such as its crest.

The relative depth for a wave is defined as the ratio of the water depth to the squared period, that is, d/T^2.

A deep water wave is one for which $d/T^2 \geq 2.56$ feet/second^2 (0.8 meters/sec^2); a shallow water wave is one for which $d/T^2 < 0.256$ ft/sec^2 (0.08 m/sec^2). All other values of d/T^2 imply waves of intermediate depth.

The significant wave height is the average height of the highest one-third of the waves in a long series of waves.

The average period is the duration of a series of waves divided by the number of waves in the series.

The relative current experienced by a wave is defined as the ratio of the mean water speed (U) to the wave period, that is, U/T.

A fetch is an area of the sea surface over which seas are generated by a wind of approximately uniform direction and speed.

The fetch length is the horizontal distance (in the direction of the wind) over which a wind of approximately uniform direction and speed generates a sea.

A decay distance is the distance through which ocean waves travel

as swell after leaving the generating area.

Wave forecasting is the empirical-theoretical determination of future wave characteristics from observed and/or predicted meteorological patterns (synoptic wind and pressure charts).

Wave hindcasting is the empirical theoretical determination of past wave characteristics, based exclusively on historic meteorological patterns (synoptic wind and pressure analyses).

Organization of the Thesis

Chapter II describes the Columbia River entrance, the nature of hazardous conditions and processes which contribute to them, and the nature of the offshore wave regime and its associated meteorological patterns.

Chapter III discusses the nature and sources of wave data at Newport which are later used as verification for the prediction methods developed.

Chapter IV reviews pertinent information on empirical-theoretical wave spectra and describes the principles and procedures involved in the semi-automated method of deep water wave forecasting. Several examples of its use are also given. A detailed documentation of the computer algorithm and program is provided in the APPENDIX.

Chapter V is an evaluation of the semi-automated method. The qualitative nature of spectra hindcast by the method is examined. Six-hourly hindcast significant heights and average periods are compared with measured ones at Newport for the 1971-1972 winter. Finally, semi-automated forecasts are simulated and compared with actual

forecasts made by manual methods.

Chapter VI examines the spectral transformations which take place when waves propagate from deep slack water to an area with finite depth and current. The corresponding changes in average heights and periods are found by integration of the original and transformed spectra. The assumptions involved and the applicability of the shoaling-current transformations are also discussed.

Chapter VII develops expressions for the probability of wave breaking in water of arbitrary depth and current. It is assumed that the wave heights and squared periods are statistically independent, have a Rayleigh probability density distribution, and that their r.m.s. values are known. In practice the r.m.s. values could be found by transformation and integration of deep water forecast wave spectra, as shown in Chapter VI. Finally, a statistical function is identified which is closely related to the probability of breaking swell. The function is not dependent on the statistical distribution of wave periods and is ideally suited as an index of bar hazard.

Chapter VIII compares hindcast significant heights and hazard indices with Newport measurements and Columbia River bar closure periods. The results suggest that if the deep water significant wave height can be correctly forecast, the hazard index should correlate well with bar closure periods (being highest when the bar is closed.)

II. PHENOMENA CONTRIBUTING TO HAZARDOUS NAVIGATION CONDITIONS AT THE COLUMBIA RIVER ENTRANCE

Introduction

The Columbia River entrance covers a large area where high winter waves frequently interact with high river flows, large tidal range, swift currents and widely varying depths to produce hazardous conditions for commercial ship traffic.

In this chapter the principal chacteristics of the river entrance are discussed as they relate to navigation hazards. The nature of hazardous conditions is examined from the point of view of the bar pilots. Periods during which the pilots will not escort ship traffic may be considered indicative of hazardous wave conditions. The bar closures are used to select periods of high waves and their related storm developments for further study. The offshore characteristics of winter waves and the evolutionary patterns of the storms which produce them are discussed. Finally, the roles of depth, current, and refraction in modifying waves and producing breakers at the river mouth are explored.

The Columbia River Entrance

The Columbia River entrance covers an extensive area with depths varying from over 50 feet along its channel to less than 30 feet over adjacent shoal areas. It is characterized by a large river discharge, swift tidal currents and shoals which continually encroach upon the channel and threaten ship traffic. A discussion of the physical features, hydrology and sediment transport at the entrance is essential to an understanding of the navigation hazards there.

Physical Characteristics

Figure 1 shows the principal physical features of the Columbia River entrance. The mouth of the river is at least two miles wide between the main jetties. It is formed by the North Jetty and Peacock Spit to the north and the South Jetty and Clatsop Spit to the south. An extensive system of numbered navigation buoys is maintained. These are well known to mariners and provide a convenient system of reference and orientation within the huge area. A shorter jetty (Jetty "A") extends southward from the north peninsula to buoy 11. The entire river entrance, which includes the mouth, extends from Jetty "A" to the most seaward buoys (1 and 2). The navigation channel has a minimum width of 1/2 mile as far upriver as Jetty "A" and a minimum depth of 48 feet, maintained by dredging.

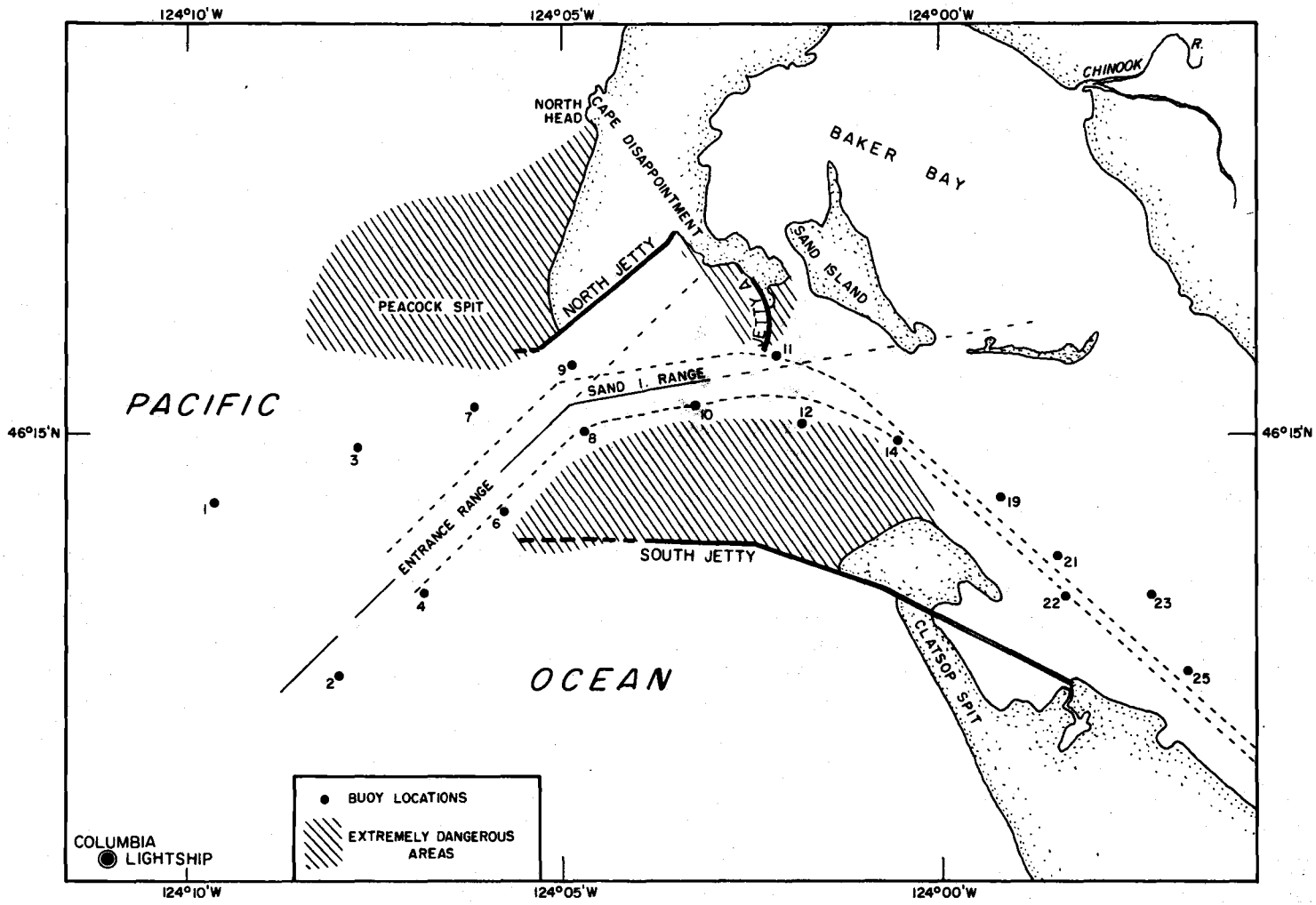

Figure 1. Map showing the principal features in the vicinity of the Columbia River entrance.

Figure 2 shows the bathymetry of the entrance area and its seaward approaches (from U.S. Coast and Geodetic Survey Chart No. 6151, surveyed in 1958). The relatively shoal area between the entrance channel and the South Jetty and extending seaward almost to buoy 6 is usually referred to as Clatsop Spit, a submerged extension of the land spit to the south. Peacock Spit is the shoal area extending seaward of the North Jetty and ending just north of and between buoys 1 and 3.

The Columbia River bar is the relatively shallow southward extension of Peacock Spit, penetrated by the entrance channel between buoys 3 and 4. A somewhat broader definition of the bar, namely the area from the jetty tips to buoys 1 and 2, would conform more closely to mariners' usuage. The portion near the jetties is commonly referred to as the "inner bar", while the seaward portion is termed the "outer bar".

The Columbia River Lightship is anchored in 200 feet of water some nine miles west of the south beach and beyond the seaward terminus of the entrance channel (Figure 1). In addition to being a navigation aid for vessels, the lightship functions as a staging area where merchant ships prepare for bar transit. Transfer of bar pilots to and from merchant ships normally takes place near the lightship.

Lockett (1963) reviewed the history of jetty construction, rehabilitation and dredging at the Columbia River. All major construction was accomplished by 1939, but rehabilitation has been conducted from time to time up into the early 1960's. It is felt that, while upper

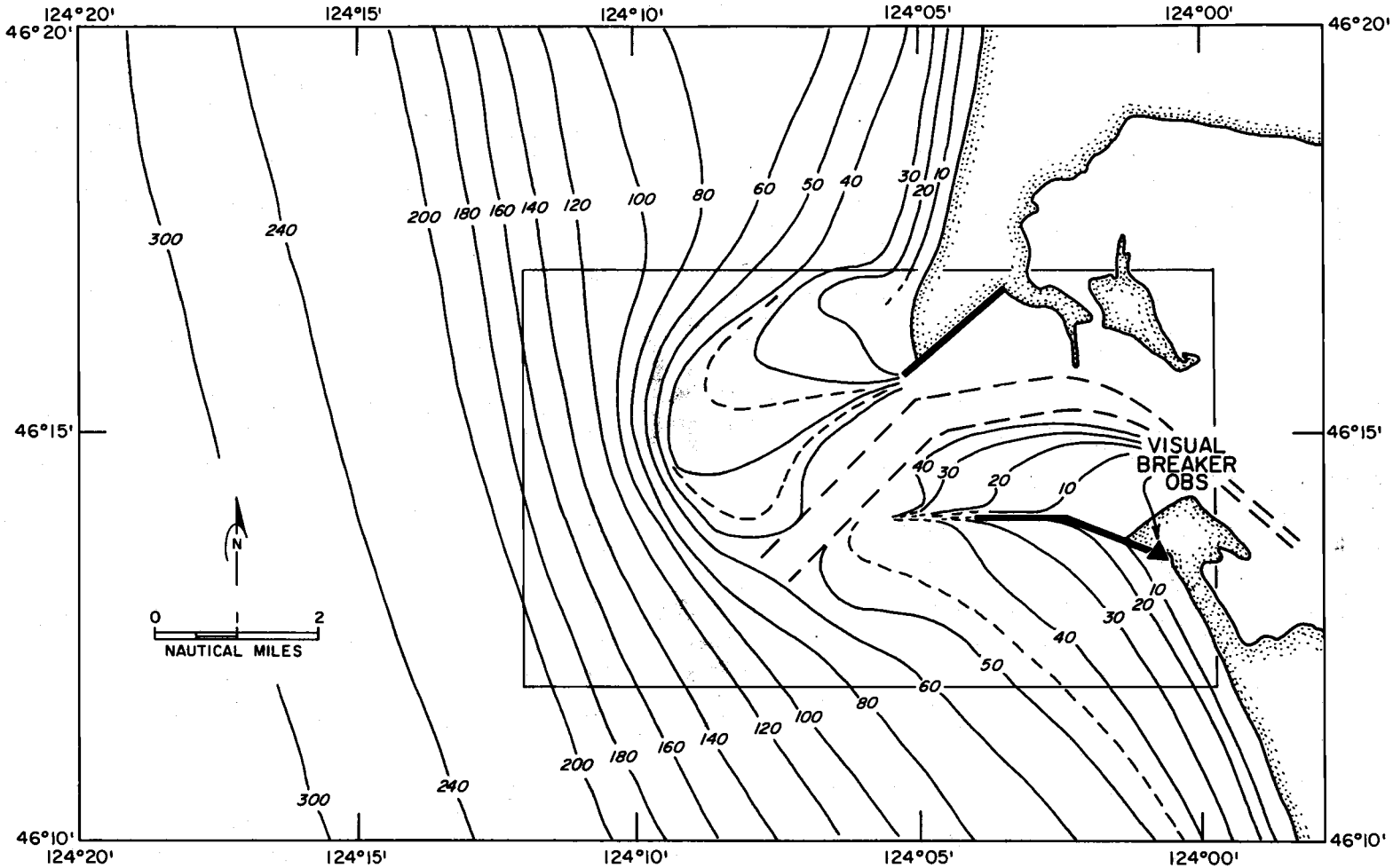

Figure 2. Bathymetry (depths in feet) in the vicinity of the Columbia River entrance. (Refraction diagrams of Figure 5 were constructed for the smaller rectangular area.)

portions of the jetties may need occasional rehabilitation due to wave damage, the bases of the structures have settled and stabilized. The construction of Jetty "A" (near buoy 11) was originally designed to constrict the ebb flow and thus induce strong enough currents to minimize dredging requirements for the channel.

Since 1956 a minimum channel depth of 48 feet has been maintained by summer dredging as far upriver as buoy 14. The south side of the channel between buoys 8 and 14 is in frequent need of dredging due to encroachment by the Clatsop Spit shoal zone. Southeastward encroachment of Peacock Spit shoal upon the entrance channel at buoy 3 has been reduced considerably as the offshore sediments approach a quasi-equilibrium configuration.

Hydrology

The Columbia River drains a large basin extending through Oregon, Washington, Idaho and Canada with surrounding elevations up to almost 14,000 feet. Much orographically induced precipitation falls in the main drainage area during the winter in the form of snow. Unlike the coastal rivers which crest soon after periods of heavy precipitation, the Columbia River freshet (high discharge) is strongest well after the storm season has subsided, when snow fields melt. The annual discharge cycle of the Columbia has become more regular and less subject to extremes through extensive dam control. The minimum discharge has been increased to 150,000 cubic feet per second (cfs) and usually occurs in September; the maximum discharge has been lowered to 600,000 cfs and occurs in May and June (Lockett, 1963). The principal effect

of large discharge rates at the river mouth is to increase the velocity and duration of the ebb flow and to increase the density stratification (Lockett; 1963, 1967). The discharge cycle is partially responsible for annual patterns of sediment deposition and scouring in the river mouth area.

In spite of the large discharge volumes, the water level at the entrance is governed mostly by tidal action. The range from mean lower low water (MLLW) to mean higher high water (MHHW) is about 8.5 feet. When spring tides are accompanied by large river discharge and/or significant storm surge, unusually high tide stages result. Coastline and harbor erosion may be greatly accelerated during such periods under conditions of strong southerly or westerly winds and high waves.

According to Neal (1972) the discharge rates and tidal stages at the Columbia River are such that partially mixed conditions usually exist. The stratification of the estuary is best developed during the late spring runoff, and may be considered well mixed at high tide during low runoff in the fall.

Tidal currents are especially strong at the river mouth (between the North and South Jetties). Bar pilots report ebb currents of five to eight knots (8 to 13 feet per second) in this area. This agrees with the maximum ebb currents predicted by tidal current tables for the channel near Jetty "A". Flood current speeds tend to be about 60% of the ebb current values.

Lockett (1963) has summarized the results of prototype current measurements* made in 1959 and subsequent hydraulic model studies of the entrance and estuary. The vertical shear of the current is such that the ebb current predominates in the upper, relatively fresh layer, while the flood current predominates in the lower, saline layer. The downstream predominance is enhanced during the late spring freshet. The 1959 current measurements showed that the current between the jetties was strongest in the channel and slightly weaker over the outer flank of Clatsop Spit, just south of the channel. Currents in the cul-de-sac north of the channel were predominantly directed upriver.

The currents measured in 1959 just south of the entrance channel (near buoy 10) went through a very regular tidal cycle. If one uses tidal prediction formulas to compute the current near buoy 11, the phase agrees almost exactly with that of the measured currents, while the magnitude of the computed current is about 15% greater. This suggests that tidal prediction formulas may be useful for studying the effects of currents on waves at the outer portion of the river mouth (between the jetty tips).

Very little is known of the current velocity distribution seaward of the jetties. The ebb effluent is a turbulent jet which discharges into a denser fluid, the ocean. It may be conjectured that the mixing and dissipation of this jet is enhanced during periods of

---

* Report of the District Engineer, U.S. Army Engineer District, Portland, "Interim Report on 1959 Current Measurement Program, Columbia River at Mouth, Oregon and Washington." dated 1 September, 1960.

low river flow (relatively weak stratification), and inhibited during high runoff periods. According to the Tidal Current Tables (Pacific coast of North America and Asia, National Ocean Survey), the tidal current at the Columbia River Lightship is rotary and weak. The current from the Columbia River masks the tidal component and sets to 295° at an average speed of 0.4 knots from October to February. This suggests that the effluent undergoes considerable dissipation between the jetties and the lightship, since much larger ebb currents occur at the mouth. Flood currents are not jet-like at the seaward approach to the mouth and only become considerable very near the jetties.

During the winter the ebb effluent seaward of the jetties appears to be quickly deflected northward by Coriolis and longshore currents, then confined to a narrow nearshore band off the Washington coast (Barnes, Duxbury and Morse, 1972). Barnes et al. noted an accumulation of fresh water just north of the river mouth, suggesting that the effluent forms an anticyclonic eddy there. Duxbury (1967) studied the currents near the mouth using aerially photographed floating mattresses. His measurements confirmed the existence of this eddy and showed that the water returned to shore near Cape Disappointment, some three miles north of the river. Mr. Ted Mather, master of the pilot boat "Peacock", has described persistent northward winter currents seaward of the jetties, evidenced when the vessel drifted several miles northward on one occasion. The evidence therefore indicates that during the winter months the ebb current does not turn southwestward with the ship channel, but straight westward and then northward.

Sediment Transport

The bathymetry of Figure 2 is based on the 1958 survey and can only be considered to show gross features. Sediments are constantly shifting in response to river discharge, tidal action, waves and littoral drift. The principal period of these processes, excepting tides, is the annual one. In winter frequent storm waves accompany a predominantly northward littoral drift and low to medium river discharge. In late spring and early summer low waves, southward littoral drift and high discharge rates predominate.

Lockett (1967) describes the principal sediment transport patterns for the Columbia River. As the ebb current flows past Jetty "A", it deposits river sediment on the flank of the Clatsop Spit shoal zone. Turbulence in the lee of the jetty scours out the northern portion of the channel to depths much greater than the project depth (48 feet) and deposits sediment in the cul-de-sac between Jetty "A" and the North Jetty.

Longshore drift is predominantly north to south over the year, explaining the accretion of sediments over the shoal north of the outer channel (Peacock Spit), and the scouring south of the South Jetty. Some of the littoral sediments move upstream into the river channel, especially when south-to-north drift is predominant. Some of the entering sediment is deposited in the cul-de-sac between the North Jetty and Jetty "A", some on Clatsop Spit, and the rest finds its way into the estuary.

Columbia River Prototype studies at the Waterways Experiment Station (Vicksburg, Mississippi) have confirmed that the saline wedge and its predominant upstream flow act like a sediment trap, resulting in unabated filling of the lower estuary. With high discharge the estuary becomes more stratified and bottom flood currents within the salt wedge predominate, not only trapping river sediments within the estuary, but also bringing in littoral sediments as well.

The continual encroachment of Clatsop Spit upon the navigation channel creates a need for frequent dredging and constitutes a serious hazard to ships. Depths of only 40 feet are found just south of the channel where the ebb currents appear to be strongest. During winter large waves first encounter this area between buoys 6 and 8. There, very large swells break relatively close to the channel, due to rapidly decreasing depths and strong ebb currents.

Hazardous Navigation Conditions at the Columbia River Entrance

This thesis involves prediction of hazardous navigation conditions at the Columbia River entrance. A precise definition of "hazardous" is difficult to formulate, since what is hazardous to a small-craft operator may be of little concern to the navigator of a large merchant vessel. Also, the degree of navigational hazard is determined by a subjective evaluation of many factors which in some way affect an operation or threaten the lives and/or equipment of mariners.

The most important of these factors is the nature of wave conditions. Considerations of wind, visibility, tide, currents, and depth

become important by the way in which these secondary factors enhance or interact with the wave hazard.

Since the scope of this thesis is limited principally to prediction of large waves generated by winter storms, it is appropriate to consider navigation hazards from the point of view of those who must navigate the river entrance under such conditions, namely the Columbia River bar pilots. Their comments given in interviews and the "closure" periods during which they would not escort ship traffic serve to identify hazardous periods.

Bar Pilot Interviews

Navigation hazards at the Columbia River can probably best be assessed by talking to those men whose livelihood and lives depend on understanding them--the bar pilots. The Columbia River bar pilots were interviewed at their Astoria office and the conversations were recorded. The more relevant portions of these interviews are summarized below.

(i) On the hazards of pilot operations:

The factors which create hazardous situations are waves, winds, lack of visibility, shoals and currents. The possible effects include physical damage to or loss of the merchant vessel, the pilot boat or the transfer launch, as well as injury to personnel and loss of life.

Hazardous situations may occur during pilot transfer near the Columbia River Lightship. As the daughter launch of the

pilot boat transfers the pilot to and from the ship, the beam of the ship is put to the oncoming swell so that the launch may approach and transfer on the protected (lee) side of the vessel. Transfer may become too hazardous if strong winds and/or cross swell eliminate the calm area normally found in the lee of the ship.

According to the pilots, the most frequent sources of danger involve high swell during the merchant vessel's transit across the inner bar and between the jetty tips. Depending on its draft, length, load and freeboard, the ship may board water, lift its screw, or even hit bottom under certain conditions of wave height, wave steepness, wave-breaking frequency and tide stage. Loss of maneuverability may expose the vessel to severe wave action or cause it to drift into shoal areas.

The danger due to the waves may be aggravated by high winds, swift currents, and lack of visibility. However, the pilots maintained that waves are always the primary consideration during their operations, pointing out that whenever winds were very strong, waves were also high.

(ii) Wave sequences at the lightship:

Except during storm passages, swell are from a generally westerly direction (west-southwest to west-northwest). Before a storm arrival, longer period swell from the west are noted. As the southerly winds of the storm's foresector begin to blow along the coast, a cross swell arrives from the southwest, often

accompanied by heavy seas; this may continue for 24 to 36 hours before the peak arrivals. Thereafter, the waves are again predominantly from the west.

(iii) Ebb current effects:

The ebb current results in steepening of the waves, whereas the flood current reduces wave steepness. If waves are long and steep, they may break even over the channel where depths are relatively large. At times the ebb current is strong enough over the outer bar to cause short period waves to break, provided the effluent follows the channel to the southwest or west-southwest. If there is a strong tendency for the ebb to turn northward past the jetties, the ebb effects over the outer bar are minimal. The large swell typically break over the inner bar and between the jetties where the ebb current is strong.

(iv) Wave breaking:

Pilots distinguish three types of wave breaking, depending on the relative size of the breakers and their persistence, that is, the length of time they are observed to break. The relatively short choppy waves in a developing sea break as short-crested whitecaps which quickly dissipate. Whitecaps are normally seen in deep water (100 feet or more) or over the outer bar during storm passages. Swell, whose crests break and topple forward with the waves for five seconds or less as they progress, are termed soft breaks. They typically occur over the inner bar against ebb currents and subside on the flood. Hence, they are

also referred to as "tide slop". Long-crested breaking swell which persist for 15 to 20 seconds or more are called running breaks. If running breaks occur at ebb tide over the channel, it is considered likely that some form of breaking will continue to occur even during the subsequent flood.

Large swell result in constant turbulent breaking over Clatsop Spit, where individual waves lose their continuity. On the ebb, breakers are largest and most frequent over the outer flank of Clatsop Spit immediately south of the channel, in about 30 to 40 feet of water. The breakers are largest when they first encounter these depths in combination with strong ebb flow; this usually occurs at the seaward portion of the spit, between the end of the South Jetty and buoys 6 and 8.

Bar Closures

When a bar pilot communicates to his Astoria office that conditions are too hazardous to warrant the risk of bar transit or of transfer to and from merchant vessels, the bar is considered 'closed'. The pilot dispatch officer turns on an amber light above the office that indicates to vessels anchored in Astoria and awaiting transit that the pilots will not escort traffic. Occasionally a vessel will decide to risk transit without a pilot, but this is rare because of insurance disclaimers regarding unpiloted transits. The judgement of pilots concerning bar conditions is respected by operators of vessels of all sizes. The amber light thus carries the same weight as if the bar transit were legally prohibited.

The pilot's decision considers the total effect of several oceanic and meteorological factors. In marginal situations the decision may depend on the particular pilot or the type of vessel to be escorted; or closure may be triggered by what is not known of bar conditions as much as what is known. This is especially true when visibility does not permit accurate extrapolation from known conditions a few hours before. The amount of ship traffic is another variable which influences marginal decisions.

The Columbia River Bar Pilots Association (Astoria, Oregon) cooperated with this study by providing records of past bar closure periods. During the seven-year period from January, 1963 through December, 1969 the bar was closed 181 times for a total of 2088 hours (87 days), or an average of 26 times per year for an average total of 300 hours, mostly during winter months.

During the seven-year period, 56% of all closures were of less than 9.5 hours duration (1½ semidiurnal tidal cycles). These closures were almost invariably associated with an ebb tide and were more frequent at night. Since the hazardous effects of waves were the primary interest of the study, extended closures lasting 9.5 hours or more were selected for further analysis. It was felt that conditions during these closures transcended purely tidal effects, and that the extended closures would serve as indicators of high-wave periods.

A total of 78 extended closures occurred from 1963 through 1969. Of these, 72% lasted for 20 hours or less; 23% lasted from 21 to 40

hours; and the remainder lasted from 41 to 80 hours. Totalled over all years, 45% occurred in December and January, 68% from November through February, and 95% from October through March. Just over 10 extended closures occurred in an average six-month "winter" (October through March) period.

The occurrences of extended closures by hour of the lunar day are shown in Figure 3a. Such closures most often included the period just before and during lower low water. Therefore, even though large waves were usually factors in producing these relatively long closures, strong ebb currents sometimes resulted in an earlier closure or a later reopening of the bar than would be the case in the absence of tidal effects.

The extended closures are grouped by hour of the solar day in Figure 3b. There is a strong tendency for closure to occur more often at night than during the day. Detailed study of the closures uncovered several instances that were not associated with severe offshore wave conditions. These were evidently due to some combination of ebb and night effects. Most closures were associated with high waves in conjunction with nightfall and/or ebb currents. To eliminate the night effect it would have been necessary to restrict attention to a much smaller sample.

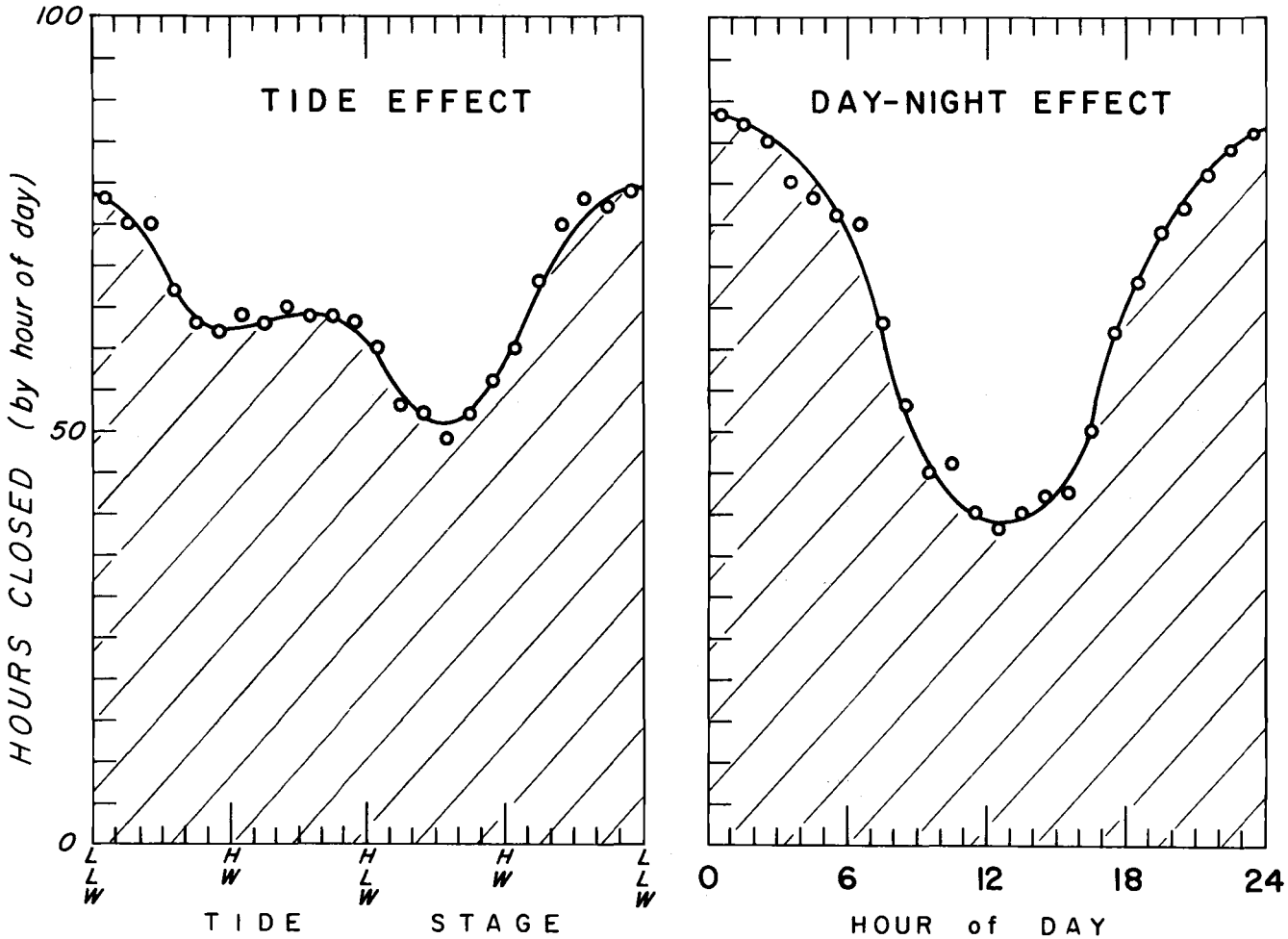

Figure 3. Influence of tidal and daylight cycles on extended (9.5 hours or more) Columbia River bar closures (1963-1969). Each small circle represents the number of times the bar was closed during that hour of the cycle.

Offshore Wave Conditions Associated With Bar Closures

What are the average offshore wave characteristics associated with hazardous conditions at the Columbia River? Virtually no measured wave data have been taken with which to compile a wave climate for the area. Only wave hindcast studies and ship reports are available for this purpose.

The National Marine Consultants (1961a) used the spectral method of Pierson, Neumann and James (1955) to hindcast waves directly offshore of the Columbia River for the three years, 1956, 1957, and 1958. Their statistics indicate that winter swell are most frequent and of greatest height and period when from the west. Since their data was compiled for all wave conditions (mild and severe), their height averages were low (about five feet) and not representative of hazardous periods at the Columbia River.

The National Marine Consultants (1961b) selected the twelve most severe storms occurring over a ten year period (1950-1960) and hindcasted the associated wave heights and periods. They computed maximum significant heights of from 23 to 30 feet, and periods from 11 to 14 seconds. The highest waves came predominantly from the west and southwest.

To complement the hindcast data, ship reported swell heights and periods were compiled for bar closure periods from 1963 through 1969. Six-hourly synoptic ship reports within 250 nautical miles of the

Columbia River were obtained for each extended closure and scrutinized for useful wave information. The observed height (nearest half-meter), period (nearest two seconds) and direction (nearest 10 degrees, true) were tabulated for each swell report. The bivariate frequency distributions for these parameters are shown in Figure 4a, b and c.

Figure 4a shows the bivariate distribution of height and period. Waves two to four and one half meters high with periods of six to eleven seconds tend to be most frequent. Heights and periods are poorly correlated.

Both heights (Figure 4b) and periods (Figure 4c) show definite modes at directions of 270° and 180°. Weak secondary modes are also suggested at directions of 315° and 230°. (These should be treated cautiously however, because there is a tendency for observers to report directions to the nearest major (octal) point of the compass.) The modal heights for west and south swell are about the same, though west swell are much more frequent. The modal periods for westerly swell are greater than for any other direction.

In summary, offshore swell heights associated with hazardous bar conditions are predominantly from 10 feet (closure-related ship reports) to 30 feet (severe storm hindcasts). The swell are most frequent, highest, and of longest period when from the west. There is a secondary tendency for southerly swell of shorter period to occur.

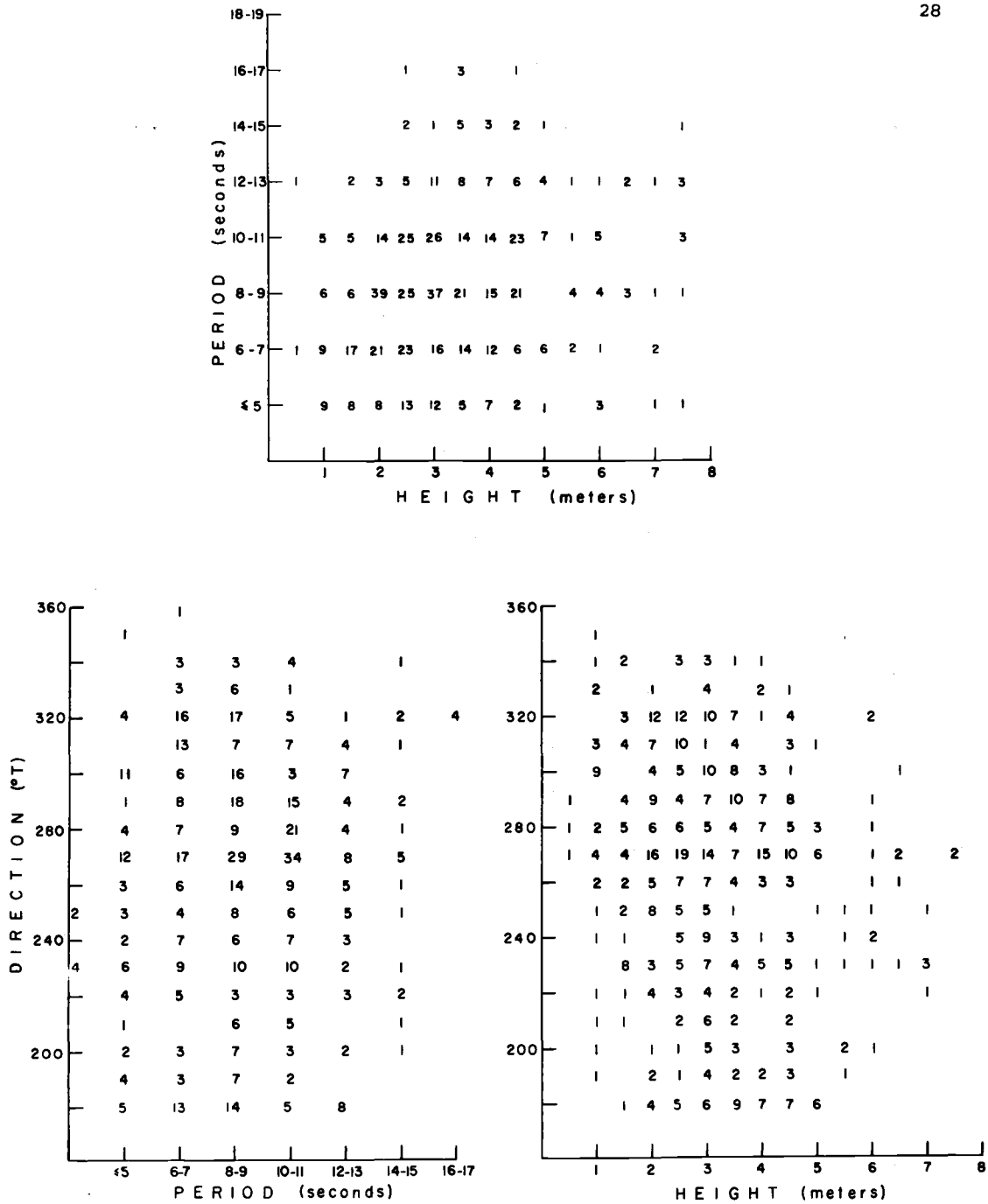

Figure 4. Bivariate plots of height, period and direction of swell reported by ships within 250 n.mi. of the Columbia River during extended bar closures (1963-1969). Numbers indicate frequency of occurrence of a bivariate pair.

Closure-Producing Storms

In order to develop predictive techniques and effectively apply them it is advisable to familiarize oneself with the characteristics of storms which frequently result in hazardous wave conditions. Toward this end, the storms associated with the extended bar closures from 1963 through 1969 were studied.

The surface pressure charts (six-hourly) for at least a three day period preceding each extended bar closure were examined. With the aid of ship reported swell and their approximate group propagation velocities, the storm developments mainly responsible for bar closure were isolated. Having eliminated (or nearly so) the tidal bias from the closure periods, it was almost always possible to find some form of cyclonic development associated with each closure. The principal data associated with each disturbance were tabulated: locations, trajectory, speed of movement, growth stage, and fetch characteristics (wind speed, fetch length, duration).

The average fetch characteristics and their ranges for closure-related storms (1963-1969) are given in Table 1:

Table 1

Fetch Characteristics	Average	Range
Wind Speed (knots)	34	20-70
Duration (hours)	31	12-84
Length (nautical miles)	500	200-800
Final Decay Distance (n.mi.)	100	0-700
Fetch Speed (knots)	17	0-40

About 60% of the storms were occluded and near maximum intensity during the periods that they significantly affected the Columbia River. Only 15% were in early stages of development, and the remainder were mature, stagnating cyclones.

Although almost all effective storms were located within 600 miles of the coast, many had traveled great distances from the mid-Pacific, along or just south of the Aleutian Islands. The moving fetches from these storms are very effective in bringing large waves to the Columbia River, as they travel with the waves they generate. The fact that the Columbia River lies directly in the path of these moving storms makes it one of the most hazardous harbor entrances in the world.

The cold sectors of cyclones moving eastward across the Pacific along or south of the Aleutians result in the everpresent westerly swell experienced at the Columbia River during the winter months. Other directions occur at intervals as cyclones mature or develop within 1000 nautical miles of the coast at different latitudes. The cold sectors of Gulf of Alaska storms typically result in northwest swell and seas. Other types generate westerly to southwesterly swell within their cold sectors. A few hours before the cold front crosses the coast the southerly winds ahead of the front briefly generate seas from the south. Cyclones in very early stages of development sometimes sweep almost northward off northern California toward the Washington coast, bringing swell and seas from the south to the Columbia River.

Waves and Breakers at the Columbia River Entrance

When waves propagate from deep water into the river entrance, they are modified due to the effects of shoaling, currents and refraction. As the average steepness of the waves increases, breaking becomes more frequent, with the form of the breakers depending mostly on the depth of water relative to the wavelength.

Shoaling produces wave height changes that compensate for changing velocity of energy propagation (group velocity) with depth. Most swell are of "intermediate" depth over the channel at the Columbia River, and little change in height results. Over nearby shoal areas, height increases of 50% or more may occur. More significant perhaps, is the fact that wavelengths may be reduced to half or less of the deep water lengths, even over the channel. Thus the waves steepen considerably, even if height changes are minimal. Because shoaling effects increase with decreasing relative depths, the longer period waves are more affected at a particular water depth.

Where currents are involved, the shorter period waves are most strongly affected. When waves encounter opposing currents (such as at a river mouth at ebb tide), the heights are increased and the lengths are decreased. Since current effects increase with increasing relative current, the shorter period waves are more affected for a particular current. Waves whose periods are less than a critical value cannot stem the ebb current and must dissipate their energy in turbulent wave breaking. Over the outer bar where ebb currents are weaker, only the locally generated seas (short periods) are seriously

affected, often breaking as short-crested whitecaps. Over the inner bar the current is strong and swell is further steepened, causing long-crested breakers to occur randomly.

The effects of shoaling and currents in modifying waves and inducing breaking will be treated in detail in Chapters VI and VII. The third process, refraction, is much more difficult to assess. Depth-controlled refraction depends on the bathymetry, which at the Columbia River is constantly changing due to sediment transport. Current-influenced refraction can only be discussed qualitatively, because the current distribution seaward of the jetties is highly variable and virtually unknown.

Since waves travel faster over channels than over nearby shoals, the wave crests are directed away from the channels and toward the shoals. This well known refraction process concentrates wave energy in shoal areas, thus increasing wave heights and enhancing the likelihood of breakers there. Over the channel, wave heights decrease. The height change is positive (increasing) for a negative (decreasing) change in orthogonal spacing (orthogonals are imaginary lines everywhere normal to the wavecrests, and initially equidistant in deep water).

To qualitatively understand the effects of refraction on swell at the Columbia River, refraction diagrams were constructed for the area by the wave crest method (Johnson, O'Brien and Isaacs, 1948). Diagrams were constructed for 12 second waves from west-northwest

(WNW, 292.5°), west (W, 270°), southwest (SW, 225°), and south (S, 180°) in deep water. The diagrams (Figure 5) clearly show the effects of convergence over Peacock Spit and divergence over the channel between the jetties, except in the case of waves from WNW. In the latter case the convergence zone shifts to the north side of the channel, between the channel and Peacock Spit; the divergent zone shifts to the south portion of the channel, near the end of the South Jetty (but not at the jetty tip, where convergence is strong and can not be calculated). Waves from SW and S approach the south side of the South Jetty with little change relative to deeper water; W and WNW waves are reduced in height in this area. Divergence over the channel is only strong between the jetties inshore of buoys 6 and 7 (Figure 1), i.e. there is little protection seaward of this point, over the outer bar. The diagrams suggest that WNW swell should be reduced the least between the jetties, but that the waves may break over Peacock Spit before reaching the channel.

At ebb tide the progress of the waves is retarded over the channel, compared to slack water. This decreases the tendency for divergence to occur and for wave heights to be lowered. During a strong ebb the currents may cause a reversal of the refractive effect over the channel resulting in convergence and height increase (Arthur, 1950). A quantitative evaluation of these effects is beyond the scope of this thesis. Research on the current distribution at the river mouth, using hydraulic and numerical models, would be very useful.

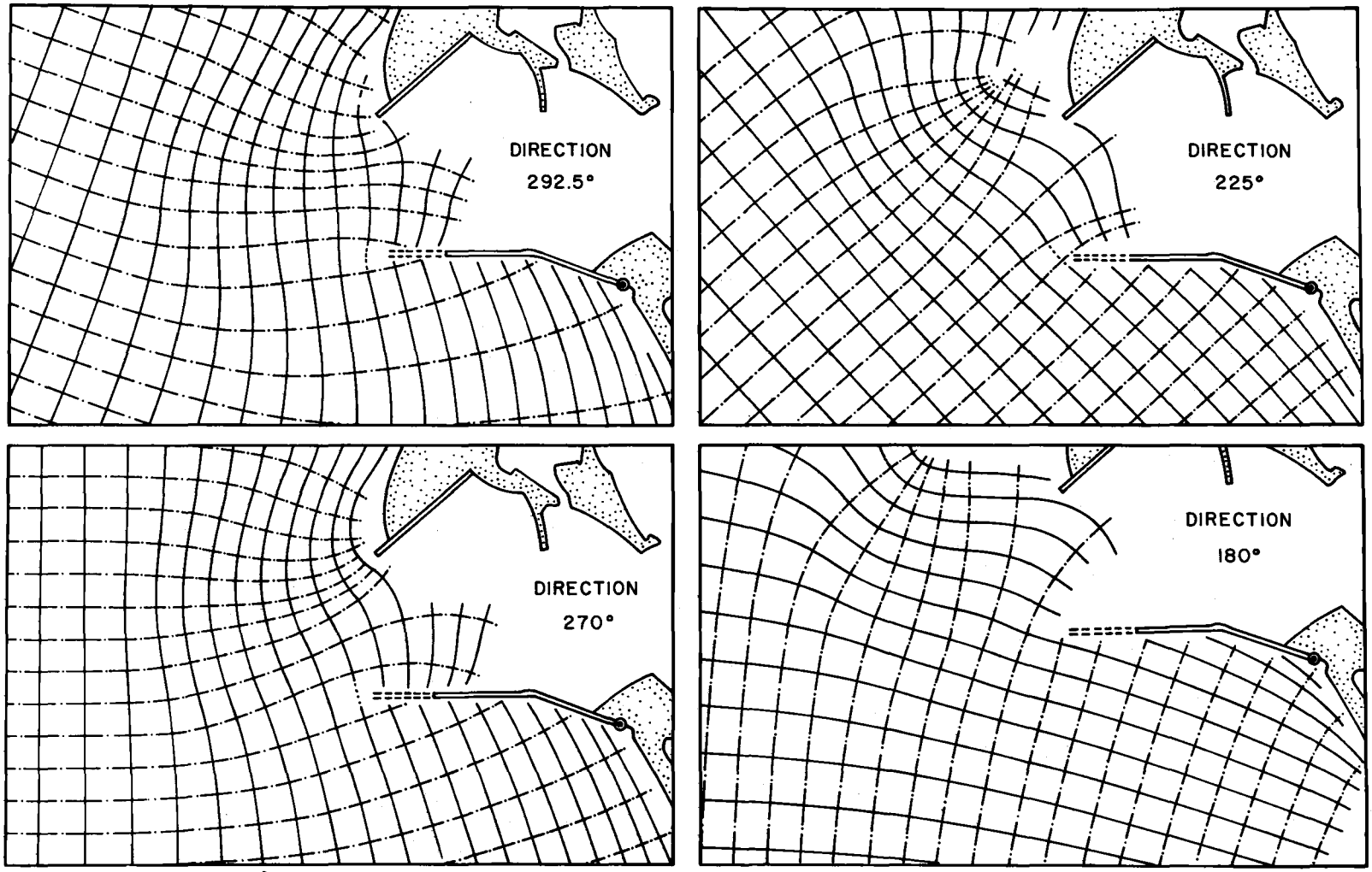

Figure 5. Wave crest refraction diagrams for 12-second waves arriving at the Columbia River from several (deep water) directions. (Bathymetry used is shown in Figure 2.)

Figures 2 and 5 suggest that the combined effects of depth, current and refraction indeed favor hazardous conditions near the seaward extremity of Clatsop Spit. Here the ebb current is still confined by the jetties and relatively strong. Depths decrease rapidly just southeast of the channel (Figure 2) and refractive divergence is not great. In addition, the swell presumably do not lose much energy in breaking prior to arrival at that point (with the possible exception of northwest swell which must first cross the outer portion of Peacock Spit).

Summary

Ship reports and bar pilot interviews suggest that offshore swell of 10 to 25 feet are usually associated with extended bar closures. Swell from the west are most frequent and of longest period, while southerly swell show a secondary frequency mode; they are of similar heights but more often locally generated than the westerly swell.

Distant storms generate waves which propagate as longer period westerly swell to the Columbia River. As storms enter the eastern North Pacific, they mature at different latitudes, causing the Columbia River entrance to experience storm waves from northwest to south. Storms usually generate closure-related waves during their occluded (most intense) development stage. Redeveloping storms in the Gulf of Alaska are often sources of high northwest swell, while prefrontal winds and young cyclones off the Oregon-California coast are often associated with locally generated sea and swell from the south sector.

Considerations of depth, current and refraction at the Columbia River entrance suggest that the area near the seaward extremity (buoys 6 and 8) of Clatsop Spit may often be quite hazardous due to steep and breaking swell.

III. WAVE OBSERVATIONS

Introduction

This chapter describes wave measurements that are used in later chapters as verification for prediction methods. Because suitable data for the Columbia River area do not exist, available measurements at Newport are used instead.

In the summer and fall of 1971 a program of wave forecast verification using visual, wave sensor and microseism observations was begun by NOAA-Sea Grant personnel at Newport, Oregon (Mr. David Zopf and Mr. Clayton Creech). (Microseisms are small vibrations on the Earth's surface of period 4-10 seconds and amplitudes up to 20 microns.) Visual observations were taken once a day (on working days) when visibility permitted. A pressure-type wave sensor installed off Newport in the fall of 1971 and again in the fall of 1972 yielded few measurements due to failures. Microseisms were recorded at six-hour intervals by a vertical long-period seismometer which correlated well with visually estimated wave heights.

The visual observations were too infrequent and sporadic to use as verification for the methods developed in this thesis. However, the seismometer at Newport provided acceptable wave-related microseism data at regular six-hour intervals, throughout the 1971-1972 winter and these data were used for verification of predictive techniques developed in subsequent chapters.

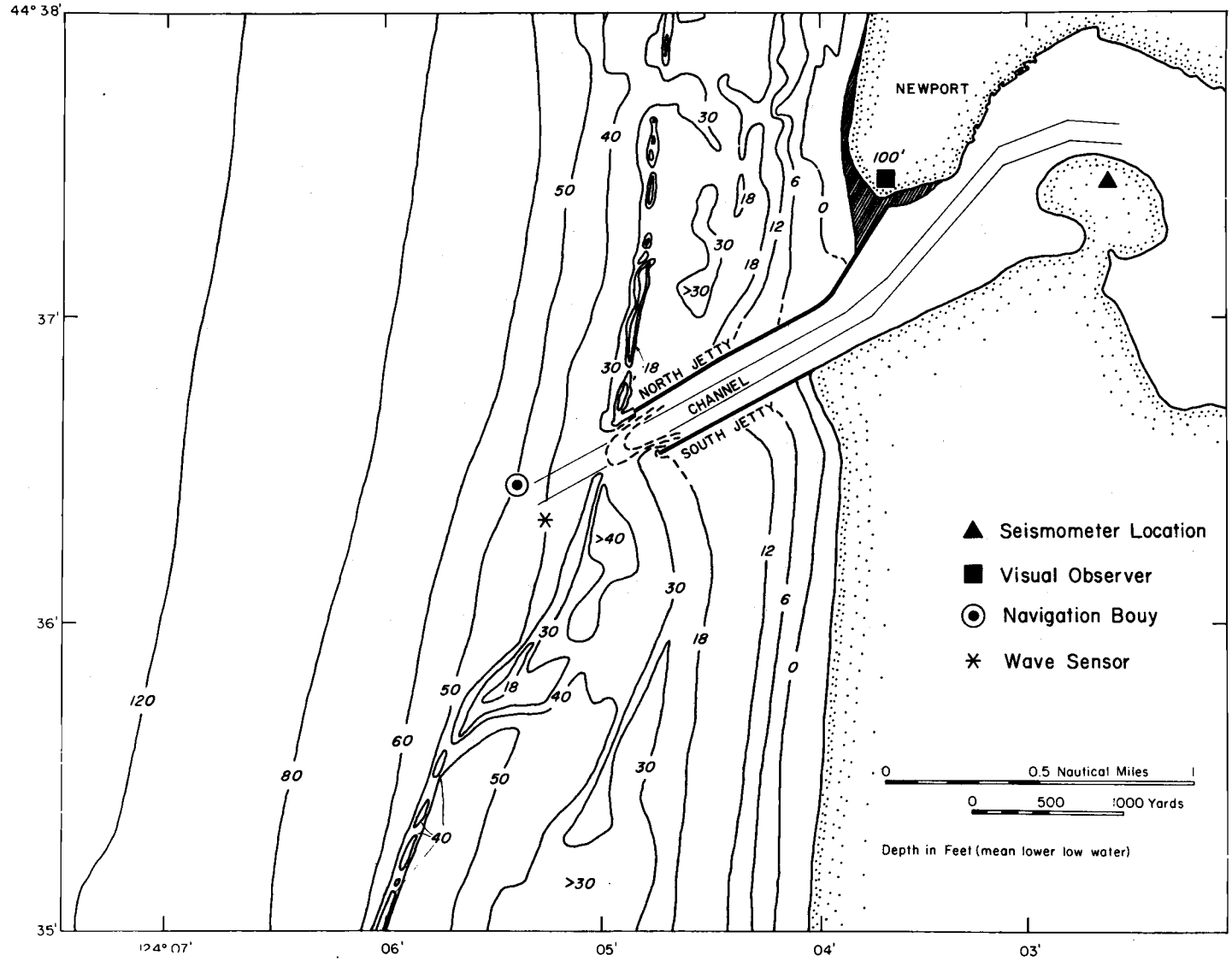

Figure 6. Map showing the bathymetry and sites of wave measurements and observations in the vicinity of Newport, Oregon.

Visual Wave Observations at Newport

Visual observations of waves from the coast at Newport were made against a 12 foot high buoy in 50 feet of water. A trained observer (Mr. Clayton Creech) estimated wave height and period from a hill about 120 feet above sea level and at a distance of 1.65 nautical miles (10,000 feet) from the buoy (see Figure 6). The observer watched the buoy through binoculars for about five minutes and estimated the wave heights from buoy features of known height (above the water line). Period was estimated by timing the passage of several well-defined waves. Observations were usually taken once a day (working days) at about 7 a.m. (Pacific Standard Time) when visibility permitted. Occasionally a second observation was taken at 5 p.m. PST.

Because of the observer's height above the water, the true wave heights were systematically underestimated at the Newport site, as shown in Figure 7 .

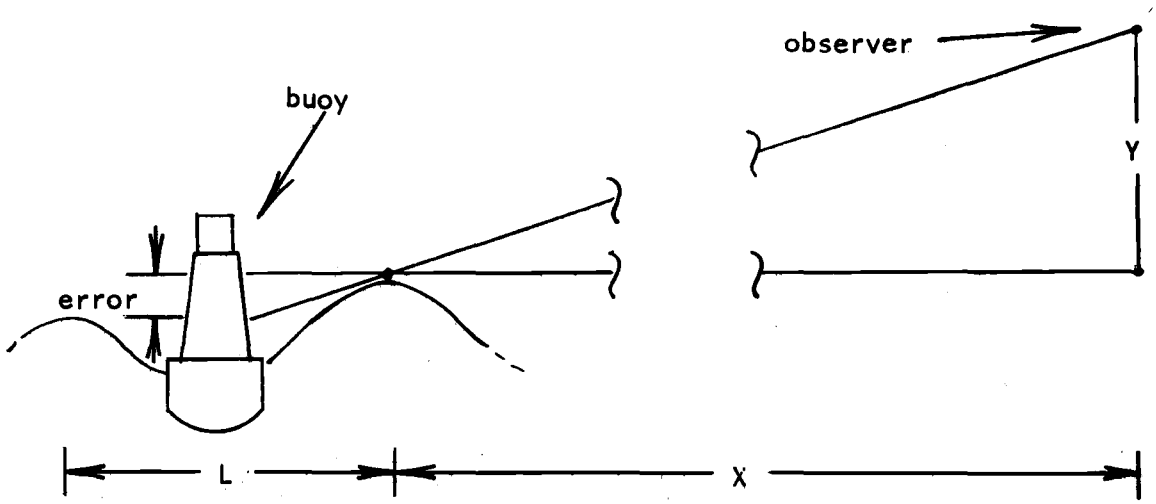

Figure 7 . Schematic for observation error.

The heights were underestimated by an amount $\frac{1}{2}L(Y/X)$, where

L = length of waves near the buoy (feet),

Y = observer's height above sea level (120 feet), and

X = distance between observer and wave (10,000 feet).

The wavelength of the observed waves can be inferred from the water depth and the estimated period and their relationship to length from small amplitude wave theory. Each height observation was corrected by adding the amount of the error, rounded to the nearest foot. The corrections varied from one foot for six second periods to four feet for 16 second periods.

Pressure Sensor Measurements at Newport

A pressure-type wave sensor was installed in 40 feet of water off Newport in the fall of 1971 (Figure 6). The system malfunctioned almost immediately and could not be reinstalled due to the onset of winter conditions. In the fall of 1972 it was again deployed at the same spot and functioned correctly from 1300 PST on October 29 to 1300 PST on November 5, at which time the system again failed.

The instrument used was a Bendix model A-2 pressure wave sensor with a time constant of 40 seconds. Prior to each set of measurements the sensor was factory cleaned, tested and calibrated against a static pressure head. Significant heights and average zero upcrossing periods were determined from six-hourly strip chart records of 12 minute duration, analyzed by the method of Tucker (1961) and Draper (1967).

Hydrodynamic pressure attenuation as a function of water depth and wave period was corrected for as suggested by Draper (1967).

Seismometer Measurements

Because it was felt that the average heights and periods might be successfully inferred from microseisms at Newport, a vertical long-period seismometer was installed. The unit is of the portable commercial type (Teledyne-Geotech, model SL-210) designed for geophysical surveys. As of this writing, the instrument has been resting on the concrete floor of the Marine Science Center building (Newport) since May 1971. The characteristics of the system were described in detail by Zopf (1972). To correctly interpret the seismometer records and correlate them to other observations, it is necessary to discuss the relation between microseisms and ocean waves.

Microseisms

Darbyshire (1963) has reviewed the theories and observations concerning the relation between sea waves and microseisms. Early investigators noted that microseism activity tended to coincide with high surf. Somewhat later (1930) it was found that microseisms at some localities were recorded before the swell arrived at the coast, suggesting that wave energy was somehow transmitted to the deep ocean floor to cause microseisms. Early attempts to explain the phenomenon failed because the effects of progressive waves are negligible at a

depth of half a wavelength. Even in shallow water the microseism wavelength is much greater than the length of ocean waves, so that the pressure effects of a succession of progressive waves tend to cancel out.

Later investigations continued to indicate a strong relation between sea waves and microseisms, and found, additionally, that the periods of microseisms were about half those of the associated ocean waves. This was confirmed by Deacon (1947) who found a close correspondence between the amplitude of waves and that of microseisms, and between the wave period and twice the microseism period.

Longuet-Higgins (1950) developed a consistent theory to explain both the deep water generation of microseisms and their "half-period". He used a previous finding by Miche (1944) as the basis for his explanation, namely, that in the second-order treatment of standing waves there is a contribution to the pressure variation that is not attenuated with depth.

When two progressive waves of the same wavelength travel in opposite directions this pressure variation is proportional to the product of the (first-order) amplitudes of the two waves and has twice their frequency. Specifically,

$$p \propto a_1 \, a_2 \, \omega^2 \cos(2\omega t) \quad , \qquad (3\text{-}1)$$

where a_1 and a_2 are the amplitudes of the two waves and ω is their angular frequency. The second-order effects ultimately predominate over the first-order effects at large depths.

Longuet-Higgins suggested that such interference could take place over sufficiently large areas of the sea floor to excite the microseism wavelengths if (1) waves or swell interact with their own reflections from a steep coast, (2) waves generated in different quadrants of a fast moving storm interfere with each other, or (3) similar swell trains travel in opposite directions from two storms. An increasing amount of observational evidence supports these explanations (Darbyshire, 1950; Haubrich, Munk and Snodgrass, 1963).

Zopf (1972) concluded that the mechanism at the Newport site is of the first type, as the arrival times of peak microseism and wave activities are not detectably different. He suggested that the clarity of the signal at Newport and the relative lack of background noise may be related to the peculiar geological structure of the area (a 50 foot layer of sand-fill overlays bedrock and extends uninterrupted to the shore, 2 kilometers away).

Record Analysis

A strip-chart recorder was programmed to register the seismometer signal for 11 minutes every six hours (01, 07, 13 and 19 PST). To determine the relation between visually observed heights and periods and the nearly simultaneous (07 PST) seismometer recordings, a representative deflection had to be extracted from each record.

Darbyshire (1950) pointed out that for a given wave height, more energy will be transmitted to the ocean floor by short waves than by

long waves (from the ω^2 dependence in [3-1]). Thus standard methods of record analysis are probably not applicable to the seismometer records.

Figure 8 shows two nearly simultaneous recordings from the pressure sensor and the seismometer. Because the chart speed for the seismometer was twice that for the pressure sensor, the spatial separations between upcrossings should by theory be equal. They are approximately equal for the greatest microseism deflections. The appearance of intervening microseism deflections of smaller amplitude and period may be due to some combination of ambient noise and short-period wave activity. In the latter case, the high frequency enhancement mentioned by Deacon may be partly responsible for their appearance. Also, short-period progressive waves are more attenuated with depth and would be absent or insignificant on the pressure sensor record.

Zopf (1972) devised the following procedure for analyzing the seismometer records:

> ...In analyzing any one record, we searched for the greatest peak-to-peak deflection and noted its zero (up)crossing period. Then the record was searched for signals of approximately the same, high amplitude but longer period, because of the strong dependence of indicated ocean wave height on period. Finally, the averages of the few greatest deflections (nearest percent of full-scale) and of their periods (nearest half-second) were selected as representing the height and (half) period ... of ocean waves during the recording.

A representative deflection and seismic period were found for each record by this procedure. An acceptable calibration of deflections in terms of average ocean wave heights may be found by correlation with visual observations, as described in the next section.

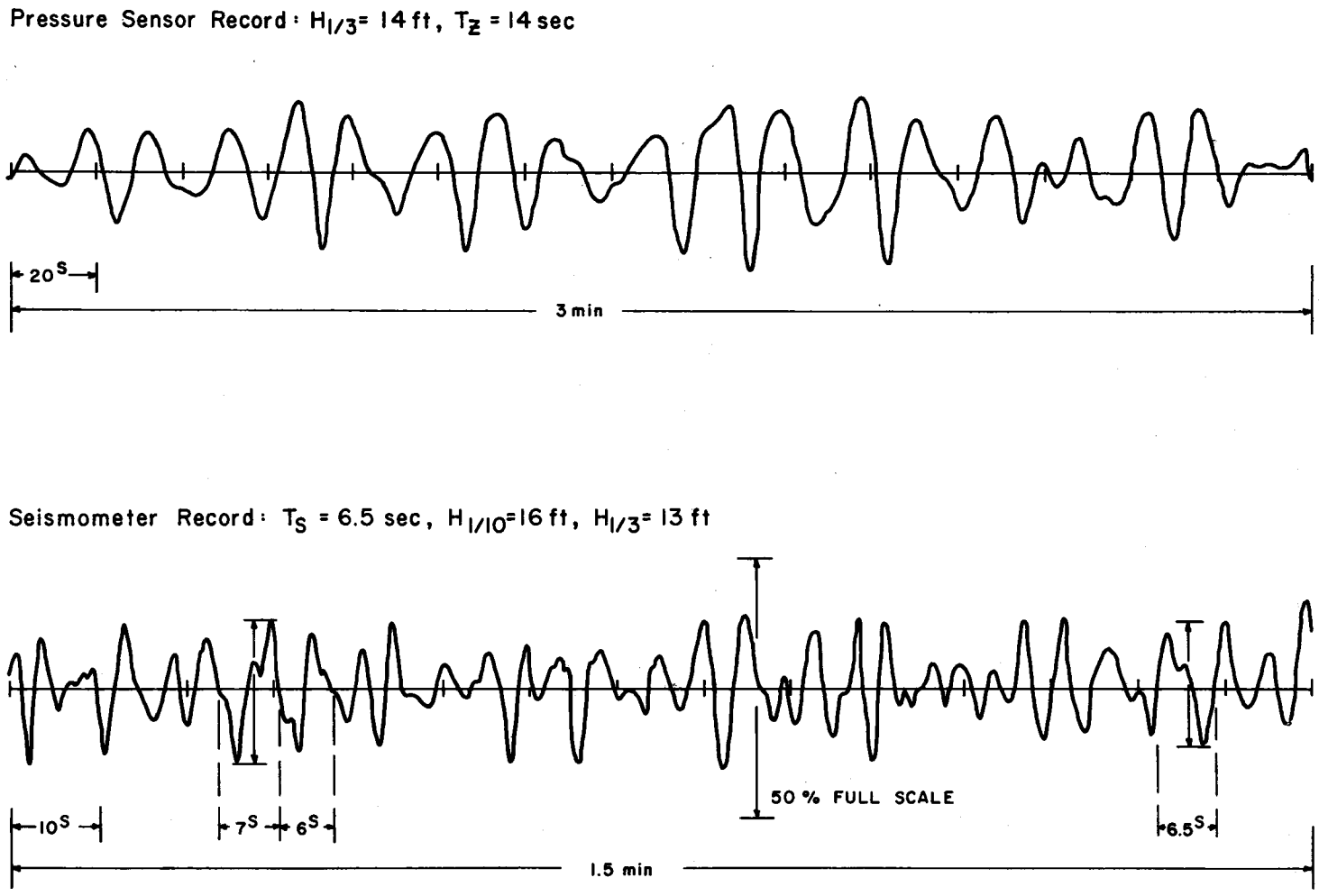

Figure 8. Nearly simultaneous pressure sensor and seismometer wave records (Newport).

Calibration

Since the Newport seismometer senses the vertical velocity of the ground motion, the chart deflection is proportional to the first derivative of the ground displacement. Zopf (1972) proposed the hypothesis that the ground displacement is linearly related to the forcing pressure field over the ocean bottom. This implies that peak-to-peak chart deflection should be proportional to the amplitude of the first derivative of (3-1), that is

$$\delta \propto H^2 \omega^3 \quad , \tag{3-2}$$

where δ is the peak deflection in percent of full scale and H is the height of the associated waves.

A straightforward way to use (3-2) as a means of calibration for the seismometer is to (statistically) regress observed wave heights on $(\delta P^3)^{\frac{1}{2}}$, where P equals the seismic half-period (π/ω). During the year from 1 August, 1971 to 31 July, 1972, 230 visual height observations were avilable that could be corrected for the systematic error discussed earlier (i.e. for which periods had also been estimated). Regression of the observed heights on $(\delta P^3)^{\frac{1}{2}}$ yielded

$$\hat{H} = 1.27 + 0.147(\delta P^3)^{\frac{1}{2}} \quad , \tag{3-3}$$

where $\hat{H}$ denotes the height predicted by the regression equation.

The predicted heights are plotted against the visually observed heights in Figure 9a. Since the two parameters are related by regression, the points fall along the 1:1 line. The computed correlation coefficient is 0.94.

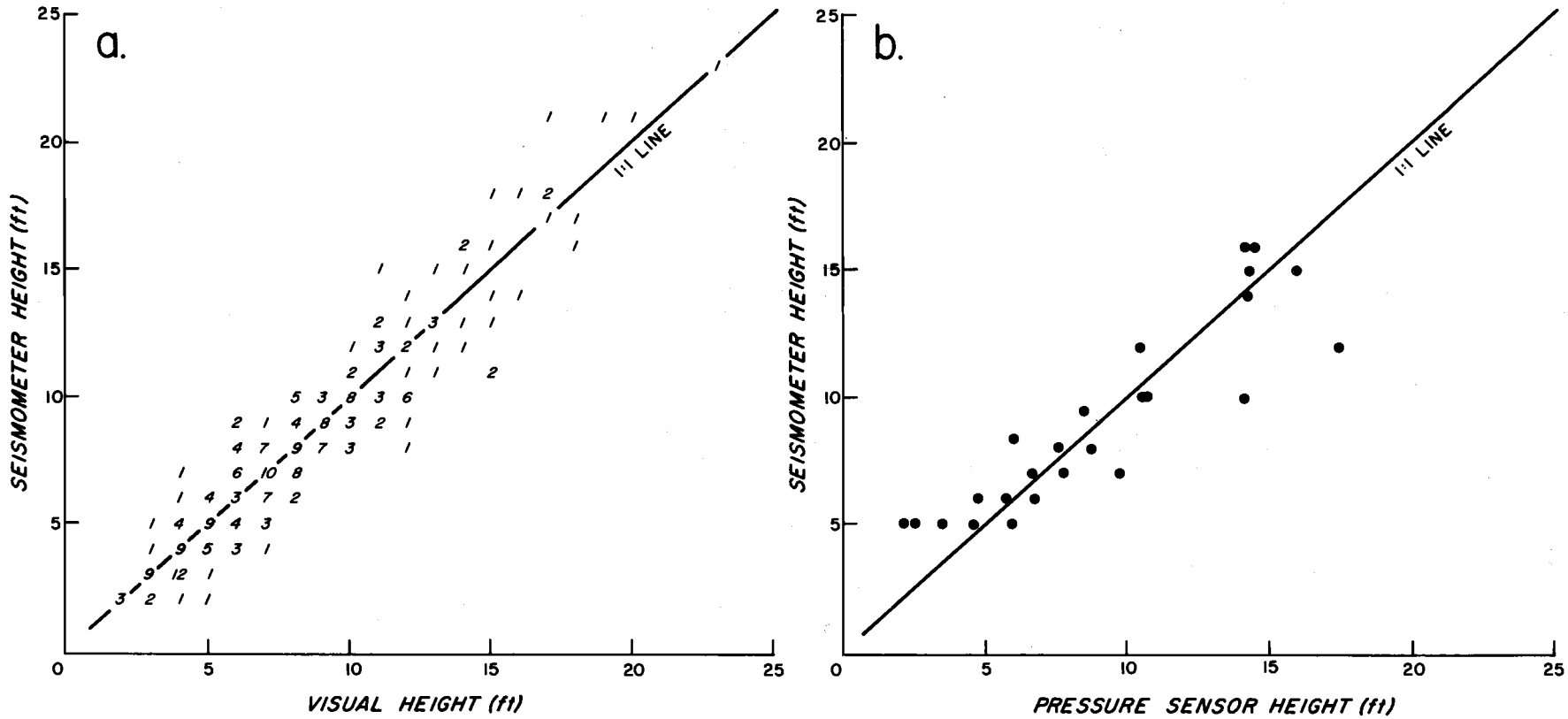

Figure 9. Scatter diagrams of seismometer-inferred heights vs. visually observed heights (a) and pressure-sensor (significant) heights (b).

The agreement shows that average wave heights are in fact closely related to microseisms at Newport, and that the hypothesis (3-2) is acceptable at that site. The inferred significant wave heights (3-3) are quite adequate for the purpose of verifying wave forecast methods. This is especially significant since direct measurements are so difficult to obtain during the Oregon winter, and visual observations can only be taken occasionally, as visibility and other circumstances permit.

It was not originally known if the observer visually estimated the significant height or not. To determine this, the significant heights from the pressure sensor records were plotted against the heights inferred by (3-3) from the nearly simultaneous seismometer records. This is shown in Figure 9b. The points also fall on 1:1 line, indicating that both the visually observed heights and the inferred heights (3-3) are close to the significant height. This is based only on one week's pressure sensor data, however, and is not conclusive.

In addition to the agreement between average wave heights and representative microseism parameters, the representative seismic period is consistently about half that of the observed average wave periods, as expected from theory and previous investigations.

Conclusion

Due to apparently ideal geological transmission characteristics for microseisms in the Newport area, recorded microseisms there correlate very well with observed average ocean wave heights (and periods). The agreement is consistent with existing theory on microseisms.

Visually observed heights from a one year period were regressed on representative seismometer deflections and periods in a manner consistent with theory. The resulting calibration equation can be used to infer six-hourly significant wave heights throughout the 1971-1972 winter. Average zero upcrossing wave periods are estimated by taking twice the representative microseism period. These data provide an acceptable means of verifying wave prediction methods developed in the following chapters.

IV. A SEMI-AUTOMATED METHOD FOR DEEP-WATER FORECASTING

Introduction

This chapter is concerned with the problem of forecasting deep-water waves off the mouth of the Columbia River.

While studying the various methods of deep-water forecasting presently in use it became apparent that all were of limited usefulness for this purpose. The classical manual methods developed during World War II or shortly thereafter were too inaccurate or cumbersome to be of value. From the manual methods, automated, ocean-wide techniques have evolved which apply the forecasting relationships at grid points, with digitized wind fields as input. The outputs are too coarse to accurately simulate wave conditions at coastal stations, where greater resolution is required, both in space and in time.

Although in principle the semi-automated technique described here can be applied at any deep-ocean site, it is primarily designed to provide coastal forecasts, for which adequate outputs do not presently exist. The method may also be used for any oceanic location of special interest as a hindcast tool.

The semi-automated method reduces the subjectivity involved in analyzing fetches from meteorological maps. It may be possible to convert the present technique into a fully automated approach, in which wind information would be input in digitized form on a specially designed grid. The grid and wind fields could then be used to generate forecasts for all major west-coast ports.

The technique is essentially a hybrid scheme which borrows from the following sources:

(a) The Pierson, Neumann, and James (1955) forecast method;

(b) The ideas of Wilson (1955) on the representation of moving fetches;

(c) The empirical-theoretical spectrum introduced by Liu (1971).

Two great shortcomings of the Pierson-Neumann-James (P-N-J) method have been remedied in the semi-automated scheme. Arbitrarily complex fetch behavior can be parameterized as input data (not formerly possible) and tedious manual computations and referencing of tables and graphs are done by computer.

Freed from tedious calculations, the forecaster can dedicate more time to an accurate and complete analysis of fetch histories. In addition the determination of fetch history is made more objective through the use of the time-distance diagram for its representation. Finally, the computerization has been greatly simplified by use of the fetch-dependent spectrum developed by Liu (1971) instead of the "fully developed" Neumann (1953) spectrum used in the P-N-J approach.

Discussion of Existing Wave Forecast Methods

Wave forecast methods are divided roughly into two categories: spectral, and non-spectral. Historically, the non-spectral method was introduced first by Sverdrup and Munk (1947) toward the end of World War II, for use in military operations. The wave spectrum approach

of Pierson-Neumann-James (1955) followed. Subsequent techniques were essentially adaptations of these methods and were principally for open-ocean, automated forecasts--of use for naval operations and merchant vessel routing.

The Sverdrup-Munk method, as revised by Bretschneider (1959) is now called the S-M-B method. The original method has been documented in Hydrographic Office Publications Nos. 601 and 604. The scientific background has been summarized nicely by Kinsman (1965). The method consists of entering certain graphs with the basic input parameters--wind speed, fetch length, wind duration, and decay distance--and reading off the desired values of significant wave height and period. The graphs were constructed from the equations of classical linear wave theory and empirical relationships involving wave age, wave steepness, conservation of energy, and the increase in predominant period with distance from decaying swell.

Kinsman (1965) has put the Sverdrup-Munk method into historical perspective by pointing out that, while many of its premises are incorrect, the approach was born of wartime necessity, utilizing to the fullest the limited observational and theoretical information available. The S-M-B techniques are still in use today because they do combine simplicity of use with acceptable accuracy, for many purposes. This is particularly true of ocean-wide automated forecasting, where the savings in computational time is multiplied many times by large numerical grids and resolution need not be great.

The P-N-J method introduced spectral concepts to forecasting. The spectrum used was the fully developed (fetch-independent) spectrum of

Neumann (1953). In practice, the spectrum is determined by the wind speed, then truncated at its low-frequency end according to the fetch length or duration, whichever is limiting. The wave energy is divided into frequency bands and "propagated" at group velocity to the forecast point. Energy components arriving simultaneously at the forecast point are summed and the energy sum is multiplied by an angular spreading factor to account for spreading losses. The net result is an energy, or "E-value" which is defined such that the area under the E curve is twice the variance, σ^2 , of the water surface elevation. The significant wave height at the forecast point is simply, $H_{1/3} = 4\sigma = 2\sqrt{2}\, E^{\frac{1}{2}}$ (Longuet-Higgins, 1952), while the range of periods to be expected is obtained directly by knowing the range of frequency components used to obtain "E".

The strengths and limitations of the P-N-J method were pointed out by the authors themselves. The spectrum provides a more complete and accurate description of wave conditions, and, qualitatively at least, of the way in which wave energy is propagated. Of particular value is the fact that the period structure of the waves is an inherent feature of the forecast. Also the use of the angular spreading factor seems to be a particularly effective innovation, accounting simulataneously for the effect of decay distance and fetch width on the amount of spreading loss.

A great disadvantage of the P-N-J method is thecumbersome nature of the techniques, which are time-consuming and tedious. The partition

and propagation of wave energy according to frequency components is done manually according to certain schemes, called "filters" by the authors. However, only two or three of the filters are easily applied and are appropriate to specific types of fetch behavior, e.g. stationary fetches (Filter II) or fetches which move with the speed of the wind (Filter IV). There is no straightforward way to treat a fetch moving at an arbitrary speed, or whose wind speed and/or fetch speed changes with time. This lack of flexibility results inevitably in oversimplifications of fetch behavior.

It is pointed out by the authors that P-N-J computations of wave height are too low for low wind speeds and short fetches, and too high for high winds and long fetches. Also, observed waves appear to arrive sooner than those that are predicted by the method. Both effects can be attributed to inadequate wind and/or frequency dependence in the Neumann spectrum. Arrival-time discrepancies may also be related to oversimplification of fetch behavior.

The Fleet Numerical Weather Central (FNWC) developed an ocean-wide fully automated forecast system in which relationships of the S-M-B type are applied at grid points, and the waves are propagated from grid point to grid point at the group velocity of the largest waves (Hubert, 1964). The method has been adapted for use by the National Weather Service (National Oceanic and Atmospheric Administration) by Pore and Richardson (1969). A clear advantage to the use of the S-M-B relationships is the savings in computation time. However, the grid size used

is too coarse to account for the detailed behavior of smaller local wind fields which affect coastal forecast points, a purpose for which the FNWC method was not intended.

The U.S. Naval Oceanographic Office wave prediction system is also of the open-ocean type, but uses the spectral relationships of the P-N-J approach, and the updated fully-developed spectrum of Pierson and Moskowitz (1964).

The reader may refer to Pore (1970) for summaries of the methods described here. Kinsman (1965) discusses the scientific aspects of the Sverdrup-Munk and P-N-J methods and Barber and Tucker (1963) give a general review of the methods.

Brief mention should be made of the techniques introduced by Wilson (1955) for the treatment of moving fetches. His approach consists essentially of using time-distance fetch diagrams together with the Sverdrup-Munk prediction method. The time-distance diagram may also be used with the spectral method, and lends itself to computerization. It is the basis for fetch representation in the semi-automated method described in this chapter.

Empirical-theoretical Spectral Forms

Short period wave forecasts could best be made from observed wave data if good data in sufficient amount existed over ocean areas. But, sea-going wave measurement systems are complex and expensive, visual observations are difficult and limited to daylight hours, and ship

distribution is quite sparse. We must therefore rely on wind measurements, which are more numerous and usually of better quality. Using the surface atmospheric pressure distribution and inferred relations with the surface wind, a fairly good surface wind pattern can be obtained. It becomes necessary, then, to determine the relationship of the wave spectra to the winds which generate them.

A number of spectral models have been proposed, based partly on theory and partly on wave observations. Most models are of the fully-developed, or fetch-independent type. Fully-developed spectral forms have been proposed by Neumann (1953), Darbyshire (1959), Bretschneider (1963a), and Pierson and Moskowitz (1964). A fetch-dependent spectrum was proposed by Bretschneider (1959) and more recently by Liu (1971).

The spectra of greatest interest to the present discussion are those of Neumann, Pierson and Moskowitz, and Liu. The Neumann spectrum is the basis of the Pierson-Neumann-James (P-N-J) forecasting technique. The Pierson-Moskowitz spectrum is the most widely accepted of the fully-developed forms, since it applies the latest theoretical knowledge to a broad observational base. The Liu spectrum approaches the Pierson-Moskowitz spectrum in its fully developed limit. This is the form used in the semi-automated forecast method, because of its fetch dependence.

General Considerations

Almost all of the proposed spectra can be reduced to a common form, proposed by Bretschneider (1963a):

$$S(f) = \hat{S} \cdot (f/\hat{f})^{-m} \exp(-m/n[(f/\hat{f})^{-n} - 1]) \quad , \qquad (4\text{-}1)$$

where f = frequency,

$\hat{f}$ = frequency of the spectral maximum,

$S(f)$ = spectral density function,

and $S(\hat{f}) = \hat{S}$ = spectral density of the spectrum peak.

The integers, m and n, are exponents which determine the form of the spectrum. The parameters $\hat{f}$ and $\hat{S}$ are in general dependent on the wind speed and fetch length. Knowing $\hat{f}$ and $\hat{S}$, the moments of the spectrum can be found by integrating (4-1):

$$M_k = \int_0^\infty f^k \cdot S(f)df \quad . \qquad (4\text{-}2)$$

The spectral moments are the basis for calculating the statistical sea state properties, namely the various average heights and periods.

The spectrum of a developing sea may be thought of as divided into two key portions: frequencies greater than $\hat{f}$ occupy the region known as the equilibrium range, governed by the power law f^{-m} in (4-1). Frequencies less than $\hat{f}$ comprise the growth range of the spectrum, governed by the exponential factor. Waves in the equilibrium range are incapable of further growth, as they are of breaking proportions--energy input by the wind is lost in wave breaking or generation of capillary waves. During spectral growth, the spectral peak frequency ($\hat{f}$) shifts to lower values and the peak energy density ($\hat{S}$) increases. Consequently, the growth range shifts to lower frequencies,

and the equilibrium range expands to occupy frequencies previously growing in energy.

The rate of spectral growth decreases as the waves approach a fully developed state. This condition occurs, approximately, when the wave component at the spectral peak has a celerity equal to the wind speed:

$$C = g/(2\pi\hat{f}) = \text{wave celerity} .$$

($\hat{f}$ in cycles per second)

If U = wind speed, it follows that fully developed conditions result when

$$\hat{f} = g/(2\pi U) \quad . \tag{4-3}$$

In all of the proposed spectra $\hat{f}$ is proportional to g/U, though the constant of proportionality varies somewhat.

To see how the statistical sea state parameters may be found from (4-1) we must first perform the integration (4-2) for the k-th spectral moment, M_k. Introducing the change of variable, $Z = (m/n)(f/\hat{f})^{-n}$, and utilizing the definite integral for the Gamma function,

$$\Gamma(q) = \int_0^\infty Z^{q-1} \exp(-Z)dz \quad ,$$

we obtain

$$M_k = \frac{\hat{f}^{k+1}\, \hat{S}\, e^{m/n}}{m} (n/m)^{q-1}\, \Gamma(q) \quad , \tag{4-4}$$

where

$$q = (m - k - 1)/n \quad .$$

The most frequently used moments are the zero-th (M_o) and the second (M_2):

$$M_o = (\hat{f}/m)\hat{S}\, e^{m/n}(n/m)^{\left[\frac{m-n-1}{n}\right]}\, \Gamma\left(\frac{m-1}{n}\right) \qquad (4\text{-}5)$$

and

$$M_2 = (\hat{f}^3/m)\hat{S}\, e^{m/n}(n/m)^{\left[\frac{m-n-3}{n}\right]}\, \Gamma\left(\frac{m-3}{n}\right) \qquad (4\text{-}6)$$

The zero-th moment is the area under the spectrum, analogous to the mass of a rigid body. The second moment is the energy-weighted sum of the squared frequencies, analogous to a moment of inertia about the origin ($f = 0$).

The basic height-related statistic is the variance of the sea surface elevation, σ^2, where $\sigma^2 = M_o$. Longuet-Higgins (1952) showed how σ^2 is related to the sea surface elevation maxima, or equivalently, mean height ($\overline{H}$), the root-mean-square height (H_{rms}), and the average height of the highest one n-th waves ($H_{1/n}$):

$$\overline{H} = 2.507\sigma = 2.507(M_o)^{\frac{1}{2}}\,, \qquad (4\text{-}7)$$

$$H_{rms} = 2.83\sigma = 2.83(M_o)^{\frac{1}{2}}\,, \qquad (4\text{-}8)$$

$$H_{1/3} = 4\sigma = 4(M_o)^{\frac{1}{2}}\,, \qquad (4\text{-}9)$$

and

$$H_{1/10} = 5.1\sigma = 5.1(M_o)^{\frac{1}{2}}\,. \qquad (4\text{-}10)$$

The average period between zero-upcrossings in a wave record ($\overline{T}$) was shown by Rice (1944) to be

$$\overline{T} = (M_o/M_2)^{\frac{1}{2}} \quad \text{(frequency in cps)}\,. \qquad (4\text{-}11)$$

Dividing (4-5) by (4-6), (4-11) becomes

$$\overline{T} = \hat{f}^{-1} \, (n/m)^{1/n} \, \left[\frac{\Gamma\left(\frac{m-1}{n}\right)}{\Gamma\left(\frac{m-3}{n}\right)}\right]^{\frac{1}{2}} \quad . \tag{4-12}$$

Thus, the average zero-upcrossing period is inversely proportional to the spectral peak frequency, the proportionality being a function of the spectral form.

Fully Developed Spectra

The Neumann (1953) spectrum became the basis for the Pierson, Neumann, and James (1955) forecasting method. The form integers for the spectrum are $m = 6$, $n = 2$. The spectrum is fully developed, the spectral peak frequency ($\hat{f}$) is inversely proportional to the wind speed (U), and the total energy is directly proportional to U^5.

Roll and Fischer (1956) pointed out a logical inconsistency in the derivation of the Neumann spectrum, concluding that the form integers should be $m = 5$, $n = 2$, but otherwise differing only by a multiplicative constant. Phillips (1958) showed by a dimensional argument that the f^{-5} power law ($m = 5$) is to be expected, provided that one assumes gravity to be the only relevant parameter under saturated wave conditions. This agrees with the result of Roll and Fischer.

Pierson and Moskowitz (1964) compared carefully measured, non-dimensionalized spectra with spectral forms for which $n = m + 1$. They found that $m = 5$ gave the best fit to the data, again confirming the f^{-5} equilibrium range law:

$$\underline{S}(\omega) = (8.1 \times 10^{-3})g^2\omega^{-5}\exp(-0.74[g/U]^4\omega^{-4}) \qquad (4\text{-}13)$$

where g = gravity and U = wind measured by weather ships (10 meters); ω is the angular frequency in radians per second (rps) and g, U, and $\underline{S}$ are given in any mutually consistent set of units. It can be seen by comparison of (4-13) and (4-1) that

$$\hat{\omega} = 0.88\ g/U \quad \text{rps} \quad , \qquad (4\text{-}14)$$

and

$$\hat{\underline{S}} = (4.4 \times 10^{-3})U^5/g^3 \quad . \qquad (4\text{-}15)$$

Using the cyclic frequency (f) in cycles per second (cps) the spectrum (4-13) becomes

$$S(f) = \hat{S}\ (f/\hat{f}\ )^{-5}\exp\{-1.25[(f/\hat{f}\ )^{-4} - 1]\} \qquad (4\text{-}16)$$

where

$$\hat{f} = 0.14\ g/U \quad \text{(cps)} \qquad (4\text{-}17)$$

and

$$\hat{S} = (2.8 \times 10^{-2})U^5/g^3 \quad . \qquad (4\text{-}18)$$

The zero-th moment of the Pierson-Moskowitz spectrum is, from (4-5):

$$M_o = \hat{S}\ \hat{f}\ e^{1.25}/5 = (2.7 \times 10^{-3})U^4/g^2 \ , \qquad (4\text{-}19)$$

and the significant height $H_s = H_{1/3}$ becomes, from (4-9):

$$H_s = 0.21\ U^2/g \quad . \qquad (4\text{-}20)$$

Finally, the zero-upcrossing period is, from (4-12) and (4-17):

$$\overline{T} = 0.71/\hat{f} = 5\ U/g \quad . \qquad (4\text{-}21)$$

Note that unlike the parameters $\hat{f}$ and $\hat{S}$, the quantities M_o, H_s, and $\overline{T}$ do not depend on the choice of angular versus cyclic frequency.

A Fetch Limited Spectrum

Liu (1971) developed a fetch limited spectrum of the Pierson-Moskowitz form through a dimensional analysis of existing wave data from many sources. He gave his equations in terms of certain dimensionless parameters which were useful in determining the empirical constants and exponents. These parameters do not lend themselves to a straightforward interpretation of the spectrum, or to comparisons with other spectra. The spectrum originally given in Liu's paper (1971) may be reduced to a more meaningful form by introducing the dimensionless parameter $X = gF/U^2$, where g is gravity, F is the fetch length, and U is the anemometer wind at ten meters (U_{10} in Liu's equations). Making this substitution, Liu's spectrum becomes:

$$S(f) = \hat{S}\,(f/\hat{f}\,)^{-5} \exp\{-1.25[(f/\hat{f}\,)^{-4} - 1]\}\ , \qquad (4\text{-}22)$$

where

$$\hat{f} = 1.3(g/U)X^{-0.222}\ (\text{cps})\ , \qquad (4\text{-}23)$$

$$\hat{S} = (2.0 \times 10^{-5})\ (U^5/g^3)X^{\,0.695}, \qquad (4\text{-}24)$$

$$X = gF/U^2\ , \qquad (4\text{-}25)$$

and g, F, and U are specified in any consistent system of units. Equations (4-23) and (4-24) together with (4-5), (4-9), (4-12) and (4-17) give us:

$$M_o = (1.8 \times 10^{-5})\ (U^4/g^2)X^{0.474} \quad , \qquad (4\text{-}26)$$

$$H_s = 0.017\ (U^2/g)X^{0.237} \quad , \qquad (4\text{-}27)$$

and

$$\overline{T} = 0.55\ (U/g)X^{0.222} \quad . \qquad (4\text{-}28)$$

Figure 10 shows the Liu spectrum for various wind speeds and fetch lengths. The effect of doubling the wind speed is clearly much greater than if the fetch length is doubled. As fetch length is increased the spectral area (M_o) increases and the peak frequency ($\hat{f}$) decreases, but at decreasing rates. Thus an absolute fully developed condition does not exist for this spectrum.

Liu pointed out that as a result of the inconstancy of S_o with changing wind speed and/or fetch length, "there is no envelope for the equilibrium range. The spectra are quite wide at early stages of the development, while they become narrower and the front face steeper as the wind speeds or fetches increase."

No single value of X will reduce all of the Liu relationships exactly to the Pierson-Moskowitz ones, but the differences are small when $X = 2.8 \times 10^4$. This is a reasonable criterion for considering the Liu Spectrum to be "fully developed".

If F is the fetch length in nautical miles and U is the wind speed in knots, the significant wave height (feet) is

$$H_s = 0.24F^{0.237}\ U^{1.526} \qquad (4\text{-}29)$$

and the sea may be considered fully developed for fetch lengths greater than

$$F_{min} = 0.41\ U^2\ (\text{n. mi.}) \quad . \qquad (4\text{-}30)$$

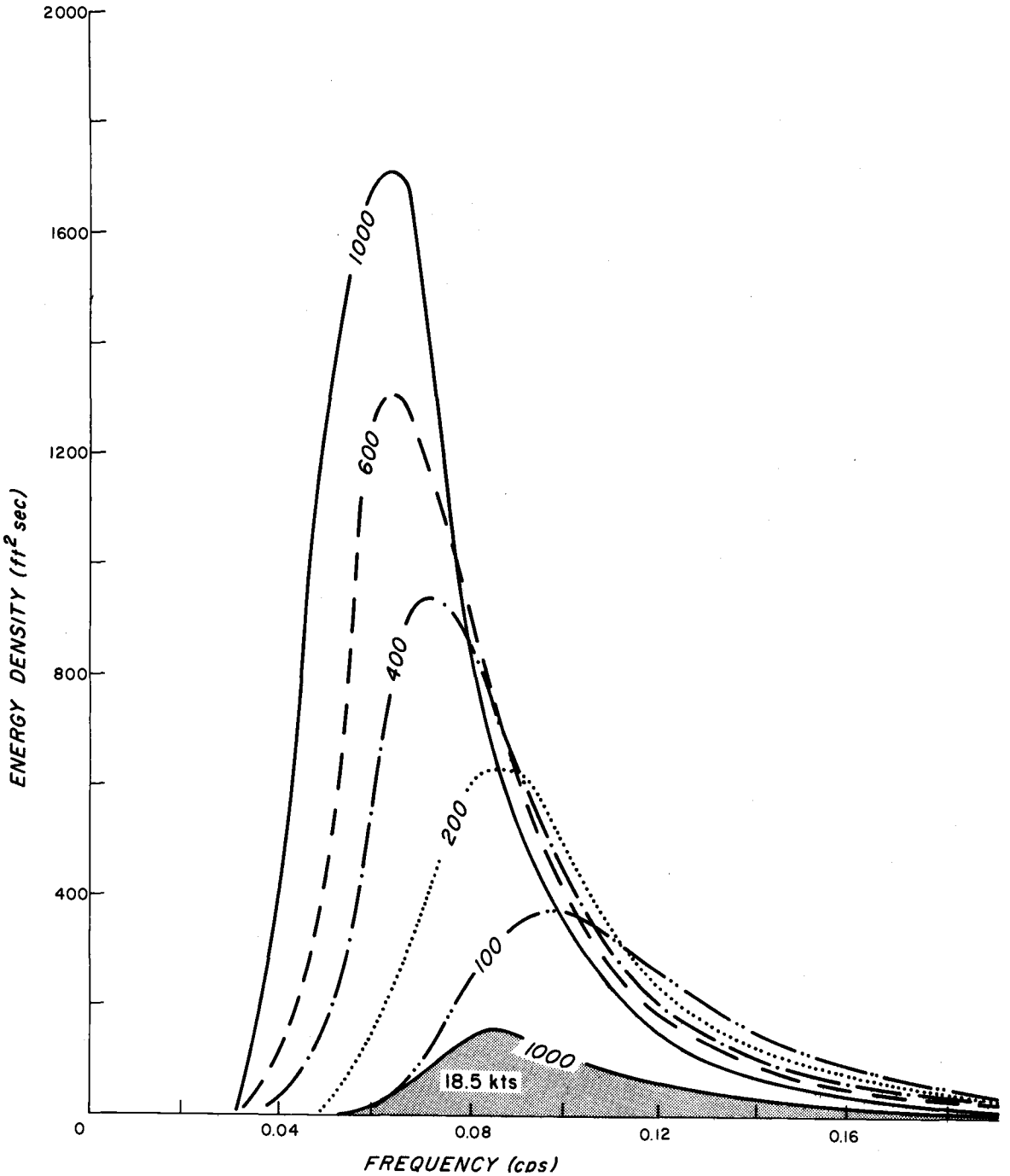

Figure 10. Unshaded: Liu spectra for 37 knot (20 m/sec) wind at various fetch lengths (n.mi.); shaded: Liu spectrum for 18.5 knot (10 m/sec) wind and 1000 n.mi. fetch length.

By differentiating (4-29) with respect to fetch length and eliminating U by means of (4-30), it can be seen that

$$\left[\frac{dH_s}{dF}\right]_{F=F_{min}} = 1.4 \text{ feet/100 n.mi.} \qquad (4\text{-}31)$$

Thus the significant wave height from the Liu spectrum increases for $F > F_{min}$, but the rate of increase is small (and decreasing).

The relationships (4-29) and (4-30) are shown graphically in Figure 11. Wind speed is clearly the most critical generation parameter for medium and long fetches, while the fetch length is critical for short fetches. The single heavy curve representing (4-30) has a dual interpretation: for a given wind speed it shows (a) the minimum fetch necessary for the sea state to be considered "fully aroused", and (b) the significant height derived from the Pierson-Moskowitz spectrum.

The "sea" states predicted by the Liu spectrum and the S-M-B and P-N-J forecasting methods are compared in Table 2. The significant height and average zero upcrossing period were computed from the Liu spectrum by (4-29) and (4-28). The S-M-B values are from the U.S. Army Coastal Engineering Research Center (1966), and P-N-J values are from Hydrographic Office Publication No. 603.

Both the heights and periods of the Liu spectrum agree closely with the S-M-B method, over most of the ranges of wind and fetch. The only significant disagreement occurs for short fetches with high wind speeds, for which the S-M-B heights are as much as 30% lower. The P-N-J heights are closest to the others for 30 knot winds, and are

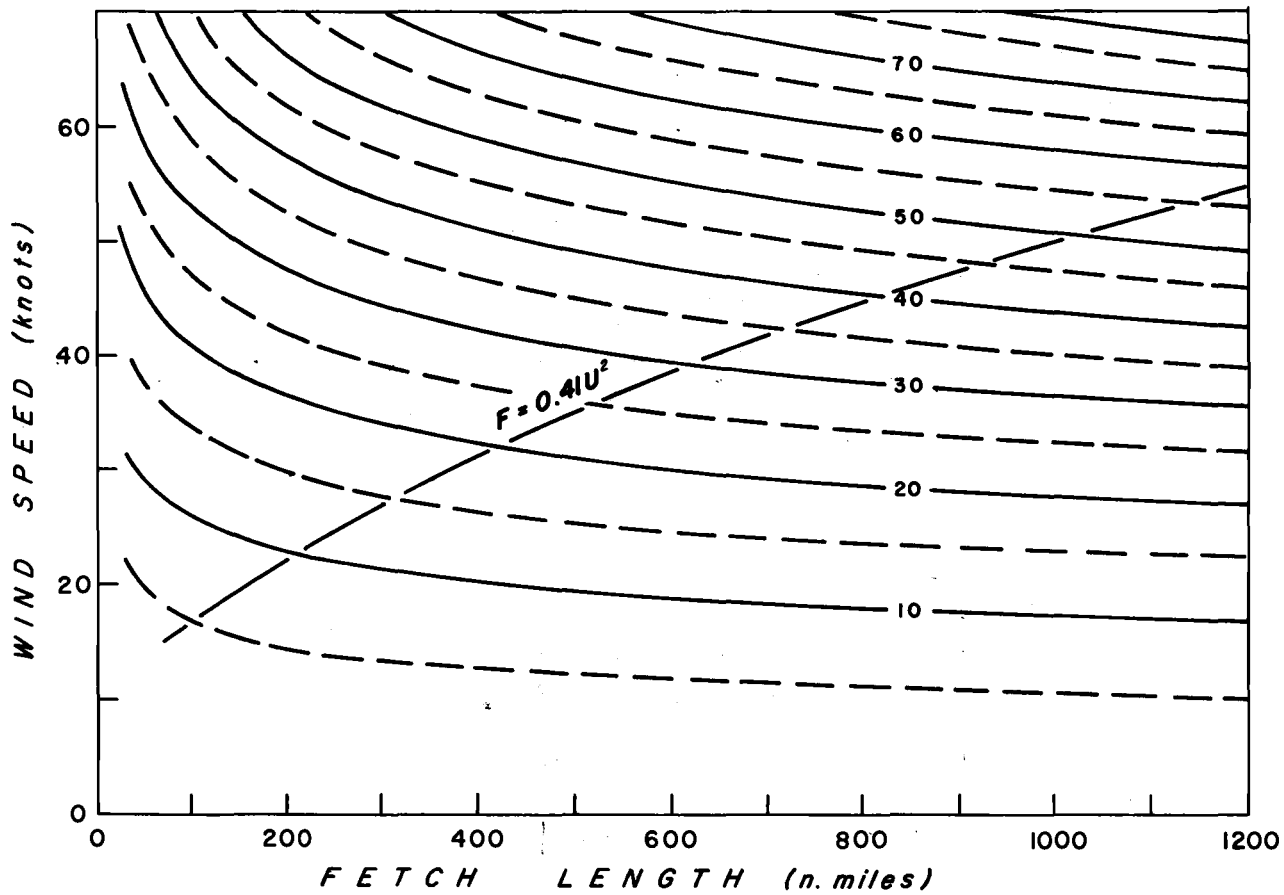

Figure 11. Multiple curves (labelled in feet): significant wave height from Liu spectrum as a function of wind speed and fetch length. Single curve ($F = 0.41\ U^2$): wind speeds and fetch lengths for which Liu spectrum approximates the fully-developed Pierson-Moskowitz spectrum.

TABLE 2. Heights and Periods Obtained from the Liu Spectrum and the Sverdrup-Munk-Bretschneider and Pierson-Neumann-James forecast methods.

Wind (kts) Speed	Fetch(n.m) Length	Sig. Height (ft)			Period (sec)		
		SMB	LIU	PNJ	SMB	LIU	PNJ
20	100	7	7	8	7	7	6
20	300	9	9	8	9	9	6
20	600	10	11	8	11	10	6
20	900	10	12	8	11	11	6
30	100	11	12	11	8	8	6
30	300	16	17	21	11	11	9
30	600	19	20	21	13	13	9
30	900	21	21	21	14	14	9
40	100	17	19	13	10	10	6
40	300	25	26	25	13	13	8
40	600	30	30	39	15	15	10
40	900	33	34	44	18	17	11
50	100	22	27	20	11	11	7
50	300	33	36	35	15	14	9
50	600	41	43	45	17	16	10
50	900	47	48	56	19	18	11
60	100	27	36	*	12	12	*
60	300	41	48	*	16	15	*
60	600	53	57	*	19	18	*
60	900	60	62	*	21	20	*

* Forecasting curves unavailable.

considerably higher for long fetches having high winds, a fact that was acknowledged by the authors (Pierson, Neumann, and James, 1955). The P-N-J periods are much lower than for either of the other two sources, the largest being 11 seconds.

In conclusion, the Liu spectrum seems to be ideally suited for computerized forecast schemes. It is of the widely accepted Pierson-Moskowitz form and closely approximates the Pierson-Moskowitz spectrum when the fetch length (n.mi.) is equal to 0.41 times the wind speed (knots) squared, an acceptable criterion for calling the Liu spectrum "fully developed". The heights and periods obtained by integrating the Liu spectrum agree closely with the sea state values predicted by the S-M-B method. It has the added advantage over its counterparts that it has an explicit functional dependence on fetch length, and can be readily programmed for use on a computer. The following sections will discuss the way in which the Liu spectrum was adapted to the semi-automated forecast method.

Principle of the Semi-automated Forecast Method

The semi-automated forecast method works on the same basic principles as the manual method of Pierson, Neumann and James (1955). That is, (1) the wave spectrum within a fetch is "generated" by an empirical-theoretical spectral formula; (2) the energy in each frequency band is "propagated" at its group velocity to the forecast point and is reduced by an amount equal to the angular spreading loss; and (3) the forecast

spectrum at some time t_f is reconstructed from all components arriving at the forecast point at t_f.

The following features of the semi-automated approach distinguish it from the P-N-J method:

The spectrum within the fetch is computed from the fetch-dependent Liu spectrum (rather than the fully developed Neumann spectrum).

The variation of wind speed, fetch length and fetch location with time is accounted for without resorting to "filters" (which usually oversimplify the fetch history).

Changes in angular spreading as a function of time and/or distance are accounted for.

All calculations are performed by computer after the forecaster inputs wind speeds, fetch lengths, durations, decay distance and angular spreading factors.

Definitions and Basic Concepts

Certain terms and concepts will be used in the following discussions which are not standard in the existing literature on wave forecasting. These are explained below. While reading, Figure 12 may be consulted for orientation.

Time-distance diagram

Time-distance diagrams were introduced by Wilson (1955) as graphic aids in the treatment of complex fetch behavior. As used

here, the distance increases to the left of the origin along the abcissa, and time increases downward. Time may be labelled in any convenient way, e.g. in six-hourly Greenwich Mean Time (GMT) increments, with dates, or in hours relative to some reference such as the distance axis.

Fetch history

On a time-distance diagram, a fetch history is a polygon (or series of polygons in tandem) which represents the distance of the fetch (front and rear) from the forecast point as a function of time. The horizontal sides of the polygon are the start and finish of the fetch and the vertical distance between them is the duration time, t_d . The sloping (or vertical) sides give the distances of the front and rear of the fetch from the forecast point as functions of time. Within the polygon the wind speed is taken to be the average for all charts on which the fetch appeared.

Propagation line

Each frequency component of the generated wave spectrum is associated with a propagation line--a straight line on the time-distance diagram which intersects the time axis at the time of arrival of the component at the forecast point. The line extends upward and to the left of the intersection and its slope is the

reciprocal of the component group velocity $C_g = 1.515 f_i^{-1}$ (C_g in knots, f_i = frequency of the i-th component in cycles per second).

Generation distance

Every spectral component whose propagation line (for a particular arrival time) crosses a fetch history polygon is associated with a generation distance. The generation distance (D_i) of the i-th component is the distance traveled by that component under the influence of the wind. It is the distance interval associated with that portion of the propagation line which lies in the fetch history polygon.

Figure 12 is a schematic of a time-distance diagram and its various graphic elements: a fetch history, two propagation lines (f_1 = 0.10 cps and f_2 = 0.20 cps), and their indicated generation distances. Distance is given in 100 nautical mile increments, and time in six-hour increments. The time origin is arbitrarily set at the top of the diagram.

The fetch history begins at t = 06 hours and ends at t = 36 hours for a total duration of t_d = 30 hours. The initial fetch length is 400 n.mi. and the final fetch length is 500 n.mi. The initial and final distances of the fetch front from the forecast point (decay distance) are 500 and 200 nautical miles, respectively, that is, the fetch moved eastward toward the coast.

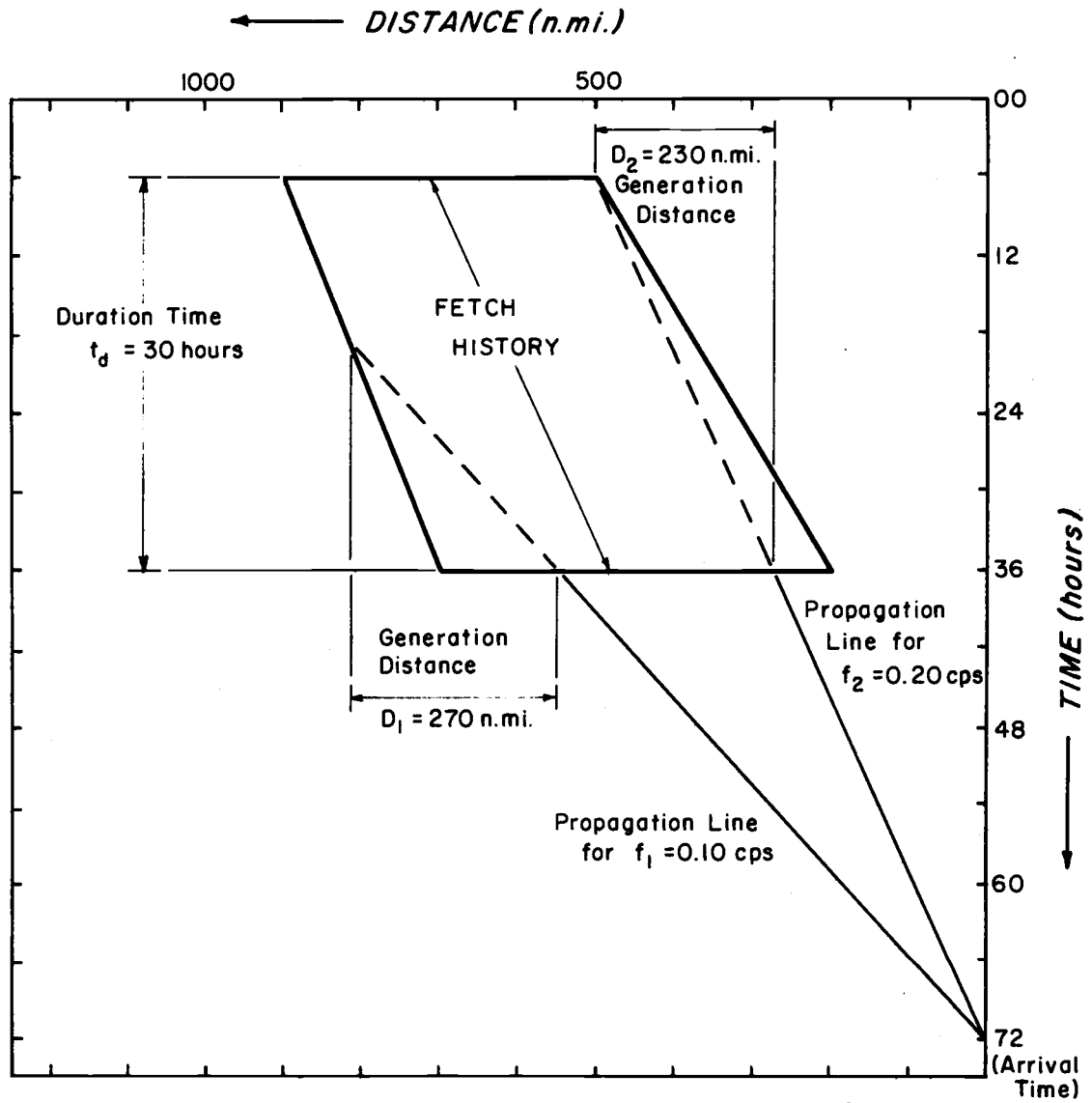

Figure 12. Example of a time-distance diagram with a fetch history and its component parts.

The propagation lines are shown for component waves of 10 second (f_1 = 0.10 cps) and 5 second (f_2 = 0.20 cps) period, arriving at the forecast point at time t = 72 hours. In order to arrive simultaneously these components must originate from different portions of the fetch. Although the five second waves were subjected to the wind for the full fetch duration (30 hours), their generation distance is smaller than for the ten second component (influenced by the wind for only 18 hours). This is because the ten-second component wave energy travels twice as far during a given time interval, due to its greater group velocity.

Angular spreading factor

Because wave energy propagates away from its generation area in many different directions, not all of the original energy will arrive at a distant point--some of it will be lost by angular spreading. The wider a fetch is, the more overlapping of energy will occur from different segments of the fetch. According to Pierson, Neumann and James (1955):

> "A storm 400 n.mi. wide which sends waves out to a point 1,000 miles away from the storm produces a completely different effect from a storm 800 n.mi. wide which sends out some waves to a point 1,000 miles away from the storm. If the waves inside the storm have the same spectrum and if all other things are equal, the waves outside the storm at the point of observation will be $\sqrt{2}$ times higher in the second case than they were in the first case, simply because of the effect of the width of the storm."

This process is accounted for by means of an angular spreading factor (A) - a number between zero and one which, when multiplied by the wave energy within the fetch just after generation is complete, yields the fraction of the original energy arriving at the forecast point. Pierson et al. give a detailed description of how the factor A may be found from weather maps using a protractor. The factor increases with increasing fetch width and decreasing decay distance.

In using the semi-automated method, the forecaster determines A twice for each fetch history: once at the rear of the fetch on the initial map (A_I) and again at the front of the fetch on the final map (A_F). These are transferred as numbers to the time-distance diagram, so that fetch width is effectively accounted for even though it is not an explicit dimension of the diagram. For west coast forecast points A_F is always larger than A_I because the storms move toward the coast. The front of the fetch on the final map is always closer to the coast than the fetch rear on the initial map. When generation is complete, the component energies begin to decay at varying distances from the forecast point. Therefore each component f_i is associated with a unique spreading factor A_i which is linearly interpolated from A_I and A_F. Accordingly, the component f_2 in Figure 12 has a larger spreading factor (A_2) than does the component $f_1(A_1)$.

Computation of Forecast Spectrum,
Significant Height and Average Period

The energy associated with each component just after generation and before decay begins is $S(f_i,D_i)\Delta f$. The function $S(f = f_i$, $F = D_i)$ is the Liu spectral energy function from equations (4-22) through (4-25), evaluated at the frequency f_i and the "fetch length" D_i (D_i is the effective fetch length for the i-th component). The wind speed (U) in these equations is just the wind speed in the fetch averaged over all charts on which the fetch appears. The bandwidth, Δf , is the frequency interval separating discrete frequency components.

The component energy after arrival at the forecast point is found by multiplying the original energy by A_i :

$$E_i = A_i S(f_i,D_i)\Delta f \qquad (4\text{-}32)$$

The zero-th moment of the spectrum is the sum of the E_i arriving simultaneously at the forecast point (the total energy):

$$M_o = \sum_{i=i\,min}^{i\,max} E_i = \sum_{i=i\,min}^{i\,max} A_i S(f_i,D_i)\Delta f \qquad (4\text{-}33)$$

and the second moment is

$$M_2 = \sum_{i=i\,min}^{i\,max} f_i^2\, A_i S(f_i,D_i)\Delta f \quad . \qquad (4\text{-}34)$$

The indices i min and i max refer to the smallest and largest frequencies whose propagation lines pass through the fetch history. Finally, the theoretically expected significant wave height and average zero upcrossing period are

$$H_s = 4\sqrt{M_o} \qquad (4\text{-}35)$$

and

$$\overline{T} = \sqrt{M_o/M_2} \quad . \qquad (4\text{-}36)$$

Figure 13 shows the fetch history for a stationary fetch of duration $t_d = 30$ hours and fetch length $F = 400$ nautical miles, the front of which remains at 300 n.mi. from the coast. The average wind speed for the fetch during the 30 hour period is 30 knots. The initial spreading factor (at the fetch rear) is $A_I = 0.5$ and the final spreading factor (at the front) is $A_F = 0.7$. Discrete frequency components of from 0.06 cps to 0.22 cps (bandwidth = 0.02 cps) pass through the fetch history and arrive at the forecast point at time $t = 60$ hours.

The generation distances, spreading factors, spectral densities and energies after spreading are listed in Table 3. Finally, by computing the sums (4-33) and (4-34), the significant height is $H_s = 11.0$ feet and the average zero upcrossing period is $T_z = 8.5$ seconds (equations [4-35] and [4-36]).

All of the data in Table 3 and the summations are calculated by a computer. The forecaster must input, via teletype, the following:

(i) the average wind speed (knots) in the fetch for all charts on which the fetch appeared;

(ii) the duration of the fetch history (hours);

(iii) the initial and final decay distances (n.mi.) or distances from the front of the fetch to the forecast point;

(iv) initial and final fetch lengths (n.mi.);

(v) initial (fetch rear) and final (fetch front) angular spreading factors.

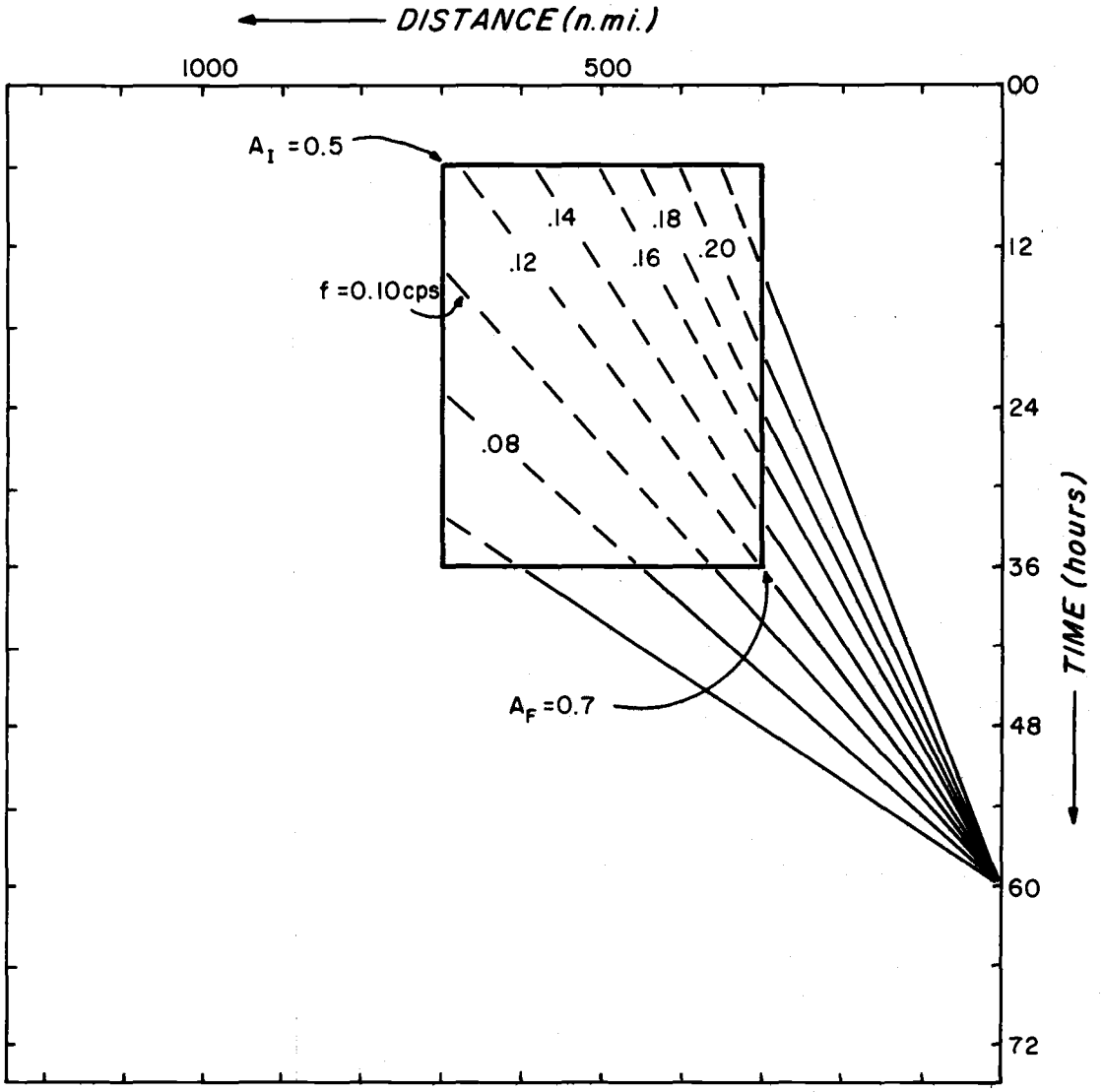

Figure 13. Propagation lines for spectral frequency components arriving 24 hours after the end of a stationary-fetch history. Initial and final angular spreading factors are also indicated. The figure corresponds to the data shown in Table 3.

TABLE 3. Data for Frequency Components, Figure 13.

units	parameter	FREQUENCY 0.06	0.08	0.10	0.12	0.14	0.16	0.18	0.20	0.22
n.mi.	Generation distance (D_i)	94	246	336	379	284	211	155	109	51
----	Spreading factor (A_i)	0.547	0.623	0.668	0.698	0.700	0.700	0.700	0.700	0.700
ft^2-sec	Spectral density $S(f_i,D_i)$	10.3	147.3	194.0	109.2	62.3	38.0	24.7	17.1	14.0
ft^2	Component energy $E_i=A_iS(f_i,D_i)\Delta f$	0.13	1.83	2.59	1.53	0.87	0.53	0.35	0.24	0.20

The foregoing descriptions illustrate the principle of the semi-automated method, but not how it is applied in practice. Procedures will be described in the following section with detailed examples.

Application of the Semi-automated Method

A given storm development may be quite complex, in terms of its associated fetch behavior. The speed of the fetch and the wind speed within it may change considerably with time. A second fetch may appear in another sector of the storm as it nears the coast. Occasionally more than one storm may contribute to the wave arrivals.

The forecaster can best judge these situations after first plotting from each chart: (1) the distance of the fetch front(s) (decay distance), (2) the distance of the fetch rear(s), and (3) the average wind speed(s). These are all plotted as a function of time on the time-distance diagram. If sustained changes in either wind speed or fetch speed are evident, he may need to draw in two or more fetch history polygons to fit the plotted data. Such polygons in tandem constitute a "complex" fetch history. When this delineation has been done, the forecaster returns to his charts and determines the initial and final angular spreading factors for each polygon.

A Simplified Example

Application of the semi-automated forecast method will be illustrated for a simplified example: an uncomplicated fetch history represented by a single space-time parallelogram (Figure 14). The

forecast procedure begins with an analysis of the fetch history from meteorological charts showing the surface pressure distribution (isobars) and plotted ship reports of wind speed and direction.

On each chart, the fetch (area of uniform wind speed and direction affecting the chosen forecast point) is approximated by a rectangular area according to techniques set forth in standard manual forecast methods (see, for example, the discussion by Shields and Burdwell, 1970). A template showing great circles radiating away from the forecast point and distances in nautical miles may be laid over the chart. The distances of the fetch front and fetch rear (from the forecast point) are recorded as points on the time-distance diagram, as shown in Figure 14. A straight line is drawn through the points for the fetch fronts. This line shows the average movement of the fetch front in time. Similarly, a second line is drawn for the fetch rears.

The start of the fetch history may be taken as half of a chart interval before the first chart on which the fetch appears. In the case shown in Figure 14 the fetch appeared first on the 1200 GMT chart. Accordingly, the fetch history begins at 0900 Z on the first day (six-hourly charts were used). Similarly, the fetch history ends at 1500 GMT on the second day, giving a fetch duration of 30 hours.

The average wind speed in the fetch is determined from each synoptic chart, using ship reports and/or winds derived from the pressure gradient. This average is written inside the fetch history polygon at the appropriate chart time (32 knots, 30 knots, etc. in Figure 14).

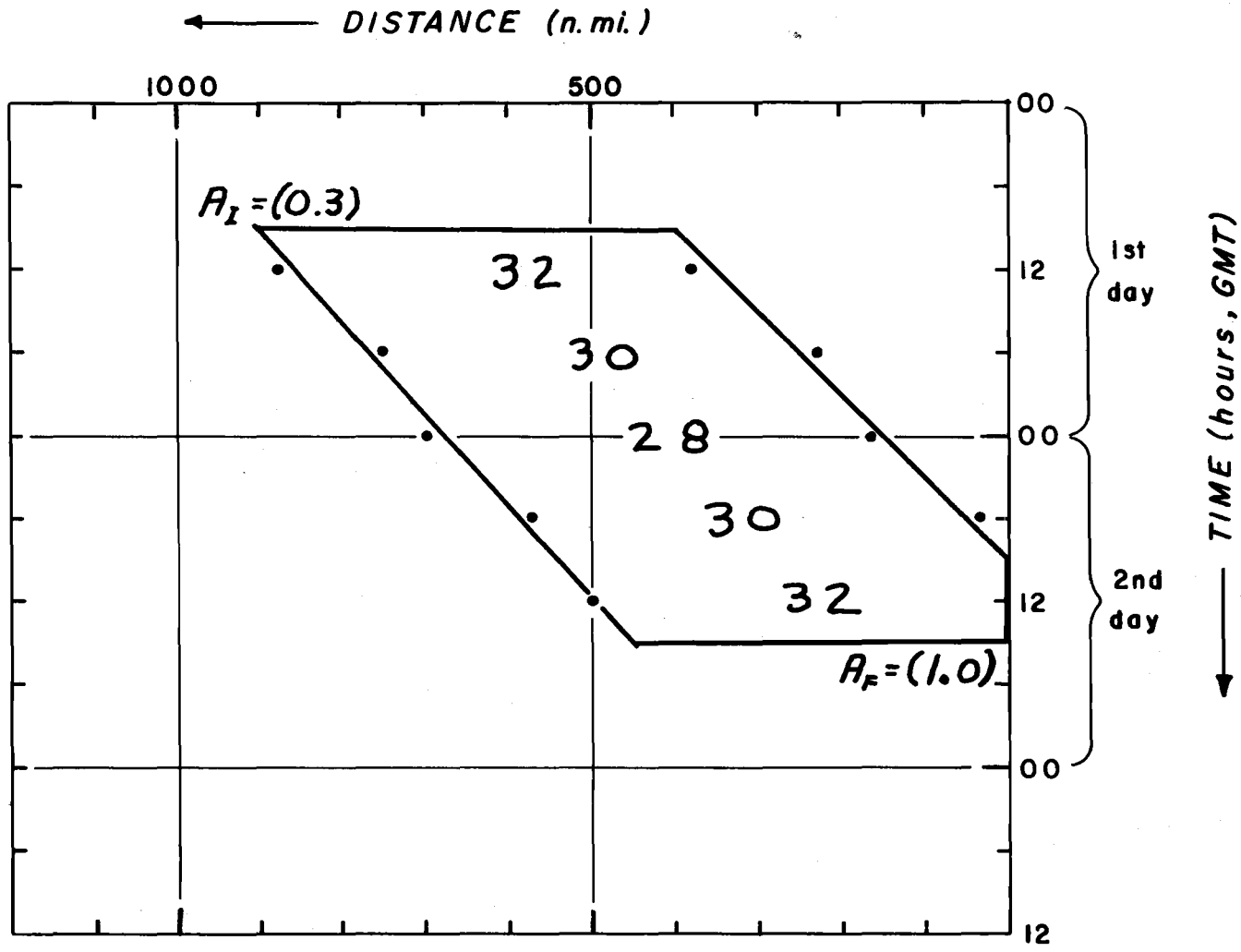

Figure 14. Time-distance diagram and plotted data for a simple fetch history. Numbers inside the polygon are the average wind speeds on individual synoptic charts; numbers in parentheses are initial and final angular spreading factors; points are plotted at distances of fetch front and rear from the forecast point.

These values are then averaged in time to give a grand mean wind speed for the fetch history (about 30 knots in the example).

After the forecaster has carried the analysis this far, he has presumably decided on definite times for the start and end of the fetch history. He then returns to the first and last charts and measures the angular spreading factor at the rear (first chart) and front (final chart) of the fetch. These values are entered on the time-distance diagram (A_I = 0.3, A_F = 1.0 in Figure 14).

Once the graphical procedure has been carried out, the wind speed, duration and initial and final values of decay distance, fetch length, and spreading factor are transferred to a table (Table 4). These data are then input to a computer in a conversational mode via teletype (Figure 15). Notice that if the fetch reaches the forecast point, as in Figure 14, the forecast program asks when the fetch arrived. This permits the truncation of the fetch history polygon at the forecast point to be correctly determined. Finally, a table of forecast significant heights and average periods is output for the 24 hours following the end of the fetch history. (Figure 15).

TABLE 4. Fetch History Data Table

Average wind speed (knots)	Duration time (hours)	Initial decay distance (n.mi.)	Final decay distance (n. mi.)	Initial fetch length (n.mi.)	Final fetch length (n.mi.)	Angular spreading factors (in/fin)
30	30	400	0	500	450	0.3/1.0

```
RUN


WHEN IS OUR FIRST FORECAST FOR?
MONTH:
OCT
DAY=2
HOUR(GMT) = 15
TIME FETCH # 1 STARTED:
MONTH:
OCT
DAY=1
HOUR(GMT) = 9
 WIND SPEED =    30
 DURATION (HOURS) = 30
 INITIAL DECAY DISTANCE =    400
 FINAL DECAY DISTANCE = 0
 INITIAL FETCH LENGTH = 500
 FINAL FETCH LENGTH =    450
 INITIAL SPREADING FACTOR = .3
 FINAL SPREADING FACTOR =    1.
DOES FETCH REACH COAST BEFORE 15Z OCT  2
(YES/NO)YES
WHEN ?
MONTH:
OCT
DAY=2
HOUR(GMT) = 9
INPUT ANOTHER FETCH(YES/NO)  ?  NO


MONTH   DAY   HOUR(PST)   SIG.HGT.   PERIOD(S)
 OCT      2        7         18.1        9.9
 OCT      2       13         16.9        9.8
 OCT      2       19         15.2        9.4
 OCT      3        1         13.1        8.8
 OCT      3        7         11.0        8.2
WANT TO DO ANOTHER FORECAST ?   NO



END OF FORTRAN EXECUTION
```

Figure 15. Teletype fetch input conversation and output heights and periods for a simple semi-automated forecast (see Figure 14 and Table 4). User responses are underlined.

The FORTRAN prediction program used for the forecast in Figure 15 is documented in APPENDIX A.

This example is intended only to illustrate the mechanical procedure, without consideration for complications which occur in practice.

Multiple Fetch Histories

Under realistic circumstances a wave forecast would need to take into account more than one fetch history polygon. It is rare for a storm to maintain the same intensity (wind speeds) throughout its development. The wind often changes by more than five knots as the cyclone gradually matures and decays, and it is common for the speed of movement to change as well--usually decreasing as the storm "deepens". The waves being proportional to the square of the wind speed, they are critically affected by sustained wind changes of five knots or more. Changes in the fetch speed can also affect the wave height, but can be especially critical to the timing of wave arrivals. (A correct height forecast that is 18 hours too early or too late is of little value.)

Other complications involve spacial rather than temporal distribution of the wind. During most of the approach of a storm, the cold (post-frontal) sector will be the only area sending waves in the direction of the forecast point. About twelve hours before the cold front reaches the coast, however, the pre-frontal, warm sector winds from the south usually begin to contribute to the arriving waves.

Along the Oregon coast these short-lived winds can often reach devastating velocities, creating extremely severe sea conditions with the addition of the "cross-swell" coming from the cold sector to the west. It is of no use to wait for analyzed charts to become available--the waves will already have done their damage before the forecast is out. Cases such as these rely heavily on the experience of the forecaster and his ability to predict the pre-frontal conditions with the aid of prognostic charts.

Spacial complications often occur. It often happens that the winds in the rear of the cold sector are considerably higher than those toward the front: 45 knots as opposed to 35 knots, for example. These situations should be analyzed as two adjacent fetches (one following the other) rather than one, even though the wind direction may be the same for both.

Another important consideration is the inclusion of more than one storm when they occur sufficiently close to each other in space-time. This is a consequence of the dispersive behavior of waves. While the late, short-period waves are arriving from one storm, early long-period waves may be arriving from its successor, simultaneously. This is especially important to mariners if the wave arrivals are from different directions.

The manner in which the effects of several fetch history polygons are combined is important. Two general situations can be recognized, each requiring special treatment as follows:

A. Separate storms may be arranged in space-time in such a way that waves arrive at the forecast point simultaneously from both sources. Also fetches in two different sectors of a local storm may be directed at large angles to each other (e.g. 90°) causing cross swell to superimpose at the forecast point. As a first approximation, it can be assumed that the wave energies from two or more such sources add linearly. The computational procedure here is simply to add the energy in a given frequency band from one fetch to that in the corresponding band of the other. Doing this to all frequency bands yields the combined forecast spectrum.

B. If adjacent fetch histories have wind directions within, say, 30° of each other, waves entering one from the other should continue to develop under the new wind. At the point of entry, the generation distance necessary to achieve the existing energy in the frequency band, but at the new wind speed, is computed and added to the geometrically determined generation distance within the new fetch. The energy computation made from the new wind speed and the revised generation distance replaces the energy value from the previous fetch. This energy continuity principle is the same one suggested in the S-M-B and P-N-J methods for the case in which the wind speed within a fetch changes in time.

Figure 16 shows a succession of fetch histories occurring over a six-day period. For the purpose of discussion the fetch histories are lettered from A to G.

Figure 16 can be imagined as a worksheet from a forecast office charged with producing wave forecasts for the Oregon-Washington coast. At 1300 PST (2100 GMT) on March 13 a forecast was to be made for the next day based on the diagnostic and prognostic charts available at the time. Fetch histories A through D were prepared on previous days from analyses (diagnostic charts). Fetch history E was prepared on March 12 and 13 from analyses. Prognositic charts and the forecaster's experience indicated that the storm associated with fetch history E could be expected to intensify somewhat and slow its advance considerably. The forecaster drew in the anticipated continuation of E in dashed lines (fetch history F). The prognoses also indicated that southerly winds of about 30 knots from the storm's foresector would begin to affect the coast at an angle of almost 90° to the westerly fetch E. The forecaster therefore dashed in fetch history G as well.

To find out which fetch histories should be included in the forecast for March 14, a plastic overlay with propagation lines for component frequencies is placed over the worksheet (use the overlay provided in the pocket of the back cover). The overlay is arranged with its time axis along the corresponding axis (right side) of the worksheet (Figure 16). The overlay is shifted vertically until the propagation lines converge at the time of the first six-hourly wave forecast, say, 1500 GMT (0800 PST) on March 14. High frequency wave energy from fetches A and C is attenuated strongly. These fetches may therefore be ignored. All of the fetch histories D, E, F and G will be needed for the forecast. The fetch history parameters for these fetches are transferred

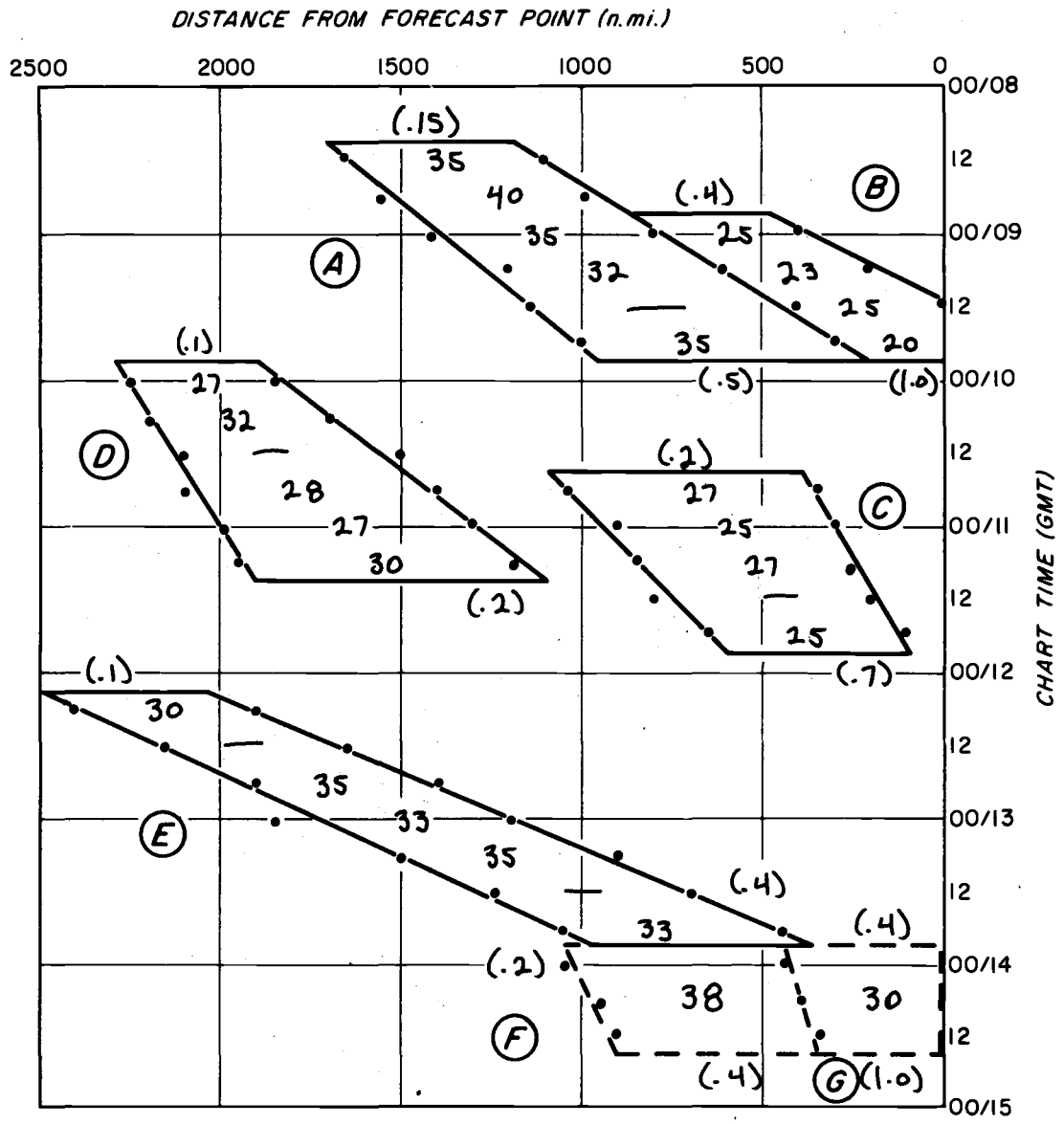

Figure 16. Time-distance diagram and plotted data for multiple fetch histories. Numbers inside polygons are average wind speeds for individual synoptic charts; numbers in parentheses are initial and final angular spreading factors; points are plotted at distances of fetch front and rear from the forecast point.

TABLE 5. Fetch History Data Table for Multiple Fetch Forecast.

Fetch	Average wind speed (knots)	Duration time (hours)	Initial decay distance (n. mi.)	Final decay distance (n. mi.)	Initial fetch length (n.mi.)	Final fetch length (n.mi.)	Initial spreading factor	Final spreading factor
D	29	24	1900	1100	400	800	0.1	0.2
E	33	42	2050	350	450	600	0.1	0.4
F	38	18	450	350	600	550	0.2	0.4
G	30	18	0	0	450	350	0.4	1

```
 LOAD,56,L=*KEITHLB
RUN
RUN



WHEN IS OUR FIRST FORECAST FOR?
MONTH:
MAR
DAY=14
HOUR(GMT) = 15
TIME FETCH # 1 STARTED:
MONTH:
MAR
DAY=9
HOUR(GMT) = 21
 WIND SPEED =   29
 DURATION (HOURS) = 36
 INITIAL DECAY DISTANCE =   1900
 FINAL DECAY DISTANCE = 1100
 INITIAL FETCH LENGTH = 400
 FINAL FETCH LENGTH =   800
 INITIAL SPREADING FACTOR = .1
 FINAL SPREADING FACTOR =   .2
INPUT ANOTHER FETCH(YES/NO)  ?  YES
CONTINUATION OF PREVIOUS FETCH (1) OR NEW FETCH (2) ? : 2

TIME FETCH # 2 STARTED:
MONTH:
MAR
DAY=12
HOUR(GMT) = 3
 WIND SPEED =   33
 DURATION (HOURS) = 42
 INITIAL DECAY DISTANCE =   2050
 FINAL DECAY DISTANCE = 350
 INITIAL FETCH LENGTH = 450
 FINAL FETCH LENGTH =   600
 INITIAL SPREADING FACTOR = .1
 FINAL SPREADING FACTOR =   .4
INPUT ANOTHER FETCH(YES/NO)  ?  YES
CONTINUATION OF PREVIOUS FETCH (1) OR NEW FETCH (2) ? : 1

TIME FETCH # 3 STARTED:
MONTH:
MAR
DAY=13
HOUR(GMT) = 21
 WIND SPEED =   38
 DURATION (HOURS) = 18
 INITIAL DECAY DISTANCE =   450
 FINAL DECAY DISTANCE = 350
 INITIAL FETCH LENGTH = 600
 FINAL FETCH LENGTH =   550
 INITIAL SPREADING FACTOR = .2
 FINAL SPREADING FACTOR =   .4
INPUT ANOTHER FETCH(YES/NO)  ?  YES
CONTINUATION OF PREVIOUS FETCH (1) OR NEW FETCH (2) ? : 2

TIME FETCH # 4 STARTED:
MONTH:
MAR
DAY=13
HOUR(GMT) = 21
 WIND SPEED =   30
 DURATION (HOURS) = 18
 INITIAL DECAY DISTANCE =   0
 FINAL DECAY DISTANCE = 0
 INITIAL FETCH LENGTH = 450
 FINAL FETCH LENGTH =   350
 INITIAL SPREADING FACTOR = .4
 FINAL SPREADING FACTOR =   1.
INPUT ANOTHER FETCH(YES/NO)  ?  NO


MONTH   DAY   HOUR(PST)   SIG.HGT.   PERIOD(S)
 MAR     14       7         16.4        9.5
 MAR     14      13         17.9       10.4
 MAR     14      19         19.1       10.9
 MAR     15       1         18.4       10.5
 MAR     15       7         16.7        9.8
WANT TO DO ANOTHER FORECAST ?   NO



END OF FORTRAN EXECUTION
```

Figure 17. Teletype fetch input conversation and output heights and periods for a multiple-fetch semi-automated forecast (see Figure 16 and Table 5). User responses are underlined.

to a table (Table 5) and are then input to the forecast program via teletype (Figure 17) and forecast heights and periods are printed out.

Summary and Discussion

The semi-automated method is a computerized coastal wave forecast system. It is based on the same principles as the manual method of Pierson, Neumann and James (1955)--the energy in each frequency band of the wave spectrum is generated, propagated at group velocity with angular spreading, and recombined with other frequency bands at the forecast point to give the predicted spectrum.

There are three principal advantages to the semi-automated method over its manual counterpart: (1) it uses a fetch-dependent spectrum of the Pierson-Moskowitz form (Liu, 1971), (2) it can treat arbitrarily complex fetch behavior through the mechanism of a time-distance diagram, and (3) virtually all computations are computerized.

For the semi-automated method the most time consuming operation is the analysis of fetches from meteorological charts. The fetch analysis would, however, carry over from one day to another, so that relatively little time would be spent at this task on any individual day. The computations performed by the computer represent a very significant savings in time over the P-N-J method. The P-N-J forecaster would not normally include all four fetches (D, E, F, G) in his forecast, or would simplify them in some way. He might treat them with the more easily applied P-N-J "filters" which are only appropriate to specific types of fetches (e.g. stationary, or moving at the speed of the wind).

Because the user of the semi-automated method is freed from the constraints of "filters" and tedious computations, he can devote his time profitably to careful analysis of fetch histories with the aid of the time-distance diagram. His most critical task is to correctly prognosticate future behavior of local fetches.

Since the wave height varies as the square of the wind speed, all available ship data should be utilized. One can draw fetch history boundaries through the plotted distances on the time-distance diagram in spite of considerable scatter (e.g. ±100 n.mi.). Where sustained changes in wind speed and/or fetch speed occur, the fetch history should be subdivided into two or more polygons.

Where very short fetches (less than 200 n.mi.) are involved, fetch lengths should be considered with great care. This is because of the sensitivity of the spectrum to fetch length for short fetches (Figure 11).

V. EVALUATION OF THE SEMI-AUTOMATED METHOD

Introduction

The semi-automated method has been evaluated to a limited extent and will undergo further study at Oregon State University. The evaluation here is based on comparisons between average heights and periods generated by the method and those inferred from microseisms at Newport (Chapter III).

For this evaluation generated heights and periods were obtained by hindcasting rather than forecasting. The forecaster only has analyzed charts available up until a few hours prior to the time of forecast issuance, and for further guidance must rely on prognostic weather charts. In contrast, a hindcast simulates past wave conditions by applying the forecasting technique to a series of analyses covering the entire period of consideration. Hindcasting is preferable for evaluating the accuracy of the forecast method because the effects of incomplete input data on analyses are minimized and the errors of prognostic charts are eliminated.

The microseism data was used for verification because it was available at six-hour intervals over a long winter period, and for a location relatively close to the Columbia River. Newport is about 130 nautical miles south of the Columbia River mouth so both areas are usually affected by the same storm and fetch developments.

The principal disadvantages of the microseism data are that (1) the seismometer was calibrated against visual observations of waves in 50 feet of water (hindcasts are for deep water) and (2) wave spectra from the microseism recordings are not available for comparison with hindcast spectra. Due to shoaling and refraction, wave heights at the observation point are somewhat less than in deep water. It would be desirable to verify the semi-automated method with measured deep-water spectra.

The semi-automated forecast method is evaluated in three ways:

(i) Six-hourly hindcast spectra were generated for a 20 day period. Their time variation was examined to see if it was consistent with the known behavior of wave spectra.

(ii) Six-hourly deep water significant heights and average periods off Newport were hindcast for a period of over four months during the winter of 1971-1972. These are compared to the significant heights and average periods as they were inferred from microseism recordings at Newport (Chapter III).

(iii) Twenty-four hour forecasts of height and period were simulated for the same place and times mentioned in (ii). This was done by limiting fetch information to that obtained from analyses available up to 24 hours before the forecast wave arrivals. The verification of the simulated forecasts and actual (manual) forecasts at Newport were compared. (This is a rather severe test of the system since ordinarily the additional guidance from prognostic weather charts would be available for the period between the last available analysis and the forecast wave arrivals.)

The Hindcast Procedure

Hindcasts were produced by the procedure outlined in Chapter IV. Six-hourly final Northern Hemisphere Surface Pressure Analyses (National Meteorological Center) were searched for fetches. Fetches up to 2500 n.mi. from Newport were considered if it was felt they would significantly contribute to the hindcast wave arrivals. The decision to include or exclude a given fetch depended on its distance, length, duration, wind speed and how accurately it was aimed at Newport. Local fetches were usually included if wind speeds of 20 knots or more were found. Distant fetches (up to 2500 n.mi.) were usually only considered for wind speeds in excess of 25 knots.

On each chart, the distances of the front and rear of each fetch from Newport were found and plotted on the time-distance diagram. The average wind speed in the fetch was found from the plotted ship reports, sometimes with the help of winds inferred from the pressure gradients. The wind speed was then plotted between the front and rear of the fetch on the time-distance diagram (at the corresponding chart time). Each fetch history was represented by one or more polygons on the time-distance diagram. Each polygon enclosed a space-time interval during which wind speeds were relatively constant (± 3 knots). Straight lines could be drawn through the plotted fetch fronts and rears with acceptable scatter (± 100 n.mi.). Polygons were terminated and new ones begun when (1) sustained departures (in time) of wind speed from previous average occurred, and/or (2) sustained departures of fetch fronts or rears from a straight line occurred.

After delineation of a polygon, the angular spreading factor at the fetch rear on the first chart was determined. Likewise, the spreading factor at the fetch front on the last chart was found. These were then plotted near the appropriate points on the polygon.

The result of this fetch history analysis generally looked very much like Figure 16. In the following section the fetch histories will be shown as they appeared over a twenty-day period.

Spectra From a Twenty-day Hindcast

Fetch histories were analyzed and hindcast spectra were generated for the twenty-day period from 7 December through 26 December, 1971. These are shown in Figure 18.

Figure 18 is divided into two parts. On the left, fetch history polygons are shown on a time-distance diagram. On the right, spectral density (ft^2-sec) is shown in a plot of frequency versus time. The time axis is vertical and common to both parts of the figure. Only the polygons and their average wind speeds are shown, not the original plotted data.

Spectra were output for six-hour intervals with a bandwidth of 0.01 cps. For the purpose of contouring, the spectral densities were linearly interpolated to a frequency interval of 0.00333 cps and smoothed with a simple binomial filter, $\bar{S}_j = \frac{1}{4}S_{j-1} + \frac{1}{2}S_j + \frac{1}{4}S_{j+1}$, where S_j is the spectral density at the j-th frequency. The traces of spectral ridges in frequency-time are shown as dotted lines in Figure 18.

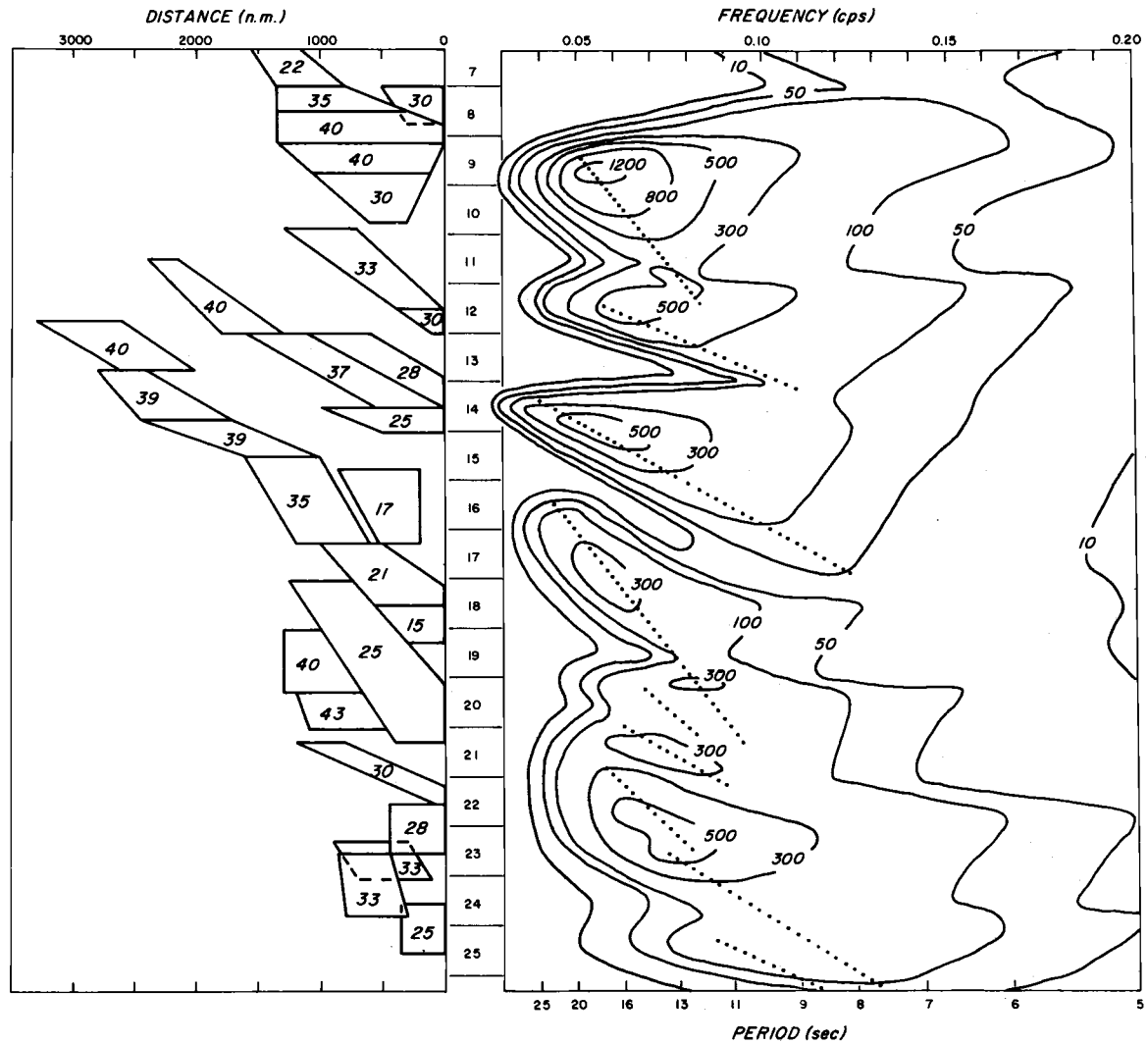

Figure 18. Fetch history diagram (left) for a 20-day period in December, 1971, and the resulting time sequence of wave spectra (right). Average wind speeds (knots) are shown for each fetch history polygon; spectral density is in ft^2-sec; dotted lines trace the decay of spectrum peaks.

To see the relationship between the fetch histories and the spectra, propagation lines drawn on a plastic template may be laid over the time-distance diagram (the template is supplied in a pocket on the back cover). The template should be placed so that the propagation lines converge to a point in time along the right side of the fetch history diagram as described in the previous chapter. The spectrum at that time is a result of the fetch histories penetrated by the propagation lines. By advancing the template in time it is possible to see how the dispersive shift in spectral peak frequency results (dotted lines on the time-frequency plot).

The spectra on December 16 and 17 were double-peaked. The propagation lines for those two days penetrate two well defined series of fetches, the first series being associated with the greater peak frequency.

It was shown by Snodgrass et al. (1966) that the time interval Δt required for the spectral peak to shift by an amount Δf (i.e. the slope of the ridge trace, $\Delta t/\Delta f$) is proportional to the distance of the storm source from the station. They used the slopes $\Delta t/\Delta f$ from measured spectra to identify the sources of swell from the opposite hemisphere. When the sources are less remote, as in Figure 18, this relationship is less well defined but qualitatively evident. The slope $\Delta t/\Delta f$ on December 16-20 is relatively large and is associated with the most remote fetches of the entire period. In contrast, the small slopes on December 24-25 are associated with very local fetches.

The dispersive frequency shift with time associated with the frequency-time ridges is shown dramatically when the spectra are plotted in pseudoperspective (Figure 19). (Figure 19 is not a true perspective because the frequency and spectral density ("vertical") coordinates suffer no distortion as one looks backward in time.)

The hindcast spectra have another characteristic in common with the measured spectra of Snodgrass et al. (1966). In both cases the maximum spectra in a series of arrivals lie within the relatively narrow frequency range of 0.05 to 0.08 cps. For spectra of the Pierson-Moskowitz form, this range corresponds to average zero upcrossing periods of from 9 to 14 seconds (by equation [4-21]). Thus, the hindcast spectra are similar to measured spectra and are consistent with the average periods of ocean swell.

Hindcast Waves at Newport During the 1971-1972 Winter

A single hindcast of significant wave height and average period was made for the period from October 18, 1971 through February 29, 1972 at Newport. Values were computed at six-hour intervals coinciding with the Newport microseism measurements. The heights and periods were integrated from the hindcast spectra over a frequency range from 0.4 cps to 0.20 cps with a bandwidth of 0.01 cps (equations [4-33] through [4-36]).

The time series of hindcast and measured (microseisms) significant height are shown in Figure 20a. The corresponding time series for average period are shown in Figure 20b. The descriptive statistics are given in Table 6.

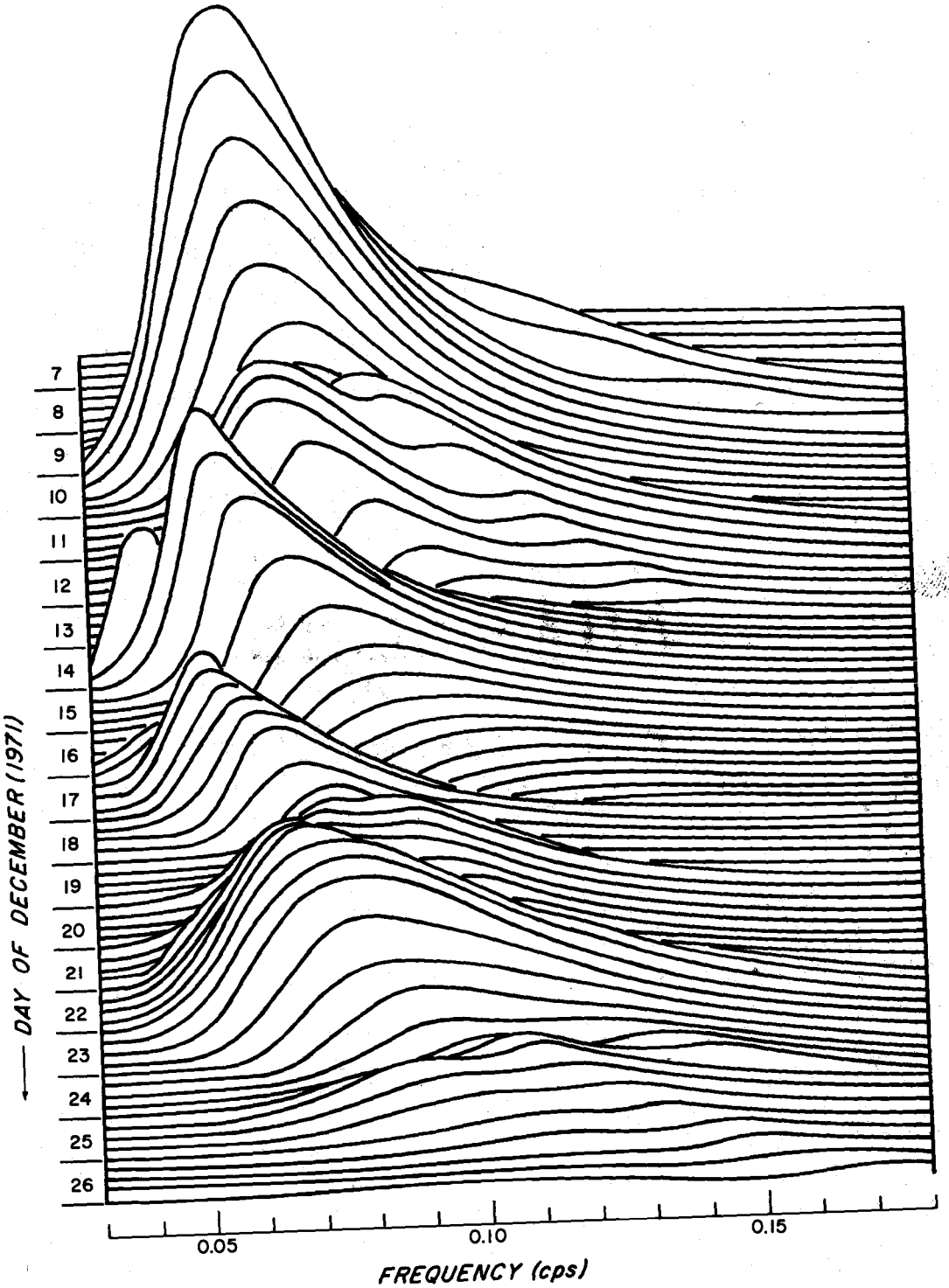

Figure 19. Twenty-day sequence of six-hourly hindcasted wave spectra, shown in pseudoperspective (December, 1971).

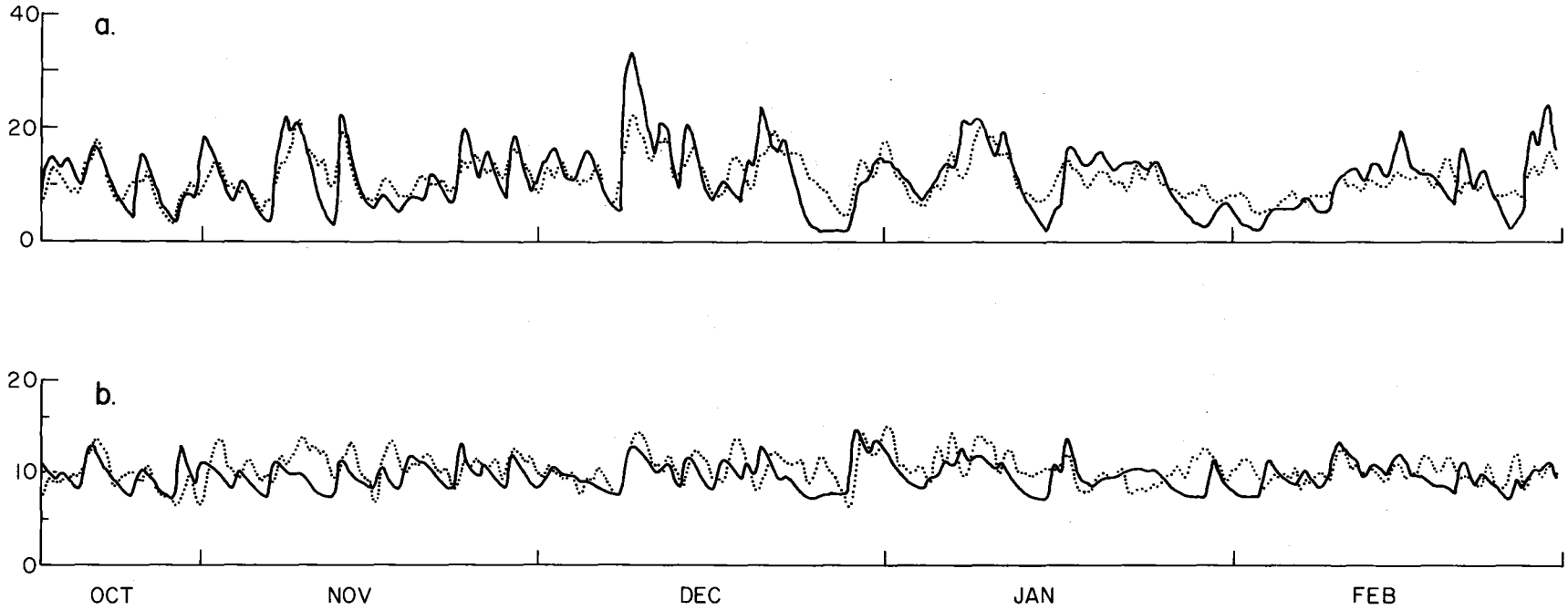

Figure 20. Part a: time series of six-hourly hindcast and seismometer-inferred significant heights at Newport during the 1971-1972 winter.

Part b: time series of six-hourly hindcast and seismometer-inferred average periods at Newport during the 1971-1972 winter.

The hindcast is plotted as a solid curve, the measured data as a dotted curve.

TABLE 6. Descriptive Statistics for Hindcast and Measured Waves at Newport.

Variable	Mean	Standard Deviation	Maximum	Minimum	Correlation Coefficient
$H^h_{1/3}$	11.1	5.5	33.0	1.5	0.77
$H^m_{1/3}$	10.9	3.4	22.1	3.2	
$H^h_{1/3} - H^m_{1/3}$	0.2	3.6	13.2	-8.8	
$\bar{T}^h$	9.7	1.6	15.0	7.0	0.31
$\bar{T}^m$	10.4	1.6	15.0	5.0	
$\bar{T}^h - \bar{T}^m$	-0.7	1.9	6.2	-5.6	

$H_{1/3}$ = significant height

$\bar{T}$ = average zero upcrossing period

Superscripts m and h refer to measured and hindcast data, respectively.

Hindcast and measured heights correlate fairly well and the difference between their means is not statistically significant. However the hindcast heights have a larger range and standard deviation. The errors (hindcast minus measured) have a large positive correlation with the hindcast heights. Thus the hindcast heights are too large during high wave periods and too low during low wave periods. This can also be seen from the time series plots in Figure 20a.

Negative errors during low wave periods are probably due to the neglect of local fetches with wind speeds of less than 20 knots (between storm wave arrivals). If it were not for the neglect of such fetches, the average hindcast wave height would have been considerably higher. It is clear from both the statistics and the time plots that high waves were usually overestimated by the semi-automated method.

At present, there seem to be three explanations for overestimation of significant height during high wave arrivals:

(1) Human error - prior to doing the hindcast, the author had been familiar with forecasting and hindcasting principles for about a year, but had relatively little practice. This was the first time the semi-automated method had been applied in such a way. Though the fetch analyses may have been systematically in error, it is not clear in what way.

(2) Error in measured heights. It has already been pointed out that the measured waves at Newport (near the navigation buoy) are systematically lower than in deep water. Shoaling results in a lowering of heights of up to 10%. Refraction may cause heights

to be lowered by as much as 50% when wave crests approach at large angles to the depth contours. (This estimate is based on refraction relationships for straight and parallel depth contours.) The exact amounts of reduction could not be estimated due to the lack of wave direction data.

(3) Errors in meteorological input data. Because average wave heights vary as the square of the generating wind speed, discrepancies in ship report data can affect the computations. The semi-automated method uses the empirical-theoretical spectrum of Liu (1971) which is parameterized in terms of U_{10} , the wind speed at a height of ten meters. However, the average anemometer height for most ocean-going ships equipped with anemometers is greater than ten meters. Assuming that the mean wind speed increases logarithmically with height z , $U(z) = U_{10} \log(z)$, we would get $U_z = U_{10}[1 + \log (z/10)]$. Thus the mean speed at 15 meters is 1.18 times that at ten meters. If 15 meter winds are used as input for the semi-automated method, significant height may be overestimated by up to 40% ($U_{15}^2 = 1.39U_{10}^2$).

In view of the human element (experience level) and the possible errors extraneous to the semi-automated methodology, the hindcast and measured heights compare quite well. Variations over several-day periods are quite well simulated by the method. Also, there is no clear tendency for hindcast arrival times to be consistently early or late relative to the measured data. The subjectivity involved in analyzing

fetch history information does not appear to seriously hamper the effectiveness of the semi-automated method as a forecast tool.

Hindcast average periods are not as well verified by measurements as are significant heights. The correlation is considerably lower and there is a tendency for maximum periods to occur sooner for the hindcast. This is because low forerunner swell of large period stand out when local fetches of low wind speed are not included in the hindcast.

It is probably not wise to attach too much importance to the apparently poor verification of hindcast periods, since it is difficult to determine period from microseism records. The measured periods are also subject to greater uncertainties than the heights due to the difficulty of obtaining visual verification.

Aside from these observational considerations, one would not expect periods to be as predictable or verifiable as heights. Wave periods are almost always more difficult to estimate on the open ocean. Recalling the spectral discussions of the previous chapter, the wave heights depend on the zero-th moment of the wave spectrum, whereas the periods depend on the second moment as well. Thus, unlike the heights, periods depend on the form of the spectrum, the location of the spectral peak frequency, and the possibility that multiple spectral peaks exist. This places much greater constraints on prediction of the wave spectrum.

Simulated Semi-automated Forecasts vs. Manual Forecasts at Newport

Under operational conditions it would not be possible to obtain wave forecasts that would verify as well against measured or observed waves as hindcasts do unless perfect prognostic charts were available. Hence, the most serious limitation of the wave forecast method is the necessity of relying on prognostic meteorological inputs.

It is desirable to conduct studies under actual forecast conditions, in which the semi-automated method is compared with the standard manual forecast methods. Such a study is currently being conducted by NOAA-Sea Grant personnel at Newport, Oregon. For this study it was decided to simulate forecasts. A simulated 24-hour forecast was made for each six-hour interval from October 18, 1971 through February 29, 1972. A significant height was computed for Newport 24 hours after each six-hourly analysis. All fetch information available prior to execution time was used as input, and any analyses during the subsequent 24 hour period ignored. These simulated forecasts are equivalent to a series of single-value 24 hour height forecasts made without the benefit of prognostic weather charts.

Twenty-four hour forecasts of significant height were made for the same period by NOAA-Sea Grant personnel at Newport, using the manual S-M-B and P-N-J methods. Mr. Clay Creech (Sea Grant) correlated those heights with the same heights from the measured microseisms. He also computed the correlation for 24-hour "persistence" forecasts with measured data. (Persistence assumes that the future height will be the

same as the present height, i.e. that no change will occur over the 24-hour interval).

In Figure 21 the correlation coefficients and their 95% confidence limits are shown for

(1) the hindcast of the previous section;

(2) the semi-automated simulated forecasts;

(3) the manual Sverdrup-Munk-Bretschneider forecasts;

(4) the manual Pierson-Neumann-James forecasts; and

(5) the persistence forecasts.

The correlation coefficient for the simulated forecasts is 0.68 as opposed to 0.77 for the hindcast heights. This is significantly lower at the 95% confidence level and reflects the partial lack of fetch information resulting from the simulation. Correlations of all forecasts except persistence are undifferentiable at the 95% confidence level. Persistence shows a correlation of 0.45, significantly lower than all other methods.

The results of these correlations are suggestive, but not conclusive, because the semi-automated simulation is not entirely comparable with the manual forecasts. The fetches used for the simulation were obtained from final analyzed pressure charts, whereas the manual forecasters used the less complete facsimile analyses supplemented by ship reports from the teletype circuit. On the other hand, the manual forecasters often extrapolated past meteorological conditions into the future with the aid of prognostic charts, whereas all "future" information was ignored in the simulation.

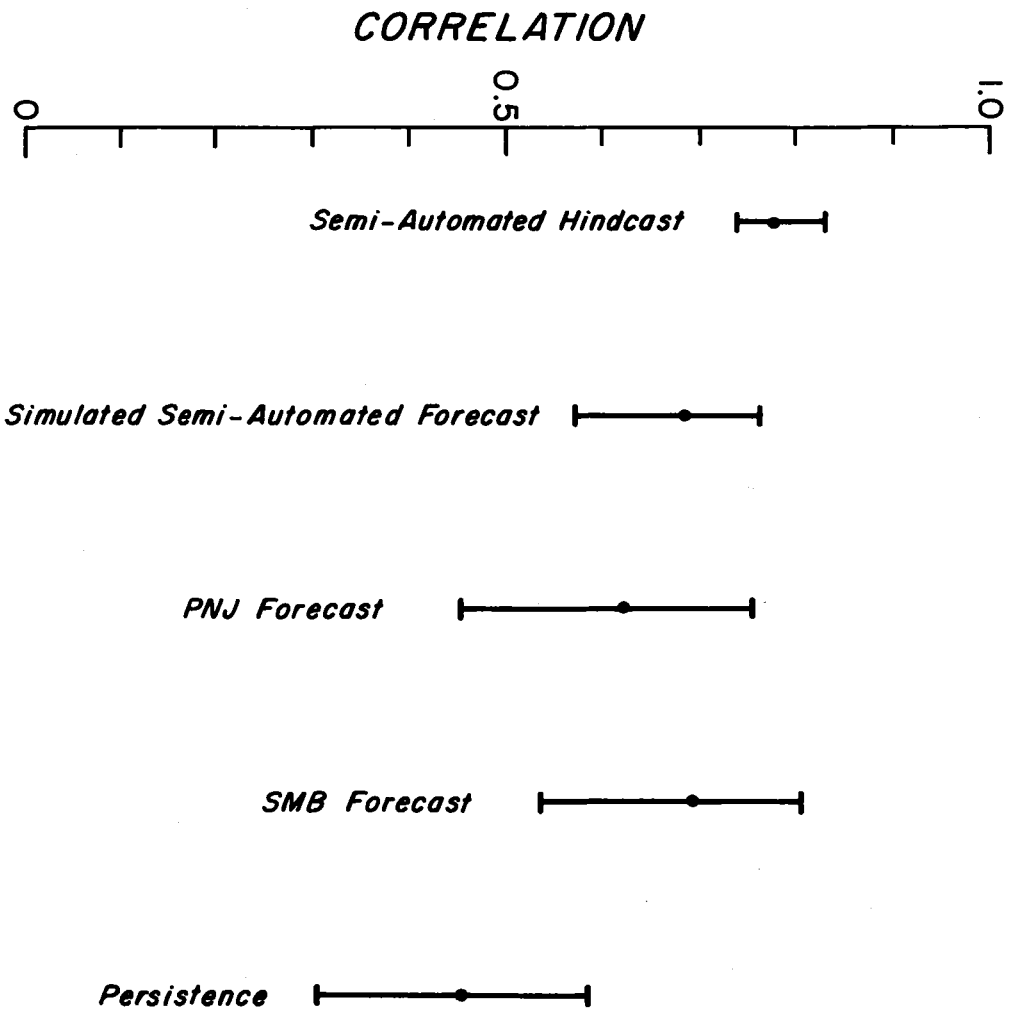

Figure 21. Correlation coefficients and 95% confidence limits for several hindcasts and 24-hour forecasts at Newport, as compared with measurements (1971-1972 winter).

It appears that the semi-automated method is capable of yielding results similar to those obtained by experienced forecasters using manual methods. However a more thorough comparison under operational conditions should be completed.

Cautions Regarding the Analysis of Meteorological Charts

Additional experience was gained by hindcasting the two previous winters for the Columbia River. The charts for the 1971-1972 winter were scrutinized again and it was found that fetch behavior had been incorrectly analyzed in a number of instances. The potential user of the semi-automated method should be cautioned in several respects.

First, when storms do not affect the eastern North Pacific, fetches must be considered which might otherwise be neglected. These include local fetches with wind speeds of less than 20 knots, and very distant fetches (over 3000 nautical miles) when winds exceed 40 knots for at least a day.

When forecasting, the short-duration local fetches in the prefrontal sectors of cyclones must be predicted with the aid of prognostic meteorological inputs. This should be done with the greatest possible care, because the wind fields are often short, with winds suddenly increasing to over 35 knots for up to 12 hours. The forecast waves will be particularly sensitive to errors in the predicted wind speed and fetch length in such cases.

The cold sectors of extra-tropical cyclones are often characterized by more intense winds toward the rear (western portion) of the

area. However, the direction of the winds may remain fairly uniform throughout the southern quadrant. This is particularly true in cases of intense cyclogenesis in the Gulf of Alaska (Winston, 1954) where cold air advected off the Alaskan Peninsula becomes very unstable over the relatively warm water of the Gulf. The intensification of the winds is greatest near the Alaskan coastline, often at the rear of long fetches extending southeastward toward Oregon and Washington. Thus, 45 to 55 knot areas may occur in the northernmost part of the fetch with lower wind speeds in the southern part of the fetch. Such situations should be analyzed as adjacent fetches with different wind speeds rather than one long fetch with an averaged wind speed.

Summary

As evidenced by a 20 day hindcast, the wave spectra computed by the semi-automated method behave very much like measured spectra. The frequency range of the (hindcast) spectral peaks and their dispersive shift with time are both consistent with the known behavior of decayed swell.

Hindcast significant heights correlate well with measured heights, with a tendency for high waves to be somewhat overestimated. There is no consistent tendency for hindcast arrivals to precede or follow the measured ones. Hindcast and measured periods are not as well correlated as heights.

Comparison of simulated semi-automated forecasts and actual manual forecasts revealed no significant differences in verification. This

suggests that the semi-automated method can give results comparable to those obtained by experienced forecasters using the manual methods.

The potential user of the semi-automated method is cautioned to use special care in analyzing local fetches and those in which wind speed is not uniform.

VI. MODIFICATION OF WAVE SPECTRA DUE TO THE COMBINED EFFECTS OF SHOALING AND CURRENTS

Introduction

Chapters IV and V discussed the semi-automated method for forecasting (or hindcasting) deep water wave spectra. The arrival of high waves offshore of harbors is itself indicative of relatively hazardous conditions near the entrances. But because of the modification of the wave spectrum as the waves propagate shoreward, the average height, period, length, and steepness change and breaking waves become more probable. To assess the altered nature of waves at the river mouth it is necessary to transform the spectrum in accordance with physical principles.

In general, the spectrum may be affected by bottom friction, percolation, refraction (by both currents and bottom contours), wave breaking, shoaling, and currents. Only the last two sources of modification are accounted for explicitly in this chapter. The probabilistic nature of wave breaking will be dealt with in the next chapter. Neglected processes are put into perspective in the next section and again at the end of the chapter.

In addition to the limitation of scope to the effects of shoaling and currents, several important assumptions are made. It is assumed that the inital spectrum in deep slack water is narrow banded, unimodal, and of the Pierson-Moskowitz form. The results of small amplitude wave theory are presumed to be adequate for transforming the

energy density at each frequency of the spectrum. For waves propagating against a current a cutoff frequency is chosen, beyond which wave energy must dissipate in turbulent breaking. It is assumed that for higher frequencies than the cutoff energy loss through wave breaking is total, while below the cutoff frequency the losses are negligible. These assumptions are discussed at the end of the chapter. Lastly, it is assumed that for the case of river mouths, the current distribution is such that energy transfer between waves and currents is negligible. This assumption will be discussed in the development of the monochromatic transformation equations.

After the initial discussion of the modification processes, the necessary transformation relationships are developed in accordance with small amplitude wave theory. These are then used to transform the energy density at each frequency of the spectrum, for a given depth and current, in the manner suggested by Bretschneider (1963b) for shoaling alone. Finally, the relative change in average height and period is determined by integration of the unaltered and transformed spectra.

Processes That Modify the Wave Spectrum

As waves propagate toward a river mouth, the wave spectrum is modified to various degrees by bottom friction, percolation, refraction, shoaling, currents, and breaking. All of these agents are selective in their action. That is, they modify the energy density more at one end of the spectrum than at the other, thereby deforming

the spectrum in a non-uniform manner. Selective modification of a complex wave group produces a shift in the frequency of the spectral peak (associated with the predominant wave period), as opposed to the case of a "monochromatic" wave group, where the frequency (period) is taken as invariant.

The effects of the various agents of modification are summarized in Table 7 . Bretschneider (1963b) noted that over the wide continental shelf of the Gulf Coast, selective attenuation of longer period waves by bottom friction and percolation is greater than their selective amplification due to shoaling. As a result, the predominant period shifts to lower values as the waves approach the coast. Along the west coast of North America bottom friction and percolation are negligible (except in the surf zone) due to the narrow and abruptly rising slope and shelf. There the shoaling effects are the more important; longer period waves are selectively amplified and the predominant period shifts toward higher values.

Near tidal inlets of the west coast, both shoaling and currents are important sources of wave modification. The relative importance of each depends on the channel depth and current speed relative to the wave period. However, during the tidal ebb the current effect is almost always appreciable. This is because channel depths and jetties are designed so that the ebb flow will be strong enough to avoid net deposition of sediment in the entrance channels. At the Columbia River mouth the ebb speeds range from six to eight feet per second (3.5 to 5 knots) during neap tides to more than thirteen fps (8 kt) during spring tides at high river stage.

TABLE 7. Processes That Modify Wave Spectra.

Modifying Process	Effect on Spectrum	Frequencies most Affected (high/low)	Frequency of Spectral Peak
Shoaling	Energy Density Increases	Low	Decreases
Bottom Friction and Percolation	Loss of Energy	Low	Increases
Following Currents	Energy Density Decreases	High	Decreases
Opposing Currents	Energy Density Increases; Total Energy Loss Above Critical Frequency (breaking)	High	Increases
Refraction Over Shoals	Energy Density Increases	Low	Decreases
Refraction Over Channels	Energy Density Decreases	Low	Increases
Refraction By Following Currents	Energy Density Decreases	High	Decreases
Refraction By Opposing Currents	Energy Density Increases	High	Increases

Wave breaking is an important modification process in shoal regions generally and specifically over entrance bars at ebb stage. The amount of breaking depends not only on the relative depth and relative current at the point in question, but on the initial (deep water) steepness of the waves as well (see, for example, the discussion of Herbich and Hales, 1972).

There is an important distinction between the modification of energy density by shoaling and currents on the one hand, and the loss of energy through breaking on the other. If energy transfer between currents and waves may be neglected, the relationship between initial and final states in the former is conservative, as there is no net loss or gain of energy to the system. During breaking, net wave energy is converted into heat and cannot be recovered. The non-conservative breaking process depends upon its history. That is, if one wishes to accurately account for energy lost in breaking, he must know the distribution of both depth and current in the area between deep water and the point in question. This is because the distribution of breaking waves is dependent on depth and current, as will be shown in the next chapter.

Refraction along the approaches to the Columbia River results from changes in depth and current speed. Refraction induced by depth changes was discussed qualitatively in Chapter II, and is most pronounced just north and south of the entrance, and upriver of the jetty tips. Current-induced refraction is especially strong during ebb flow over the outer bar. Neither of the effects is treated here due

to inadequate bathymetric data and the almost non-existent data on currents seaward of the jetties.

To summarize, the situation to be treated in this chapter is an idealized one. It is equivalent to considering waves which propagate eastward toward a tidal inlet of simple proportions on a north-south coast with parallel, north-south depth contours. Depth and current are assumed to deepen and disperse (respectively) seaward of the inlet with sufficient abruptness that the effects of bottom friction, percolation, and wave breaking are minimal prior to arrival of the waves at the inlet opening. This simple model focuses attention on the effects of shoaling and currents, the two most consistent causes of wave modification at the mouth of the Columbia River. In practice, even over the relatively deep entrance channel the history of refraction and wave breaking may be important, depending on wave height, period, direction, and tidal current.

Modification of Small Amplitude Monochromatic Waves By Shoaling and Currents

Consider a train of small amplitude waves of height H, length L, and period T. The celerity of such waves, according to small amplitude (first and second order) theory, is

$$C = \left[\frac{gL}{2\pi} \tanh\left(\frac{2\pi d}{L}\right)\right]^{\frac{1}{2}} , \qquad (6\text{-}1)$$

where g is the acceleration due to gravity and d is the water depth.

In the limit of large depths ($d > L/2$), (6-1) reduces to

$$C_o = \left[\frac{gL_o}{2\pi}\right]^{\frac{1}{2}} \quad , \tag{6-2}$$

where the "o" subscript denotes deep water, and

$$L_o = \frac{gT^2}{2\pi} \quad . \tag{6-3}$$

Equations (6-2) and (6-3) are sufficiently good approximations provided the depth is at least half of the deep water wavelength, or

$$d \geq \frac{gT^2}{4\pi} \quad . \tag{6-4}$$

If the waves propagate with or against a current, equation (6-1) is to be interpreted as the celerity in a reference frame moving with the current. To a stationary observer, the period of the waves would be

$$T = \frac{L}{C + U} \quad , \tag{6-5}$$

where U is the current speed and is taken to be negative if it opposes the waves. The usual kinematic assumption is that the period remains constant as the depth and current speed change. Thus, as the waves propagate from deep slack water to an area of influencing depth and non-zero current,

$$\frac{L_o}{C_o} = \frac{L}{C + U} \quad , \tag{6-6}$$

or

$$\frac{L}{L_o} = \frac{C + U}{C_o} \quad . \tag{6-7}$$

From (6-1), (6-2), (6-3), and (6-7), the celerity and length of waves in water of depth d and current U, relative to deep, slack water, are

$$\frac{C}{C_o} = \left[\frac{L}{L_o} \tanh\left\{2\pi \frac{d}{L_o} \cdot \frac{L_o}{L}\right\}\right]^{\frac{1}{2}} , \qquad (6\text{-}8)$$

and

$$\frac{L}{L_o} = \left[\frac{L}{L_o} \tanh\left\{2\pi \frac{d}{L_o} \cdot \frac{L_o}{L}\right\}\right]^{\frac{1}{2}} + \frac{U}{C_o} . \qquad (6\text{-}9)$$

Equation (6-9) is transcendental in L/L_o but can be solved for L/L_o by computing iteratively until successive differences are acceptably small. Subtraction of the constant term, U/C_o, yields the corresponding value of C/C_o.

Equations (6-7) and (6-8) were first discussed by Unna (1942). He assumed that the speed of wave energy propagation past a stationary observer is

$$V = nC + U , \qquad (6\text{-}10)$$

where

$$n = \tfrac{1}{2}\left(1 + 4\pi \frac{d}{L} \Big/ \sinh\left[4\pi \frac{d}{L}\right]\right) . \qquad (6\text{-}11)$$

The quantity n is the ratio of group velocity to phase velocity for small amplitude waves in the reference frame moving with the current.

Denoting the wave energy density (energy per unit horizontal area) as E, we require that the rate of energy transfer past a stationary point remain invariant or, using (6-10),

$$\frac{\partial}{\partial X} \left(E[nC + U]\right) = 0 , \qquad (6\text{-}12)$$

where χ is the horizontal coordinate in the direction of wave travel. This means that the energy density relative to deep slack water becomes

$$\frac{E}{E_o} = \frac{\frac{1}{2}C_o}{nC + U} = K^2 \qquad (6\text{-}13)$$

where $n = \frac{1}{2}$ in deep water and K^2 is a convenient symbol to denote the energy amplification factor. Wiegel (1964) discusses the application of equations (6-7), (6-8) and (6-13) to the case of waves in deep water which encounter a current along the χ axis.

Longuet-Higgins and Stewart (1961) pointed out that, although frequently cited in the literature, the assumption (6-10) (and therefore also its consequences, (6-12) and (6-13)) is not correct generally. Thus (6-10) is equivalent to assuming that there is no net energy transfer from the mean current to the waves, or vice versa. The authors show that as the waves propagate through a current gradient, the degree of interaction between current and waves will depend on how much of the non-uniformity in the χ-direction is due to horizontal compensation (lateral inflow or outflow) or to vertical compensation (upwelling or downwelling).

Longuet-Higgins and Stewart applied their theory to two special deep water cases. In their development the energy balance equation reduces to

$$\frac{\partial}{\partial \chi}\{E(\tfrac{1}{2}C + U)C\} = 0 \qquad (6\text{-}14)$$

for pure upwelling (downwelling), and

$$\frac{\partial}{\partial \chi}\left\{E\,\frac{(\tfrac{1}{2}C + U)}{C}\right\} = 0 \qquad (6\text{-}15)$$

for pure lateral inflow (outflow). The energy amplifications are, respectively,

$$\frac{E}{E_o} = \frac{C_o}{C}\left(\frac{\tfrac{1}{2}C_o}{\tfrac{1}{2}C + U}\right) = K'^2 \qquad (6\text{-}16)$$

and

$$\frac{E}{E_o} = \frac{C}{C_o}\left(\frac{\tfrac{1}{2}C_o}{\tfrac{1}{2}C + U}\right) = K''^2 \quad , \qquad (6\text{-}17)$$

if the waves are assumed to be in initially slack water.

If wave-current interaction is neglected, (6-13) yields

$$\frac{E}{E_o} = \frac{\tfrac{1}{2}C_o}{\tfrac{1}{2}C + U} \qquad (6\text{-}18)$$

for deep water. Comparison of (6-16), (6-17), and (6-18) suggests that (6-18) corresponds to a case intermediate between the two extremes. In fact, one can show that (6-18) results if equal amounts of vertical and lateral compensation are involved. Herbich and Hales (1972) pointed out that in a prototype tidal inlet situation some condition between the extremes probably exists as the current converges (diverges) from (toward) all directions.

The actual degree of wave-current interaction cannot be determined for the Columbia River because the details of the current distribution seaward of the jetties are unknown. In view of this lack of

data, the assumption leading to (6-18) appears to be satisfactory. It will be assumed, therefore, that (6-13) correctly describes the energy amplification for the Columbia River entrance.

It can be seen from (6-13) that a discontinuity occurs when $U = -nC$; as this limiting value is approached, the amplification tends to infinity. In this limit the speed of energy propagation is reduced to zero (Unna, 1942). Unna noted that for depths greater than $L_o/20$ the discontinuity may be approximated by the condition

$$U = -\tfrac{1}{4}C_o \quad . \tag{6-19}$$

He further pointed out that waves of finite steepness must break before the current reaches the limiting condition of equation (6-19). Wave breaking would presumably continue (perhaps sporadically) as the limit is approached and additional energy is lost through breaking. Since the wave energy is proportional to the squared height, the height amplification from (6-13) is just

$$\frac{H}{H_o} = \left\{\frac{\tfrac{1}{2}C_o}{nC + U}\right\}^{\frac{1}{2}} = K_{sc} \quad . \tag{6-20}$$

The amplification, K_{sc} , can be termed a shoaling-current coefficient in analogy to the shoaling (K_s) and refraction (K_r) coefficients often cited in the literature. In fact, K_{sc} reduces to K_s in the limit of zero current, as it should.

Noting that

$$\frac{U}{C_o} = \frac{2\pi}{g}\left(\frac{U}{T}\right)$$

and

$$\frac{d}{L_o} = \frac{2\pi}{g}\left(\frac{d}{T^2}\right) \quad ,$$

The coefficient K_{sc} can be computed for various values of relative depth (d/T^2) and relative current (U/T). The result is shown in Figure 22. The salient features of Figure 22 may be summarized as follows:

(a) In the limit of deep slack water K_{sc} approaches unity.

(b) Along the null-current line $(U = 0)$, K_{sc} reduces to the shoaling coefficient, K_s.

(c) For a given value of D/T^2, K_{sc} increases with greater opposing current speeds $(U/T < 0)$ and decreases with greater following current speeds $(U/T > 0)$.

(d) For a given value of relative current (U/T), K_{sc} is minimum at intermediate values of relative depth.

(e) The rate of increase of K_{sc} is greatest for shallow depths and strong opposing currents.

In some applications (e.g. H.O. Pub. 234, "Breakers and Surf: Principles in Forecasting", 1954) it is assumed that statistical averages of H, C, and L can be transformed (shoaling only) by the equations of small amplitude theory and that the average period is unchanged. The assumption is correct in the limit of waves of infinitesimal steepness with a "line" spectrum, where energy is unaffected by

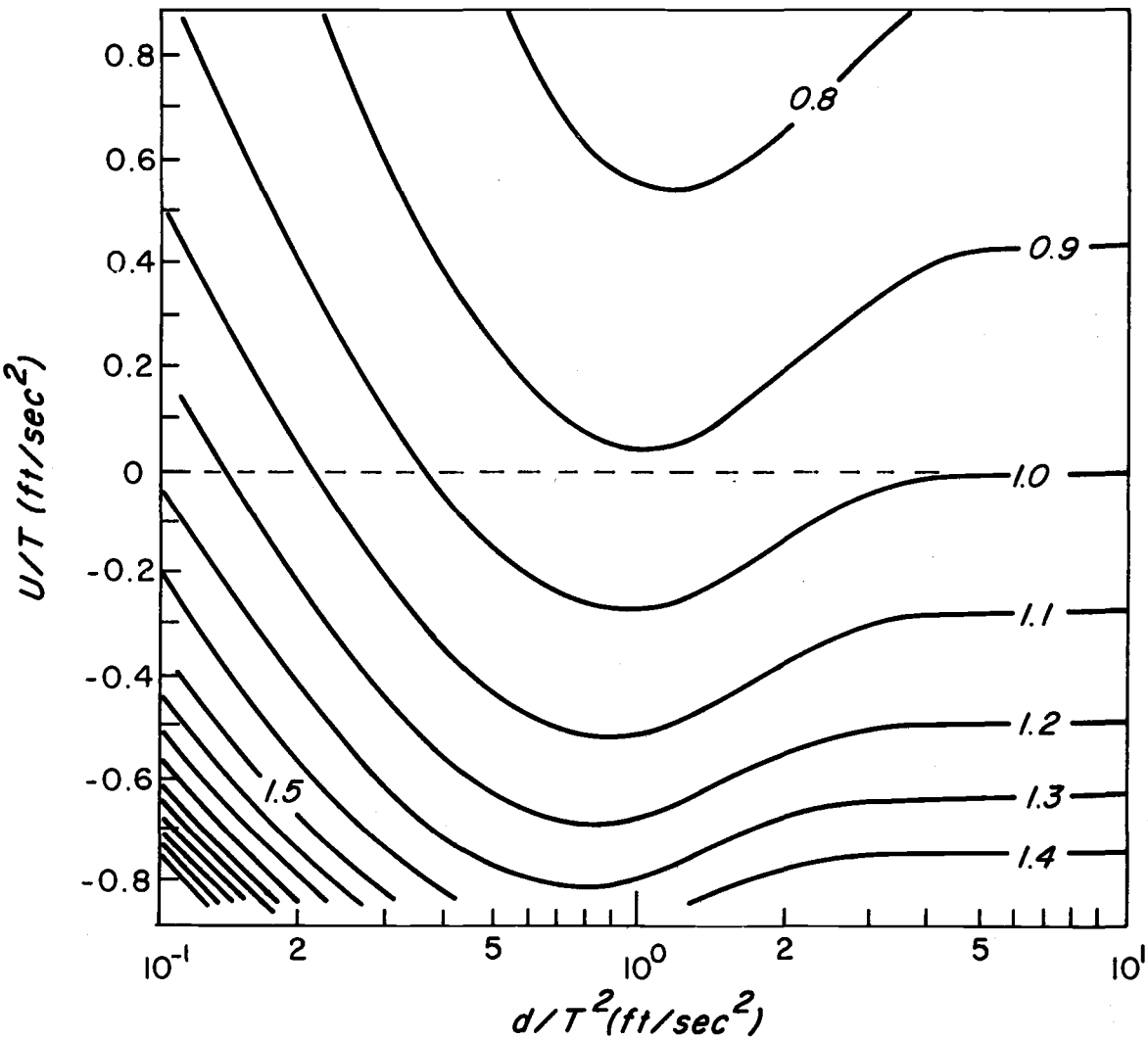

Figure 22. Shoaling-current coefficient (K_{sc}) for monochromatic waves as a function of relative depth (d/T^2) and relative current (U/T).

other processes mentioned in the preceding section. The assumption becomes increasingly unacceptable as the actual waves depart from this idealized condition. In the case of storm waves it is necessary to transform the entire spectrum.

Transformation of Wave Spectra By Shoaling and Currents

Bretschneider (1963b) transformed wave spectra by applying the shoaling coefficient K_s to the energy densities of the deep water period spectrum, $S_o(\underset{\sim}{T})$:

$$S(\underset{\sim}{T}) = K_s^2 \, S_o(\underset{\sim}{T}) \quad , \tag{6-21}$$

where $K_s = [C_o/2nC]^{\frac{1}{2}}$ as determined by small amplitude theory,

$$S_o(\underset{\sim}{T}) = A\underset{\sim}{T}^3 \exp(-B\underset{\sim}{T}^4) \quad , \tag{6-22}$$

$$\underset{\sim}{T} = T/\overline{T}_o \quad , \tag{6-23}$$

A and B are constants and $\overline{T}_o$ is the average wave period in deep water, before transformation.

Each period component of the spectrum is subjected to a relative depth

$$d/T^2 = (d/\overline{T}_o^2) \div \underset{\sim}{T}^2 \quad . \tag{6-24}$$

The coefficient K_s varies across the spectrum accordingly; it will affect the longer periods to a greater extent due to their smaller relative depth.

Bretschneider (1959) showed how the frequency spectrum may be obtained from the joint probability distribution of wave heights and periods. If heights and squared periods are both Rayleigh-distributed and independent, the frequency spectrum corresponding to (6-22) is

$$S_o(\underset{\sim}{f}) = a\underset{\sim}{f}^{-5} \exp(-b\underset{\sim}{f}^{-4}) \quad , \tag{6-25}$$

where $\underset{\sim}{f}$ is the frequency as normalized by a characteristic value, and a and b are constants appropriate to the choice of normalization. Depending on the specific form which (6-25) takes, and its dependence on wave generation parameters, it may be alternatively referred to as the Bretschneider spectrum (Bretschneider, 1959) or the Pierson-Moskowitz spectrum (Pierson and Moskowitz, 1964).

If the frequency is normalized by the spectral peak frequency, f_o^{max}, and the spectral density by the peak energy density, S_o^{max}, the normalized spectrum becomes simply

$$\underset{\sim}{S}_o(\underset{\sim}{f}) = \underset{\sim}{f}^{-5} \exp(-\tfrac{5}{4}\{\underset{\sim}{f}^{-4} - 1\}) \quad , \tag{6-26}$$

where $\underset{\sim}{f} = f/f_o^{max}$, and the "o" subscript refers to the unaltered deep water spectrum, as before. The shoaling transformation of (6-26) is

$$\underset{\sim}{S}(\underset{\sim}{f}) = K_s^2 \, \underset{\sim}{S}_o(\underset{\sim}{f}) \quad . \tag{6-27}$$

The period corresponding to the spectral peak frequency is

$$T_o^{max} = [f_o^{max}]^{-1} \tag{6-28}$$

and is related to the mean period, $\overline{T}_o$, by a constant factor. If $\overline{T}_o$ is taken as the average period defined by the zero upcrossing method, it can be shown that (e.g. Bretschneider, 1959)

$$T_o^{max}/\overline{T}_o = 1.4 \quad , \tag{6-29}$$

For a given initial value of $d/\overline{T}_o^2$, each frequency component is subjected to a shoaling coefficient corresponding to the relative depth at that frequency:

$$d/T^2 = \left(\frac{\overline{T}_o}{T_o^{max}}\right)^2 \left(\frac{d}{\overline{T}_o^2}\right) \div \underset{\sim}{f}^2 = 0.5\left(\frac{d}{\overline{T}_o^2}\right) \div \underset{\sim}{f}^2 \tag{6-30}$$

In Figure 23 the transformed (normalized) spectra are shown for various values of $d/\overline{T}_o^2$. The spectrum corresponding to $d/\overline{T}_o^2 =$ 12 ft/sec^2 is essentially the unaltered deep water one, (6-26). Although the form of the spectrum changes little with changing depth, the peak frequency shifts and the area under the spectrum changes. At $d/\overline{T}_o^2 = 2.4$ ft/sec^2 (intermediate depth) the spectral area is less and the spectral peak frequency shifts to higher frequencies. At the shallower depths the spectral peak frequency shifts to lower values and the spectral area increases.

The desired transformation for the spectra of waves approaching the Columbia River is one which combines the effects of shoaling and currents. Figure 24 shows the result of transforming the normalized spectrum (6-26) with the shoaling-current amplification factor discussed in the previous section:

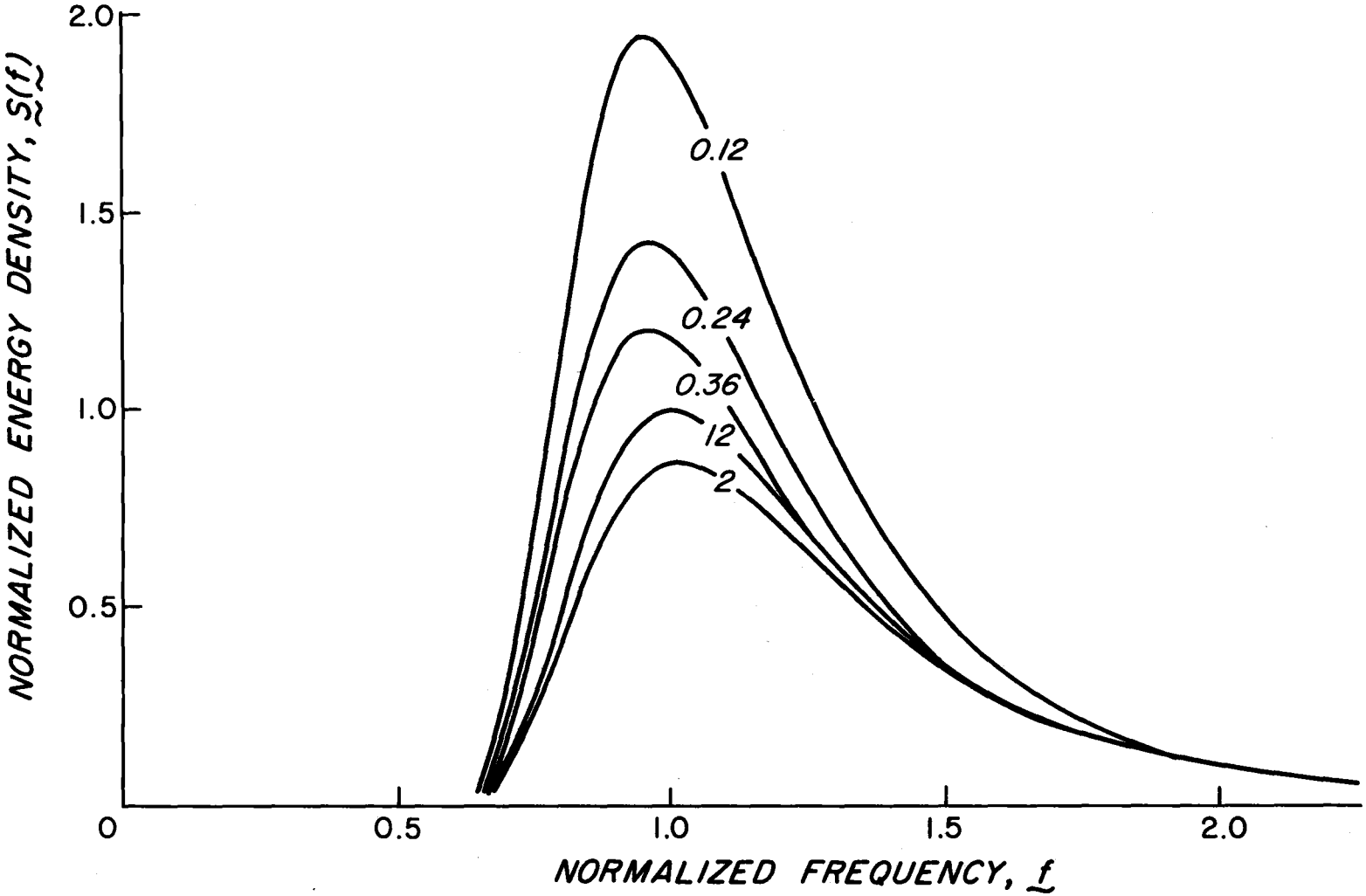

Figure 23. Normalized wave spectra in slack water at several relative depths (plotted numbers, ft/sec^2). Frequency and energy density are normalized by the frequency and energy density of the spectral peak for deep water (where $d/\bar{T}_o^2$ = 12 ft/sec^2).

$$S(f) = K_{sc}^2 \, S_o(f) \qquad (6\text{-}31)$$

where

$$K_{sc}^2 = \frac{\frac{1}{2}C_o}{nC + U} \quad . \qquad (6\text{-}13)$$

All curves in Figure 24 are for a relative depth $d/\overline{T}_o^2 = 0.36$ ft/sec^2. This would correspond, for example, to waves with an average zero upcrossing period of 12 seconds at a depth of about 50 feet. The range of relative current $(U/\overline{T}_o)$ shown is equivalent to current speeds of from 5.5 fps (flood) to -11 fps (ebb) for the same example. These are typical figures for storm waves over the Columbia River navigation channel, say, between the jetty tips.

Several prominent features of Figure 24 may be noted:

(1) The spectral peak frequency shifts slightly to higher values with increasingly negative (opposing) relative current. This is to be expected as (6-13) is larger for shorter waves (larger frequencies).

(2) Energy density increases for opposing currents and decreases for following currents.

(3) For opposing currents a relative minimum occurs, beyond which energy density rapidly increases (dotted portion of curves).

The frequency at which the energy density approaches infinity is the theoretical limit where the group velocity is equal and opposite to the current velocity.

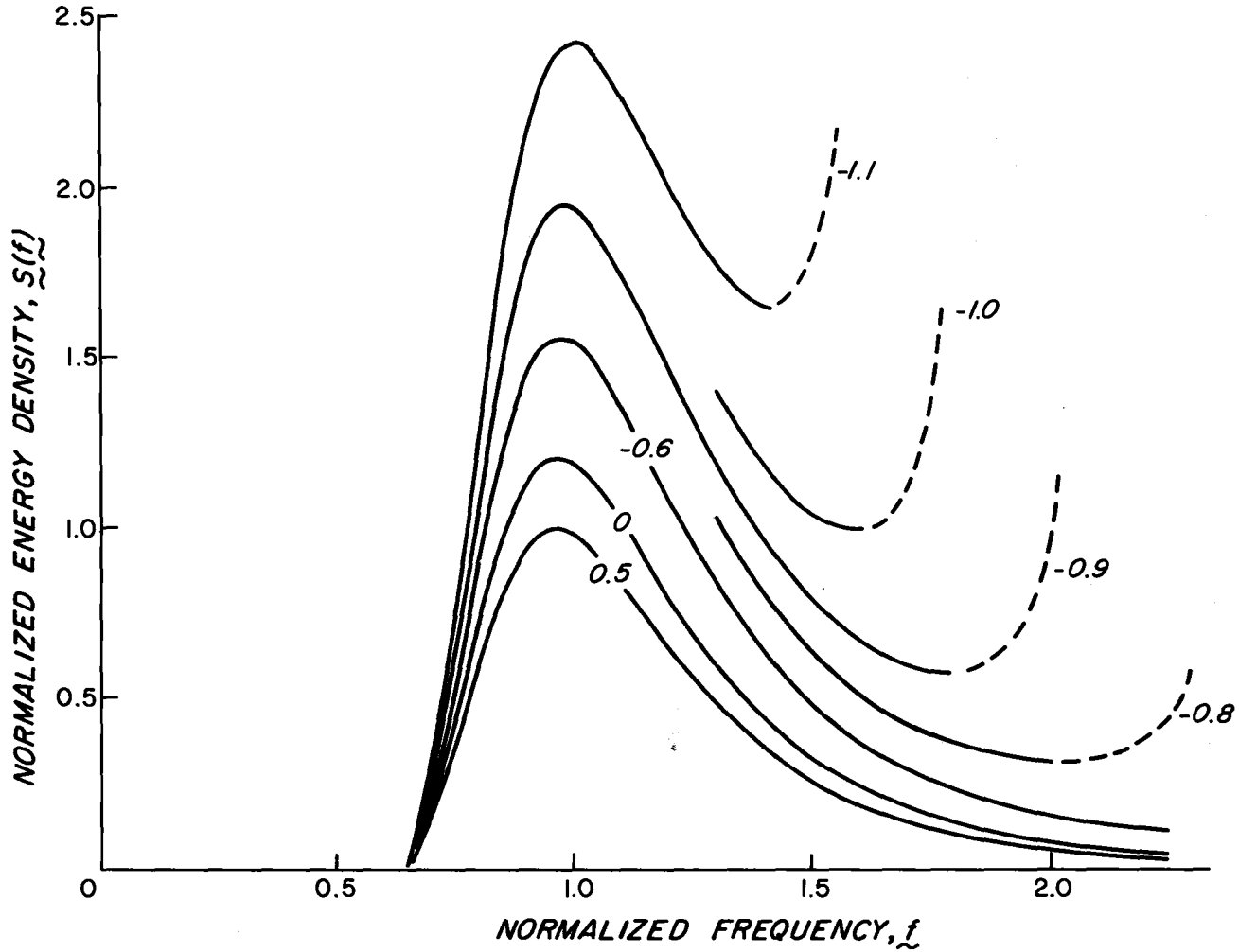

Figure 24. Normalized spectra for a relative depth $d/\overline{T}_o^2 = 0.36$ ft/sec^2, and several relative currents (ft/sec^2). Spectra were transformed from the spectrum for deep slack water. Frequency and energy density are normalized by the frequency and energy density of the spectrum in deep slack water.

Huang et al. (1972) performed transformations on deep water spectra where opposing and following currents were involved. They arbitrarily chose the energy amplification factor (6-16) and applied it to the Pierson-Moskowitz spectrum obtaining results similar to Figure 24. They pointed out that no waves can exist beyond the theoretical limit and that waves would break before reaching it. They added that:

> In actual cases, the spectrum will show an overshoot or energy pile-up at the frequency just below (the critical frequency), and the sea state becomes extremely rough caused by the breaking.

The effects of shoaling and currents on averaged wave height and period will now be examined by integration of the unaltered spectrum in deep slack water and the transformed spectrum in water of arbitrary depth and current.

Change in Average Wave Heights

The variance of the sea surface elevation is equal to the zero-th moment of the energy spectrum, or the spectral area. Longuet-Higgins (1952) showed theoretically that for a narrow banded spectrum the square root of this variance is related to the mean wave height and the average of the highest one n-th waves by constant factors. The relative change in average height resulting from the spectral transformation (6-31) is therefore equal to the square root of the relative change in spectral area. That is,

$$\frac{\overline{H}}{\overline{H}_o} = \left[\frac{\int_0^\infty S_\zeta(f)df_\zeta}{\int_0^\infty S_{\zeta o}(f)df_\zeta} \right]^{\frac{1}{2}} , \qquad (6\text{-}32)$$

where the computed ratio applies to mean height as well as to the average height of the highest one n-th waves.

In practice, of course, one could choose a non-infinite upper frequency limit for the integrations, consistent with the expected range of wave periods. For this study the upper frequency limit was chosen to be four times the spectral peak frequency. For an average zero upcrossing period of 12 seconds, this would mean neglecting periods of four seconds or less.

In the case of opposing currents, a cutoff frequency for the transformed spectrum must be chosen that is less than the limit just mentioned. This limit was taken as the frequency at which the spectral density is a relative minimum, f_{ζ} min . The choice is arbitrary, as it is not possible to say how the energy lost through breaking is distributed across the spectrum. As noted earlier, this depends on the history of depth and current encountered by the waves as they propagate to the point in question.

There is a probability, however small, that waves will break in any part of the spectrum. It will be shown in the next chapter that in deep water breaking waves are most probable at high frequencies, but that at depths smaller than a critical value there is a sudden shift of the maximum breaking probability toward lower frequencies.

It will be assumed therefore that the frequency $\underset{\sim}{f}$ min is a reasonable cutoff point before depths become so shallow that the largest waves frequently break. For the purpose of computation the relative change in average wave height becomes

$$\overline{K} = \frac{\overline{H}}{\overline{H}_o} = \left[\frac{\int_0^{\underset{\sim}{f}\,\min} S_{\underset{\sim}{f}}(f)\,df_{\underset{\sim}{f}}}{\int_0^{4} S_{\underset{\sim}{f}_o}(f)\,df_{\underset{\sim}{f}}} \right]^{\frac{1}{2}} , \qquad (6\text{-}33)$$

where

$$\underset{\sim}{f}\,\min \leq 4 \ .$$

The distribution of $\overline{K}$ with relative depth $d/\overline{T}_o^2$ and relative current $U/\overline{T}_o$ is shown in Figure 25 ($\overline{T}_o$ denotes the initial average zero upcrossing period). The behavior of $\overline{K}$ is very similar to that of K_{sc}, the shoaling-current coefficient for monochromatic waves (Figure 22). The most notable difference is that $\overline{K}$ is less than K_{sc} for strong opposing currents. This is because the increase in energy density for $\underset{\sim}{f} \leq \underset{\sim}{f}\,\min$ is partially compensated for by the loss of all energy where $\underset{\sim}{f} > \underset{\sim}{f}\,\min$ (breaking).

Change in Average Wave Periods

The relative change in average period with shoaling and currents can be computed by integration of the normalized spectra in deep water and in water of arbitrary depth and current. Using Rice's (1944) definition of $\overline{T}$ discussed in Chapter IV (equation [4-11]),

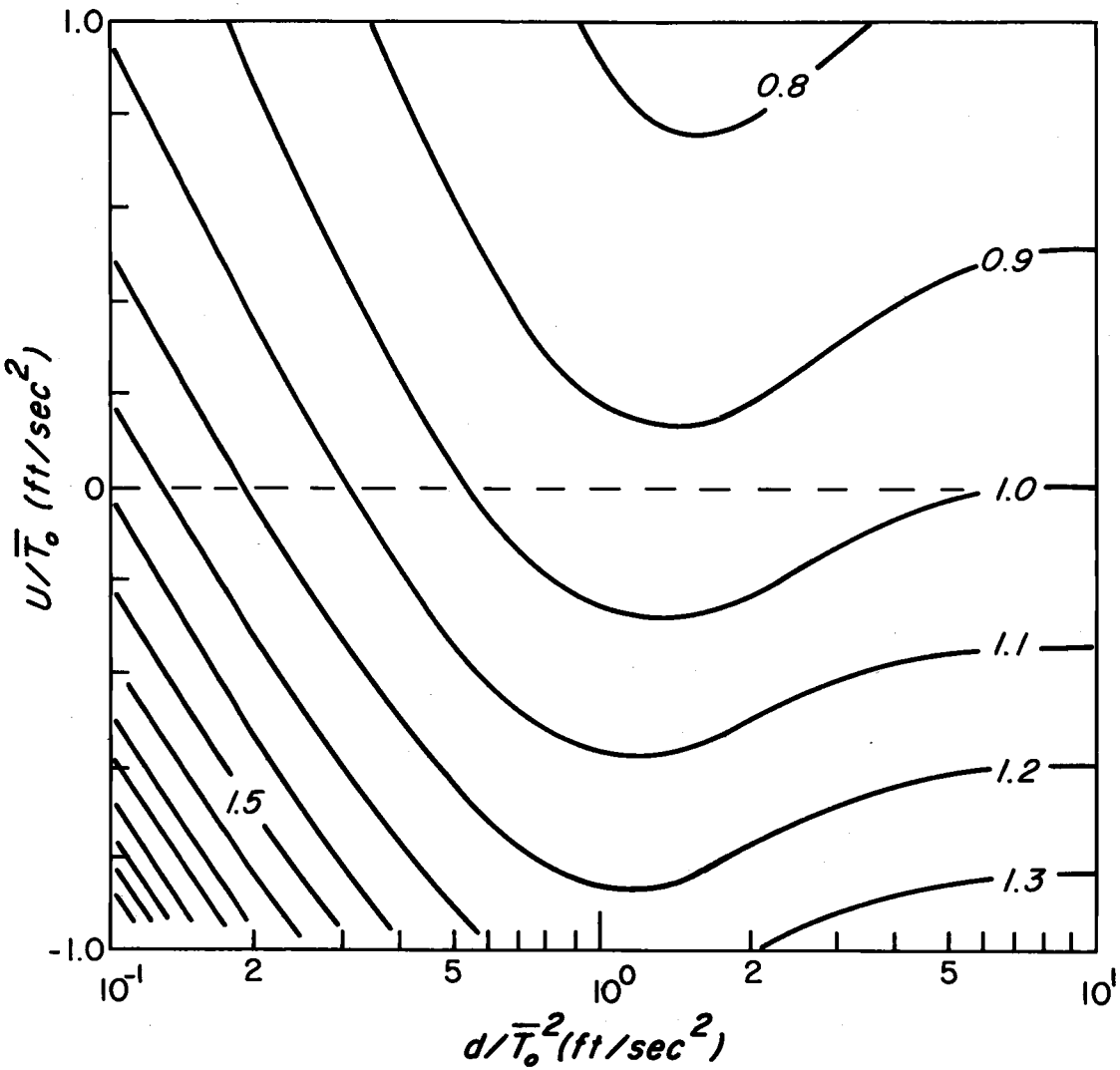

Figure 25. Height amplification factor ($\overline{K}$) derived from spectral transformations, as a function of relative depth ($d/\overline{T}_o^2$) and relative current ($U/\overline{T}_o$).

$$\frac{\overline{T}}{\overline{T}_o} = \left[\frac{\int_0^{f_{min}} S(f)\,df \Big/ \int_0^{f_{min}} f^2 S(f)\,df}{\int_0^{4} S_o(f)\,df \Big/ \int_0^{4} f^2 S_o(f)\,df} \right]^{\frac{1}{2}}, \qquad (6\text{-}34)$$

where f_{min} is as defined in (6-31).

The variation of $\overline{T}/\overline{T}_o$ is shown in Figure 26 as a function of $d/\overline{T}_o^2$ and $U/\overline{T}_o$. The amount of variation is not great over most of the domain of $d/\overline{T}_o^2$ and $U/\overline{T}_o$. The average period decreases somewhat at relatively large depths and moderate opposing currents. This reflects the increase in the spectral peak frequency discussed earlier in connection with Figure 24. This tendency is weakened as depth decreases because shoaling has the opposite effect on the spectral peak frequency. For strong opposing currents the truncation of the transformed spectrum becomes important, causing the average period to increase over the value in deep slack water.

Discussion and Conclusion

The results of this chapter should not be treated as having quantitative significance, except insofar as an actual situation satisfies the assumptions which have been made. At the entrance to the Columbia River, further modification of the wave spectrum can be expected due to refraction. Previous wave breaking below the cutoff frequency and departures from the idealized unaltered spectrum are also important sources of discrepancies.

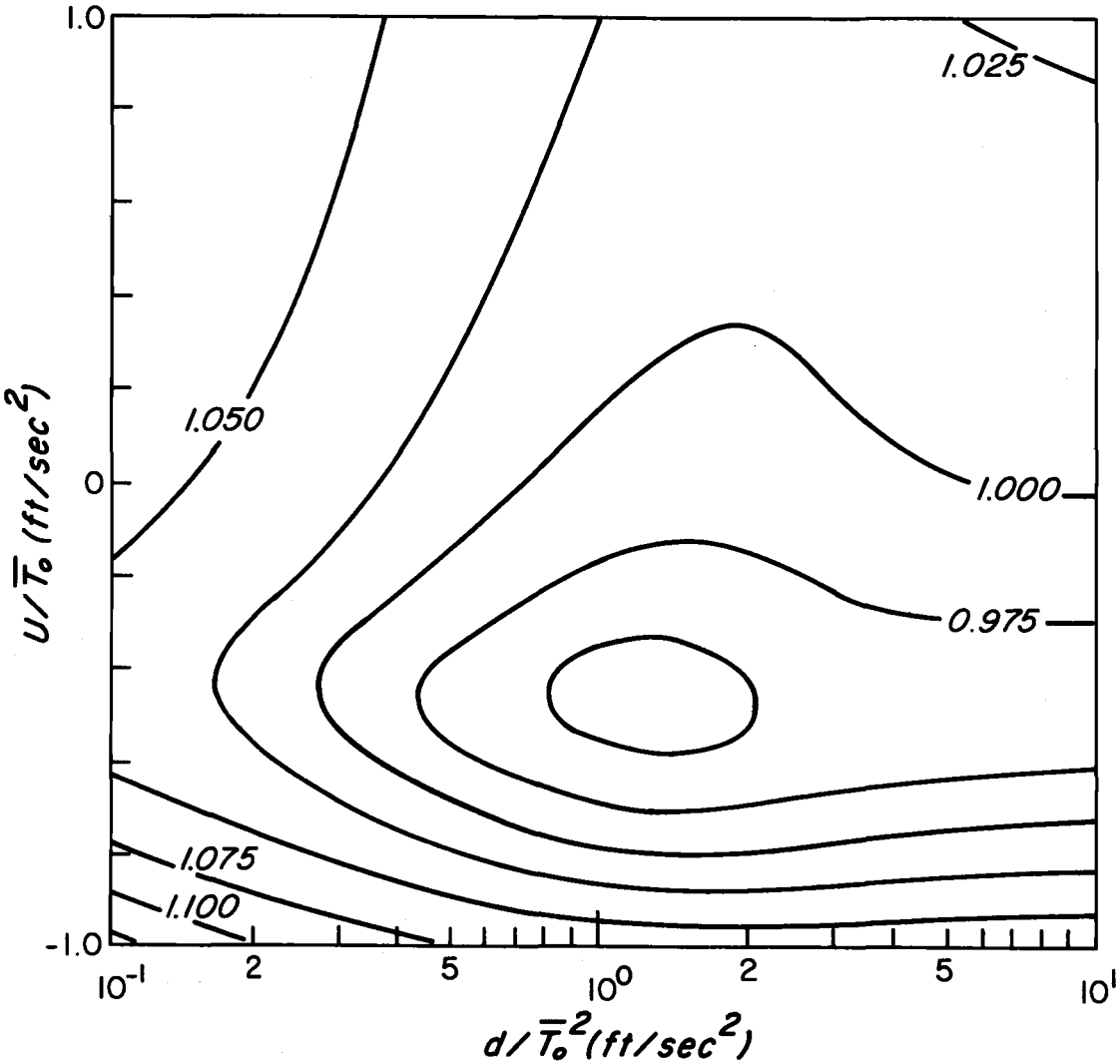

Figure 26. Period amplification factor derived from spectral transformations, as a function of relative depth ($d/\overline{T}_o^2$) and relative current ($U/\overline{T}_o$).

Refraction effects will be strongest in the areas of Peacock and Clatsop Spits, whereas it is appropriate to study the navigation hazard over the channel. Due to the channel depth, these effects will usually not be great. During ebb conditions, current and water depth induce refraction of opposing tendency (see discussion of refraction, Chapter II). The current effect is probably stronger during strong ebb conditions, causing additional increases in average height.

The history of wave breaking prior to arrival of the waves at the point in question will result in departures from the (average) height and period changes suggested in Figures 25 and 26. If swells arrive from west-northwest and a strong ebb current jet flows directly toward the oncoming waves seaward of the jetties, considerable wave breaking could occur over the shoal area off Peacock Spit. This would result in lower average heights between the jetty tips than would be expected from Figure 25. The effect on average period would depend on the period of the most probable breaking waves over the shoal area.

The assumption that the wave spectrum in deep slack water is narrow banded and of the Pierson-Moskowitz form is another limitation. The assumption is probably best after the cold front of a storm passes inland and the cross swell caused by the southerly winds of the storm's foresector disappears. At this time the spectrum, if previously bimodal, becomes unimodal. It should be noted, however, that deviations from the idealized spectrum are automatically accounted for if one performs transformations on the forecast or hindcast spectra. The results then depend on the ability of the forecast method, the forecaster and his data to simulate the actual spectra.

In spite of the difficulties in applying the techniques of this chapter to actual situations, the results agree qualitatively with physical logic and are useful in understanding the combined effect of shoaling and tidal streams on waves arriving at river mouths.

Nothing has been said of the effects of depth and current on wave steepness. The waves will be shorter and steeper at intermediate and shallow depths than in deep water. Ebb currents will induce additional steepening. However, a study of the statistical nature of wave breaking for such conditions is more useful than steepness in understanding the navigation hazard. Also, parameters related to breaking reflect on the steepness as well. The results of this chapter provide a useful basis for developing statistical indices related to wave breaking. This is done in the following chapter.

VII. DERIVATION OF A HAZARD INDEX FOR RIVER ENTRANCES FROM THE PROBABILITY OF BREAKING WAVES

Introduction

Wave breaking is in general random, even in the surf zone, except when only very regular swell are involved. This randomness is especially true during the winter along the Oregon-Washington coast. During the arrival of storm waves the surf zone becomes quite wide, with the largest waves breaking at its seaward edge and breaker heights decreasing toward shore.

Even over ship channels random breaking may occur, especially during ebb tide. As storm waves encounter the outer (weakest) portion of the ebb effluent, the short waves become extremely rough and break frequently. As the waves approach the jetties, the current becomes stronger and the period range of tumultuous wave breaking will shift toward higher values.

Waves whose periods are beyond this critical range will break randomly with increasing frequency. The random breaking of the longer "swell" is the most hazardous to pilots and navigators of large vessels. Occasionally, during severe storms, very hazardous conditions transcend the ebb tide effects and continue on the flood.

Given the capability of predicting deep water wave conditions, it is desirable to estimate the degree of navigation hazard which can be expected. This is in part a problem of transforming the wave spectrum according to physical principles (Chapter VI). Assuming the transformed

spectrum can be estimated for some point near the river entrance, one may arrive at the probability that a given wave will break, provided the statistical properties of wave heights and periods are known.

Related to this probability is a statistical function which emphasizes the breaking probability of waves in the period range associated with swell. This function is insensitive to assumptions about the distribution of wave periods. It therefore appears to be an ideal index of navigation hazard at river entrances during storm conditions.

In the following section the breaking index is developed as a function of depth and current. Then some of the pertinent literature regarding wave statistics is reviewed, with emphasis on the Rayleigh distributions for wave heights and squared periods.* Expressions are developed and discussed for breaking wave statistics in deep slack water as well as water of arbitrary depth and current. A useful statistical index for navigation hazard at river entrances is discussed and illustrated in an example.

The Breaking Index in Water of Arbitrary Depth and Current

A very useful parameter for many design purposes is the height of a breaking wave. The breaking height (H_b) is important to the development of this chapter because the probability that a given wave is breaking is related to the probability that the height exceeds H_b. For a

* Unless otherwise specified it will be assumed that heights and periods refer to those of zero upcrossing waves.

given depth and current, the breaking height depends on the wave period. Thus it is convenient to determine the breaking index H_b/T^2 as a function of relative depth and relative current:

$$\frac{H_b}{T^2} = \nu(d/T^2,\ u/T) \quad . \tag{7-1}$$

The functional form taken by (7-1) should be consistent with the known behavior of breaking waves in the absence of currents. The Stokes criterion for wave breaking is that the water particle velocity at the crest is just equal to the wave celerity. This leads to the result that the wave breaks in deep water when a critical steepness is attained,

$$\left(\frac{H_b}{L_b}\right)_{max} = 0.142 \quad , \tag{7-2}$$

where L_b is the wavelength of the breaking wave (Michell, 1893). Michell further showed that the deep water breaking length is greater than that expected from small amplitude wave theory (L_o). Specifically,

$$\frac{L_{ob}}{L_o} = 1.2 \quad , \tag{7-3}$$

where

$$L_o = \frac{gT^2}{2\pi} \quad . \tag{7-4}$$

Together, these equations yield

$$\frac{H_b}{T^2} = 0.875 \text{ ft/sec}^2 \tag{7-5}$$

for deep water. Since only waves in a developing sea break in deep water, the breakers are short crested and cusp-shaped, usually termed "white-caps".

As waves move into shallow water ($d < L_o/20$) they become "solitary" waves, that is, they behave independently of each other, or of the wavelength. Assuming that the Stokes criterion applies to solitary waves, McCowan (1894) showed that

$$\frac{H_b}{d} = 0.78 \quad , \tag{7-6}$$

i.e., the breaking height is determined only by the depth. Equations (7-2) through (7-6) are summarized by Dean and Eagleson (1966).

In water of intermediate depth the breaking height depends on both length and depth. Miche (1944) gives the limiting steepness as

$$\frac{H_b}{L_b} = 0.142 \tanh\left(\frac{2\pi d}{L_b}\right) \tag{7-7}$$

for water of arbitrary depth. The data of Danel (1952) show that (7-7) is satisfactory from an engineering standpoint (see discussion by Wiegel, 1964).

From small amplitude wave theory, the celerity and wavelength are given by

$$C^2 = \frac{gL}{2\pi} \tanh\left(2\pi\frac{d}{L}\right) \quad , \tag{7-8}$$

and

$$L = L_o \tanh\left(2\pi\frac{d}{L_b}\right) \quad . \tag{7-9}$$

Equation (7-9) follows from (7-8), (7-4) and the necessary condition that $C = L/T$. The fact that breaking waves are faster and longer than small amplitude waves might be accounted for by generalizing (7-3) to all depths. By this hypothesis, (7-8) and (7-9) become (for breaking waves)

$$C_b^2 = 1.2 \frac{gL_b}{2\pi} \tanh\left(2\pi \frac{d}{L_b}\right) , \qquad (7\text{-}10)$$

and

$$L_b = 1.2\, L_o \tanh\left(2\pi \frac{d}{L_b}\right) . \qquad (7\text{-}11)$$

By using (7-10) to eliminate the hyperbolic tangent in (7-7), we may obtain the breaking index

$$\frac{H_b}{T^2} = 0.12 \frac{2\pi}{g} \left(\frac{C_b}{T}\right)^2 . \qquad (7\text{-}12)$$

C_b may be found from (7-10) after L_b is successively approximated by iteration of (7-11) on a computer. The curves of H_b/T^2 and L_b/T^2 are shown in Figure 27 as functions of the relative depth, d/T^2. For comparison, the values given by stream-function theory are also shown (Dean, 1970).

At relative depths of 1 ft/sec^2 or less, the curve for H_b/T^2 approaches the line for 1:1 correspondence with d/T^2. This means that H_b becomes relatively independent of wave period at these depths. This is of considerable importance to the development of an index of navigation hazard at the river mouth, to be discussed in a subsequent section. The agreement shown in Figure 27 is sufficient for the purposes of this study.

Equations (7-10) and (7-12) may be easily extended to include the case of non-zero current. Assuming that the period is constant for a wave which eventually breaks in water of current U, then

$$\frac{L_b}{L_o} = \frac{C_b + U}{C_o} \quad , \tag{7-13}$$

where $C_o = gT/2\pi$ and $L_o = gT^2/2\pi$ may be assumed to apply to deep slack water (small amplitude theory yields good approximations until shortly before the limiting steepness is reached). Substituting (7-13) into (7-10), and expressing C_o and L_o in terms of T, one obtains,

$$\left(\frac{C_b}{T}\right) = 1.2\,\frac{g}{2\pi}\left(\frac{C_b}{T} + \frac{U}{T}\right)\tanh\left(\frac{2\pi d/T^2}{C_b/T + U/T}\right) \tag{7-14}$$

which may be solved directly by iteration.

The breaking index from (7-12) and (7-14) varies with d/T^2 and U/T as shown in Figure 28. For a given depth and period, the breaking height is less for opposing currents than for slack water or following currents. The wavelength is decreased when waves encounter an opposing current, so that the height must also be less when the limiting steepness for breaking is reached.

The insensitiveness of H_b to wave period for $d/T^2 \leq 1$ ft/sec^2 also applies to cases where currents are involved. This condition extends to somewhat greater depths for following currents, and somewhat lesser depths for opposing currents.

It is readily seen that in the limit of shallow depths (where the hyperbolic tangent may be approximated by its argument) equations (7-12)

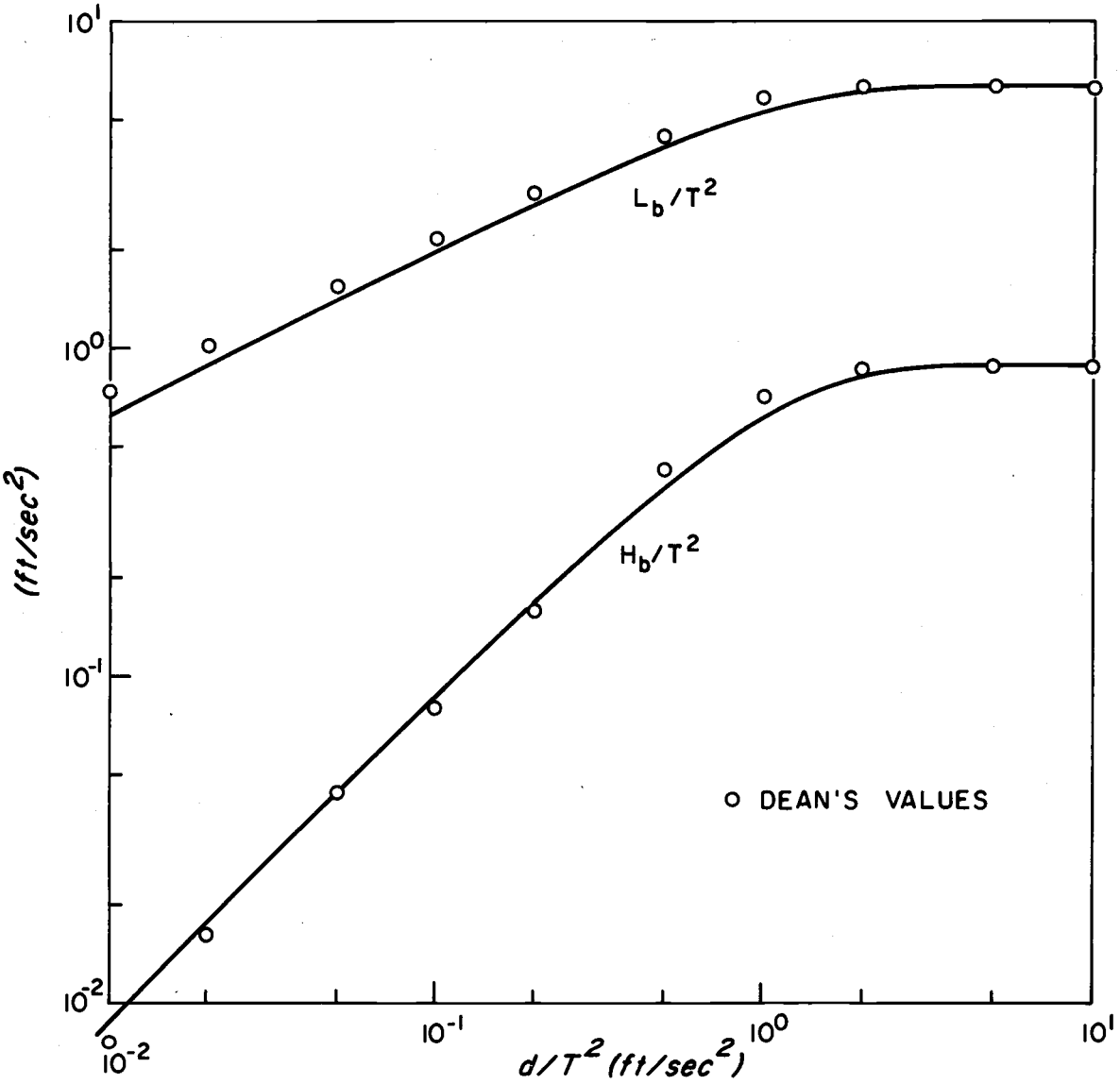

Figure 27. Heights (H_b) and lengths (L_b) of breaking waves relative to squared period, shown as functions of relative depth (d/T^2). Solid curves are given by equations (7-10), (7-11) and (7-12); plotted points were numerically computed from stream function theory by Dean (1970).

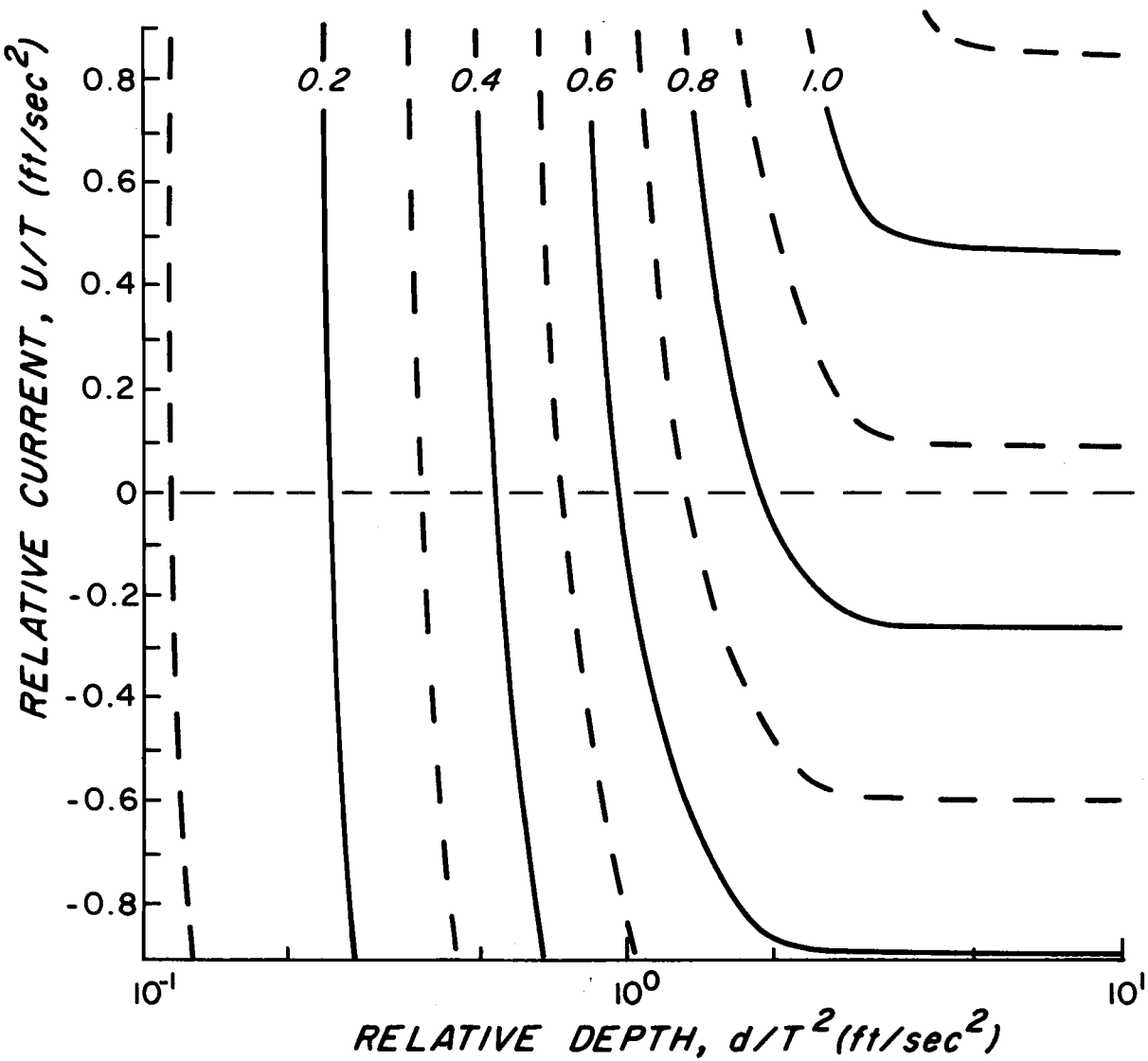

Figure 28. Breaking index, H_b/T^2 (ft/sec^2), as a function of relative depth and relative current.

and (7-14) give $H_b \doteq 0.142(2\pi)d = 0.89d$. Thus these relationships give a higher breaking height in very shallow water than (7-6). This discrepancy is less at greater depths, and is reversed at intermediate depths (Figure 27). Though the functional relationships do not conform perfectly to theory, they provide a practical means of computing $\nu = H_b/T^2$ as a function of both depth and current.

Height and Period Statistics

It is well known that the heights and periods of ocean waves are not regular but statistically distributed. Various mathematical functions have been proposed to account for these distributions, the foremost being the Rayleigh distribution for wave heights, and the Rayleigh distribution for squared wave period. The moments of these distributions are simply related by the gamma function.

Longuet-Higgins (1952) showed theoretically that when the wave spectrum is narrow-banded, the maxima of water surface elevation follow a Rayleigh distribution. For such a spectrum the wave height is twice the surface elevation maximum, and therefore is also Rayleigh-distributed. Thus,

$$P(H \leq h) = F_H(h) = 1 - \exp[-(h/\eta)^2] \qquad (7\text{-}15)$$

and

$$f_H(h) = \frac{dF_H}{dh} = 2h/\eta^2 \exp[-(h/\eta)^2] \quad . \qquad (7\text{-}16)$$

Here, F_H and f_H are referred to respectively as the cumulative distribution function and the marginal probability density function (p.d.f.) for the random variable H (height). The notation P(A) denotes the

probability that H occupies the sample subspace A, h refers to a particular value or realization of H, and η is the root mean square (r.m.s.) value of H.

The Rayleigh distribution for wave heights has been shown by Bretschneider (1959), Goda (1970) and others to have a wide applicability. Moreover, Goda found that the distribution is applicable over a wide range of spectral width. Thus the assumption that (7-15) holds is a reasonably good one.

Longuet-Higgins (1952) determined the relationship of the various average wave heights to the r.m.s. height for narrow banded spectra:

$$\begin{aligned} \overline{H} &= 0.89\,\eta \\ H_{1/3} &= 1.41\,\eta \\ H_{1/10} &= 1.80\,\eta = 1.28\,H_{1/3} \end{aligned} \qquad (7\text{-}17)$$

Goda confirmed these numerically and found them to vary from (7-17) for sufficiently broad spectra. His results show that they are applicable to waves with a Pierson-Moskowitz spectrum.

There is much less uniformity regarding the distribution of wave periods. Various distributions such as the Putz or log-normal distributions have been proposed, but the Rayleigh distribution for squared periods is the most widely accepted. Bretschneider (1959) gave both physical arguments and considerable observational evidence for the Rayleigh distribution. Goda (1970) numerically simulated waves from spectra of varying functional shapes and compared the resulting distributions with the theoretical ones. He found the T^2-Rayleigh distribu-

tion to be in fair agreement with that of the Pierson-Moskowitz spectrum, but considerably different from those of other spectral forms, especially double-peaked spectra.

The T^2-Rayleigh distribution is given by

$$P(T^2 \leq t^2) = F_{T^2}(t) = 1 - \exp[-(t^2/\tau^2)^2] \qquad (7\text{-}18)$$

where τ^2 is the r.m.s. squared period and t is a realization of the random variable T(period). The corresponding marginal p.d.f. for periods is

$$f_T(t) = \frac{4t^3}{\tau^4} \exp[-(t/\tau)^4] \quad . \qquad (7\text{-}19)$$

The kth moment of (7-19) is given by

$$M_k = \overline{T^k} = \int_0^\infty t^k f_T(t)dt = \tau^k \Gamma(1 + \tfrac{k}{4}) \ , \qquad (7\text{-}20)$$

from which the average period becomes

$$\overline{T} = 0.91\tau \quad . \qquad (7\text{-}21)$$

It has been shown by Bretschneider (1959) and confirmed experimentally by Goda (1970) that

$$\overline{T} = 0.71\hat{f}^{-1} \quad , \qquad (7\text{-}22)$$

where $\hat{f}$ is the spectral peak frequency for a spectrum of Pierson-Moskowitz form.

By setting the derivative of (7-19) equal to zero, the most probable period, t_m, is

$$t_m = 0.93\tau = 1.03\overline{T} \qquad (7\text{-}23)$$

and

$$t_m = 0.73\ \hat{f}^{-1} \quad . \qquad (7\text{-}24)$$

The relationship between wave spectra of the Pierson-Moskowitz form and the T^2-Rayleigh distribution has been demonstrated by Bretschneider (1959) and Goda (1970). This relationship and (7-21), (7-22) and (7-23) should remain valid under the shoaling-current transformations described except in the case of opposing currents. They presumably break down if extensive losses of wave energy occur due to bottom friction, percolation, and wave breaking. Bretschneider (1963b) argued that a single-peaked spectrum in deep water may become double-peaked in the surf zone due to the successive action of bottom friction, percolation and shoaling (Gulf of Mexico).

The correlation between heights and periods and its variation with spectral characteristics have not been studied extensively enough to draw definitive conclusions. Bretschneider (1959) found correlation coefficients from 0.08 to 0.65 between heights and squared periods, increasing for decreasing spectral width. Bretschneider suggested that "zero correlation quite likely exists between H and T for a fully developed sea" and that "non-correlation is perhaps the most likely to be encountered by engineers and oceanographers".

Goda (1970) found the correlation between (zero upcrossing) heights and periods to be strongly affected by spectral width, increasing with increasing width. This is seemingly contrary to Bretschneider's results. Goda concluded that further field analysis is needed to clarify this.

The Truncated Distribution For Wave Periods

The effects of opposing currents on the wave spectrum were discussed in the previous chapter. Waves cannot propagate against a current if the wave period is less than some critical value. They therefore dissipate all of their energy in breaking and the spectrum is truncated at high frequencies. Though this phenomenon has been noted visually by observers (e.g. Isaacs, 1948), there is no observational evidence (to my knowledge) regarding the statistical distribution of such waves after this truncation has been effected.

If the wave-breaking activity takes place chiefly at periods near and below the "cutoff" period, then the shape of the distribution for longer periods should not be affected. That is, the probability density of the remaining periods should be increased equally, in proportion to the "lost" probability.

This may best be seen by expressing (7-18) in terms of the most probable period, t_m :

$$F_T(t) = 1 - \exp\{-\frac{3}{4}(t/t_m)^4\} \qquad (7\text{-}25)$$

(since $t_m^4 = 3/4\ \tau^4$). The choice of t_m is appropriate because the most probable period should maintain its relationship with the spectral peak frequency (7-24), whereas truncation will bring about an increase in all moment-related periods, such as τ . The truncated distribution $F_T'(t)$ is limited to the sample space $t_c < t < \infty$, where t_c denotes the cutoff period. Therefore (7-25) must be normalized by the total probability that a period lies in this range. Thus,

$$F_T'(t) = \frac{F_T(t) - F_T(t_c)}{1 - F_T(t_c)}$$

$$= 1 - \exp\{-\tfrac{3}{4}[(t/t_m)^4 - (t_c/t_m)^4]\} \quad , \qquad (7\text{-}26)$$

and the corresponding p.d.f. becomes

$$f_T'(t) = 3t^3/t_m^4 \exp\{-\tfrac{3}{4}[t/t_m)^4 - (t_c/t_m)^4]\} \qquad (7\text{-}27)$$

where $t_c < t < \infty$.

The expression relating τ to t_m may be obtained from the fourth moment of $f_T'(t)$. Letting z denote the argument of the exponential in (7-27) we obtain, after some manipulation,

$$\tau^4 = \overline{T^4} = \int_{t_c}^{\infty} t^4 f_T'(t)dt$$

$$= \frac{4}{3} t_m^4 \int_0^{\infty} ze^{-z}dz + t_c^4 \int_0^{\infty} e^{-z}dz$$

$$= \frac{4}{3} t_m^4 + t_c^4 \quad . \qquad (7\text{-}28)$$

Thus τ increases with t_c as expected. But because τ is proportional to the fourth root of (7-28), its increase in not large until t_c nears t_m . Solving for t_m^4 , (7-27) may be expressed in an alternate form,

$$f_T'(t) = \frac{4t^3}{(\tau^4 - t_c^4)} \exp\{-(\frac{t^4 - t_c^4}{\tau^4 - t_c^4})\} \quad . \qquad (7\text{-}29)$$

When $t_c = 0$, both (7-28) and (7-29) reduce to the corresponding relationships for the untruncated distribution, (7-19) and (7-23). However, the relationship between the most probable period and the spectral

peak frequency should remain as given by (7-24) even when $t_c \neq 0$, provided (1) wave-breaking is confined predominantly to low period values and (2) the truncation period remains low enough that waves of period $T = t_m$ do not frequently break. If these conditions are not satisfied, the distribution (7-29) may only be reasonable at the onset of breaking.

One is forced to conclude that for strong opposing currents even the largest waves will break frequently and the period distribution will become unstable and degenerate. If the waves are initially distributed as T^2-Rayleigh, the truncated distribution (7-29) is reasonable for moderate opposing currents until just after water depths are shallow enough for the largest waves to break (i.e. swell).

Even when (7-29) may be considered applicable there exists some probability that random wave breaking will occur. This is to be taken up in the next section.

Breaking Wave Probability

The subject of this section is the breaking wave probability, or the probability that a given wave will break. This is to be distinguished from the tumultuous breaking which occurs at short wavelengths (periods) at ebb tide, i.e., at periods near or below the cutoff period (t_c) discussed in the previous section. For verification purposes the breaking-wave probability may be considered the fraction of breaking waves in a wave record.

Much insight to the following development was obtained from the work of F. L. Ramsey and J. H. Nath, which has not yet been published. They are developing expressions for the probability distribution functions of breaking waves in the Eastern North Pacific Ocean, verified with observations and measurements from the Canadian weather ship at station Papa. In particular, I am indebted to them for the derivation of the probability that a wave is breaking in deep slack water.

To illustrate the logic of the statistical arguments, the breaking probability is first derived for deep slack water. These arguments are then extended to include water of arbitrary depth and (opposing or following) current. The variations of statistical breaking properties with depth and current are illustrated by means of an example.

The expressions for the breaking wave probability evolve from the following assumptions:

(i) wave heights are Rayleigh distributed without exceptions;

(ii) squared wave periods are Rayleigh distributed in water of arbitrary depth and/or following currents;

(iii) the distribution of wave periods is given by the truncated distribution when the mean current opposes the waves;

(iv) heights and periods are uncorrelated.

Application of these ideas to the wave spectra transformed from deep slack water requires the additional assumption that

(v) the most probable period is related to the spectral peak frequency by an invariant factor (7-24).

Deep Slack Water

The probability that a given wave is breaking may be restated as the probability that the limiting height is exceeded:

$$P_{bw} = P(H > H_b) = P(H > \nu T^2) \quad , \tag{7-30}$$

Where ν is the breaking index defined by (7-1) and H and T are the random variables for height and period.

The probability that a wave of period $T = t$ is breaking is (with the aid of [7-15])

$$\begin{aligned} P(H > \nu t^2) &= 1 - P(H \leq \nu t^2) \\ &= 1 - F_H(\nu t^2) \\ &= \exp[-(\nu t^2)^2/\eta^2] \quad . \end{aligned} \tag{7-31}$$

The probability that $t < T < t + dt$ is (from [7-19])

$$P(t < T < t + dt) = f_T(t)dt = \frac{4t^3}{\tau^4} \exp[-(t/\tau)^4]dt \quad . \tag{7-32}$$

If heights and periods are independent, the probability that $t < T < t + dt$ and the wave breaks is the product of (7-31) and (7-32):

$$\begin{aligned} g(t)dt &= P(H > \nu T^2 \text{ and } t < T < t + dt) \\ &= \exp[-(\nu t^2)^2/\eta^2]\exp[-(t/\tau)^4] \frac{4t^3}{\tau^4} dt \\ &= \exp[-(t/\tau)^4(1 + Q^{-2})]\frac{4t^3}{\tau^4} dt \quad , \end{aligned} \tag{7-33}$$

where $Q = \eta/\nu\tau^2$. The parameter Q is the ratio of the r.m.s. wave height to the height of a breaking wave of period $T = \tau$. Finally,

the probability that the wave breaks regardless of its period is the integral of the product function $g(t)$ over all periods. In deep slack water the breaking index is a constant, $\nu = 0.875$ ft/sec^2 , so that (7-33) is easily integrated in closed form. With the change of variable $z = t^4/\tau^4$,

$$\begin{aligned} P_{bw} = P(H > \nu T^2) &= \int_0^\infty g(t)dt \\ &= \int_0^\infty \exp[-z(1 + Q^{-2})]dz \\ &= (1 + Q^{-2})^{-1} \quad . \end{aligned} \tag{7-34}$$

The marginal p.d.f. for breaking-wave periods, $f_T^*(t)$, is related to the relative frequency of the event "$t < T < t + dt$ <u>given</u> that $H > \nu T^2$". From (7-33) and (7-34),

$$P(t < T < t + dt | H > \nu T^2) = \frac{P(t < T < t + dt \text{ and } H > \nu T^2)}{P(H > \nu T^2)}$$

$$= f_T^*(t)dt = P_{bw}^{-1}\, g(t)dt \quad .$$

In other words,

$$f_T^*(t) = (1 + Q^{-2})\, \exp[-(t/\tau)^4(1 + Q^{-2})]\frac{4t^3}{\tau^4} \quad . \tag{7-35}$$

Using (7-20) and the change of variable $z = (t/\tau)^4(1 + K^{-2})$ the <u>k</u>th moment of (7-35) is

$$\begin{aligned} M_k = \overline{T_b^{\,k}} &= \tau^k(1 + K^{-2})^{-k/4} \int_0^\infty z^{k/4}\, e^z dz \\ &= (P_{bw})^{k/4}\, \tau^k \Gamma(1 + k/4) \\ &= (P_{bw})^{k/4}\, \overline{T^k} \quad . \end{aligned} \tag{7-36}$$

Thus any representative period $(\overline{T_b^k})^{1/k}$ for breaking waves has the same simple relationship with the corresponding period for all waves $(\overline{T^k})^{1/k}$:

$$(\overline{T_b^k})^{1/k} = (\overline{T^k})^{1/k} \, P_{bw}^{1/4} \quad ; \tag{7-37}$$

specifically,

$$\tau_b/\tau = P_{bw}^{1/4} \quad . \tag{7-38}$$

As an example of (7-34) and (7-38) consider waves in deep slack water with an r.m.s. height $\eta = 14$ feet and periods such that $\tau = 10$ seconds. The probability of wave breaking is 2.5% and $\tau_b/\tau = 0.4$ -- that is, periods of breaking waves are generally a little less than half those for all waves.

Probability of breaking in water of arbitrary depth and current

In water of arbitrary depth and current the breaking index depends upon wave period and the period distribution may in general be truncated at low periods (opposing currents). From (7-29) and (7-31) the product function $g(t)$ becomes

$$g(t) = \exp[-(\nu t^2)^2/\eta^2] \exp\left[-\left(\frac{t^4 - t_c^4}{\tau^4 - t_c^4}\right)\right] \frac{4t^3}{\tau^4 - t_c^4} \quad . \tag{7-39}$$

Then

$$P_{bw} = \int_{t_c}^{\infty} g(t)\,dt \quad ,$$

the p.d.f. for periods of breaking waves is

$$f_T^*(t) = P_{bw}^{-1} g(t) \quad , \text{ and}$$

$$\tau_b/\tau = \tau^{-1} \left[P_{bw}^{-1} \int_{t_c}^{\infty} t^4 \, g(t)\,dt\right]^{\frac{1}{4}} \quad .$$

Because of the complicated functional dependence of ν on period, these integrations are done numerically on a computer.

An example

The behavior of $P(H > \nu t^2)$, $f_T(t)$, $g(t)$, P_{bw} and τ_b/τ as functions of depth and current are shown in Figures 29 and 30. At each depth and current the spectrum (deep slack water) of waves with η_o = 15 feet and τ_o = 10 seconds was transformed as described in Chapter VI. Thus the r.m.s. height (η) at the depth and current in question is the result of applying the amplification factor of Figure 25, where $\overline{T}_o$ = 0.9 τ_o. The corresponding value of τ was obtained from the spectral peak frequency of the transformed spectrum using (7-24) and (7-28).

Variations with depth (no current) are shown in Figure 29a,b,c,d. The conditional probability of wave breaking at period t, $P(H > \nu t^2)$, is shown in Figure 29a, while Figure 29b shows the period probability density $f_T(t)$. Figure 29c shows the product function, $g(t)$, and Figure 29d gives the variation of P_{bw} and τ_b/τ with depth. The following features may be noted:

a. The conditional probability of breaking in deep water is appreciable only for periods less than six seconds, where the probability density for periods is low. Thus P_{bw} is small and breaking periods are short relative to all periods, i.e. τ_b/τ is small. This condition might apply to short-crested whitecaps in a developing sea.

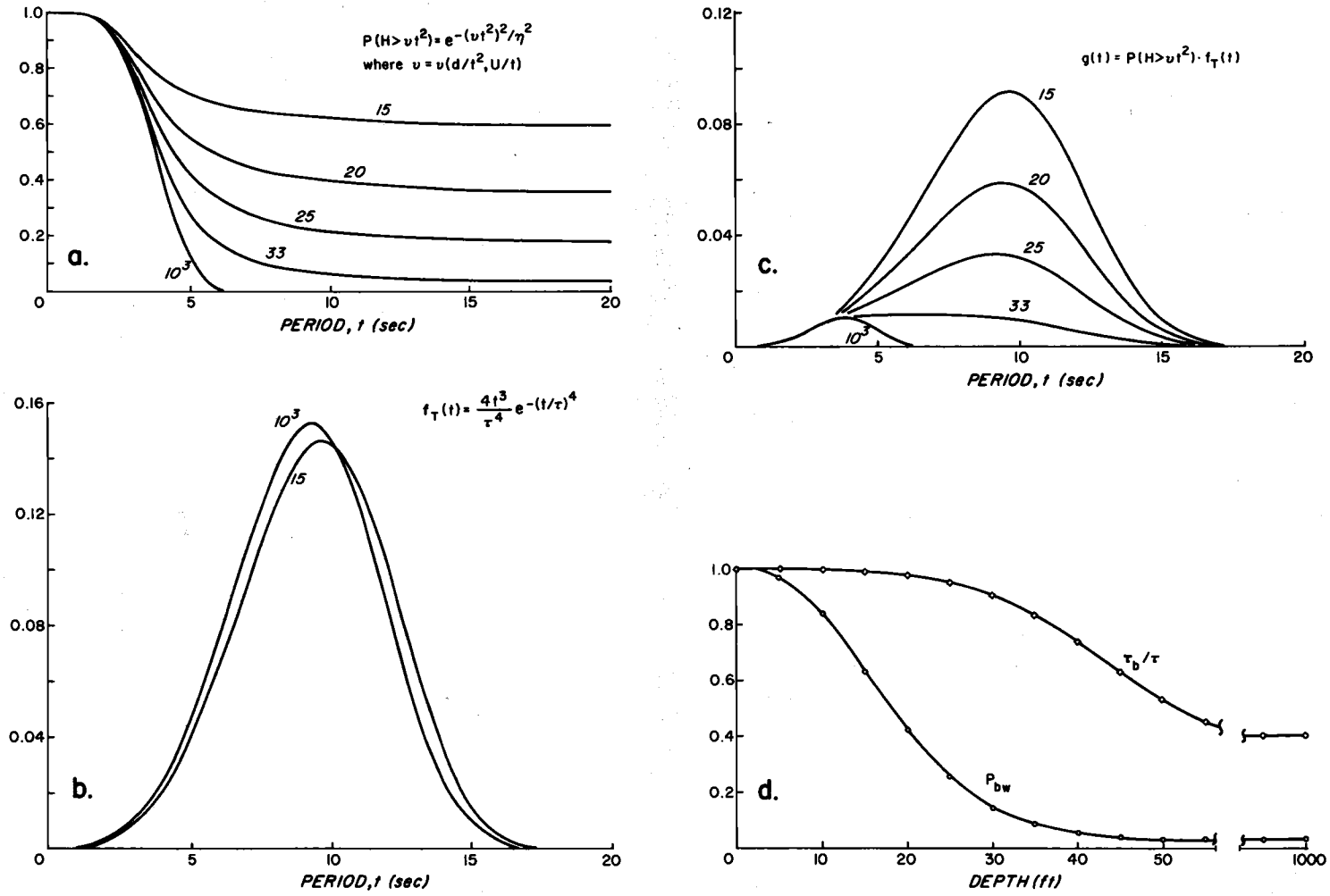

Figure 29. Statistical properties of waves and breakers at several depths (feet) in slack water. Symbols and functions are defined in the text; η and τ were found by spectral transformation from deep slack water where η_o = 15 feet and τ_o = 10 seconds.

b. At intermediate and shallow depths the conditional probability of breaking increases. At periods near or beyond the most probable period (say $t \geq 8$ seconds) it becomes insensitive to period change (because of the behavior of the breaking index noted in the second section of this chapter). At depths for which the conditional probability of breaking becomes appreciable at longer periods, the product function g(t) at those periods also becomes significant.

c. The apparent shift of the predominant breaking wave period from lower to higher values occurs at a depth of 33 feet. This is an intermediate depth for waves with the average zero upcrossing period (nine seconds). Waves with the average period become strictly "shallow" when $d = (g\bar{T}_o^2/2\pi)/20 = 21$ feet. At "shallow" depths τ_b/τ is almost unity and P_{bw} rises very rapidly, indicating entry into a surf zone.

d. The transition from low to high values of τ_b/τ takes place over a relatively narrow range of depths, from 50 feet to 30 feet. At depths of over 50 feet breaking waves have essentially the same statistical characteristics as in deep slack water, even though waves of average upcrossing period are not "deep" until depths exceed 200 feet.

e. Shoaling has relatively little effect on the probability distribution of wave periods except to increase somewhat the predominant period. Shoaling therefore affects breaking wave statistics principally through the behavior of the conditional probability of breaking (Figure 29a).

Variations with current (depth = 30 feet) are shown in Figure 30a, b,c,d. The parameters shown are those of the corresponding portions of Figure 29, but for varying current (negative currents are opposing). The following features may be noted:

f. The conditional probability of breaking (Figure 30a) decreases for following currents and increases for opposing currents, the effect of opposing currents being greater. At periods near or longer than the predominant period it is relatively unchanging as a function of period. However, the dependence on period increases somewhat for opposing currents.

g. There is little change in the most probable period (Figure 30b). The truncation of the probability distribution for periods results in higher probability densities since the area under the curve $f_T(t)$ must be invariant. The increases in the product function $g(t)$ are therefore a result of increases in both the probability density of periods and the conditional probability of breaking.

h. The increase of P_{bw} with opposing current (Figure 30c) is mainly the result of the increase in the conditional probability of breaking. This is at first surprising in view of the previous observation. It is because the increase in $g(t)$ due to the increase of $f_T(t)$ is compensated for by the truncation. This means that the area under $g(t)$ (proportional to P_{bw}) is relatively insensitive to changes in $f_T(t)$. This fact is of importance in the following section.

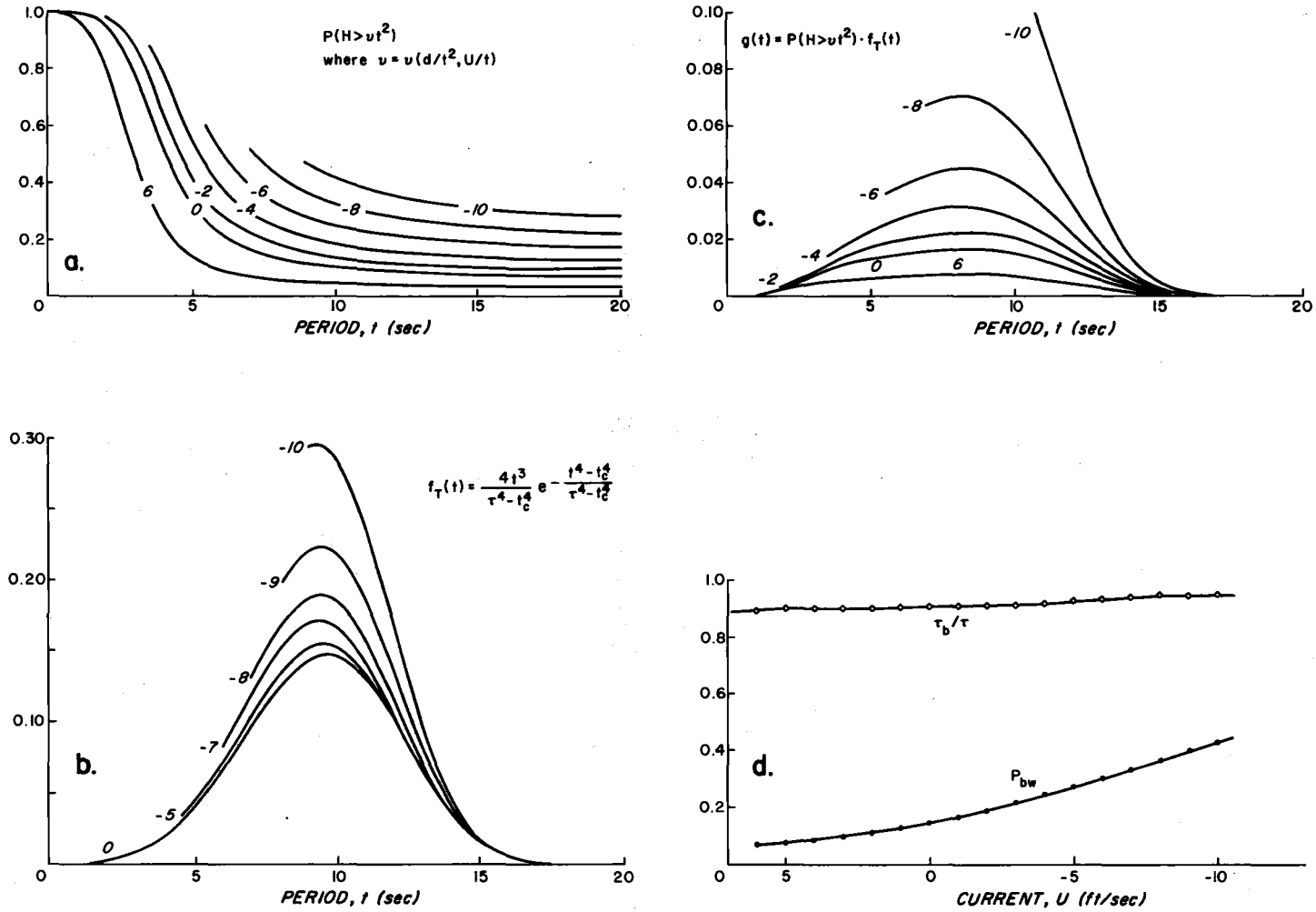

Figure 30. Statistical properties of waves and breakers at several current strengths (ft/sec) and a water depth of 30 feet (negative currents are opposing). Symbols and functions are defined in the text; η and τ were found by spectral transformation from deep slack water where η_o = 15 feet and τ_o = 10 seconds.

i. For the particular depth chosen in Figure 30c, there is little change in τ_b/τ , which is uniformly high. For depths greater than the transition depth (33 feet), a considerable increase of τ_b/τ from medium to high values is observed for opposing currents (due to truncation of the lower periods).

The following results are especially significant in regard to the statistics of breaking waves in water of arbitrary depth and current:

(1) The probability that a given wave breaks at water depths of up to 50 feet appears to be insensitive to the exact form of the probability distribution for periods. Variations of P_{bw} result mainly from changes in the conditional probability of breaking (at the period $T = t$). Because of the previously noted behavior of the breaking index, the conditional probability is insensitive to period changes at periods near or longer than, say, the average zero upcrossing period in deep slack water.

(2) In slack water where waves of average zero upcrossing period have a relative depth $d/\overline{T}_o^2 \geq 0.6$ ft/sec^2 , the breaking wave statistics are essentially those of very deep water. Thus, for example, storm waves for which $\overline{T}_o = 12$ seconds would have a breaking probability given by the simple closed-form equation (7-34) at a platform in 85 feet of water (in contrast to 380 feet as expected by the classical criterion for deep water, $d/\overline{T}_o^2 \geq 2.56$ ft/sec^2). This simplifies greatly the problem of studying breaking wave excedances at offshore platforms.

(3) During a strong ebb in a tidal inlet, the periods of random breaking waves are near the predominant periods (for all waves) in deep slack water, no matter what the relative depth $d/\overline{T}_o^2$ may be over the channel. This is due to truncation of the probability distribution at lower periods. This truncation is due to tumultuous wave breaking at low periods seaward of the point in question (e.g. over the outer bar).

An Index of Navigation Hazard At River Entrances

Every navigator knows that when waves are large offshore, conditions will be hazardous at a river mouth, especially during ebb tide. But there exists no reliable measure of the hazard from one such situation to the next. This is because of the complex interaction of many factors -- in the case of the waves themselves the most important elements are the depth, current, and average height and period of the waves offshore. One expects the wave conditions to vary as some function of the parameters $H_{os}/\overline{T}_o^2$, $d/\overline{T}_o^2$, and $U/\overline{T}_o$ (H_{os} denotes the significant height in deep slack water).

The weakest assumption of the previous section is probably that the squared periods are described by the Rayleigh (or truncated Rayleigh) distribution. Yet this is not crucial to the determination of P_{bw} at the water depths typical of river entrances. This is because of the insensitivity of the conditional breaking probability to the longer wave periods.

For any given situation there exists some period t' such that

$$P_{bw} \approx P(H > \nu t'^2) \int_0^\infty f_T(t)dt \quad . \tag{7-40}$$

In deep water, t' is much less than $\overline{T}_o$. However, in relatively shallow water (e.g. $d/\overline{T}_o^2 \leq 0.4$ ft/sec^2), t' is near the predominant period, and slight deviations from t' do not seriously affect (7-40). This means that for zero upcrossing periods of 10 to 11 seconds or more in deep water (typical of storms), P_{bw} may be approximated by the conditional probability of breaking at $T = \overline{T}_o$, namely $P(H > \nu_o \overline{T}_o^2) = \exp[-(\nu_o \overline{T}_o^2/\eta^2)]$. Since the significant height at the point in question is $H_s = \sqrt{2}\eta$,

$$P_{bw} \simeq \alpha = \exp[-2(\nu_o \overline{T}_o^2)^2/H_s^2] \quad , \qquad (7\text{-}41)$$

where α is the desired hazard index, and $\nu_o = \nu(d/\overline{T}_o^2, U/\overline{T}_o)$. Note that the remaining quantity in the argument of (7-41) is $H_s/\overline{T}_o^2 = \overline{K} H_{os}/\overline{T}_o^2$, where $\overline{K}$ is the height amplification factor of equation (6-33). Thus the index α is in fact a function of all three parameters, $H_{os}/\overline{T}_o^2$, $d/\overline{T}_o^2$ and $U/\overline{T}_o$.

The index α is a satisfactory approximation to P_{bw} for storm waves at the Columbia River entrance. The following characteristics of α are useful for wave forecasting applications.

(i) it depends only on the statistical assumption that wave heights are Rayleigh distributed (a relative tenable assumption);

(ii) it is not necessary to determine changes in average period with changes in depth and/or current;

(iii) it is not sensitive to errors in forecast of $\overline{T}_o$; and

(iv) computation is straightforward.

The principal difficulty in the use of α lies in its sensitivity to H_s. Use of the deep water significant height (H_{os}) would ignore entirely the effects of shoaling and currents on heights. Modification of the significant height by an amplification factor such as that of Figure 25 would be an improvement, and probably sufficient for forecasting purposes, where other errors are large. For hindcasting and engineering purposes, however, a detailed study of refraction due to both depth and currents is probably advisable.

The breaking index can be rewritten as

$$\alpha = \exp[-2(H_b/H_s)^2] \qquad (7\text{-}42)$$

where $H_b = \nu_o \overline{T}_o^2$ (the breaking height for waves of period $T = \overline{T}_o$). The function (7-42) is shown in Figure 31. When the ratio H_b/H_s is unity, $\alpha = 13\%$. If H_s is doubled, keeping H_b constant, then the ratio is also doubled and α increases to 60%. For swell at water depths of 50 feet or less, ν_o is approximately proportional to $d/\overline{T}_o^2$, so that H_b and α are nearly independent of $\overline{T}_o$. Thus the significant height influences the hazard index much more than the average period does.

Figure 32 shows the behavior of the hazard index and the breaking probability with varying depth and current (H_s and $\overline{T}_o$ kept constant). The plots show the variation of tide stage, currents, P_{bw} and α over two diurnal cycles, at bathymetric depths of 30 and 50 feet. These depths are typical of the outer portion of Clatsop Spit and the navigation channel at the Columbia River, respectively. The significant

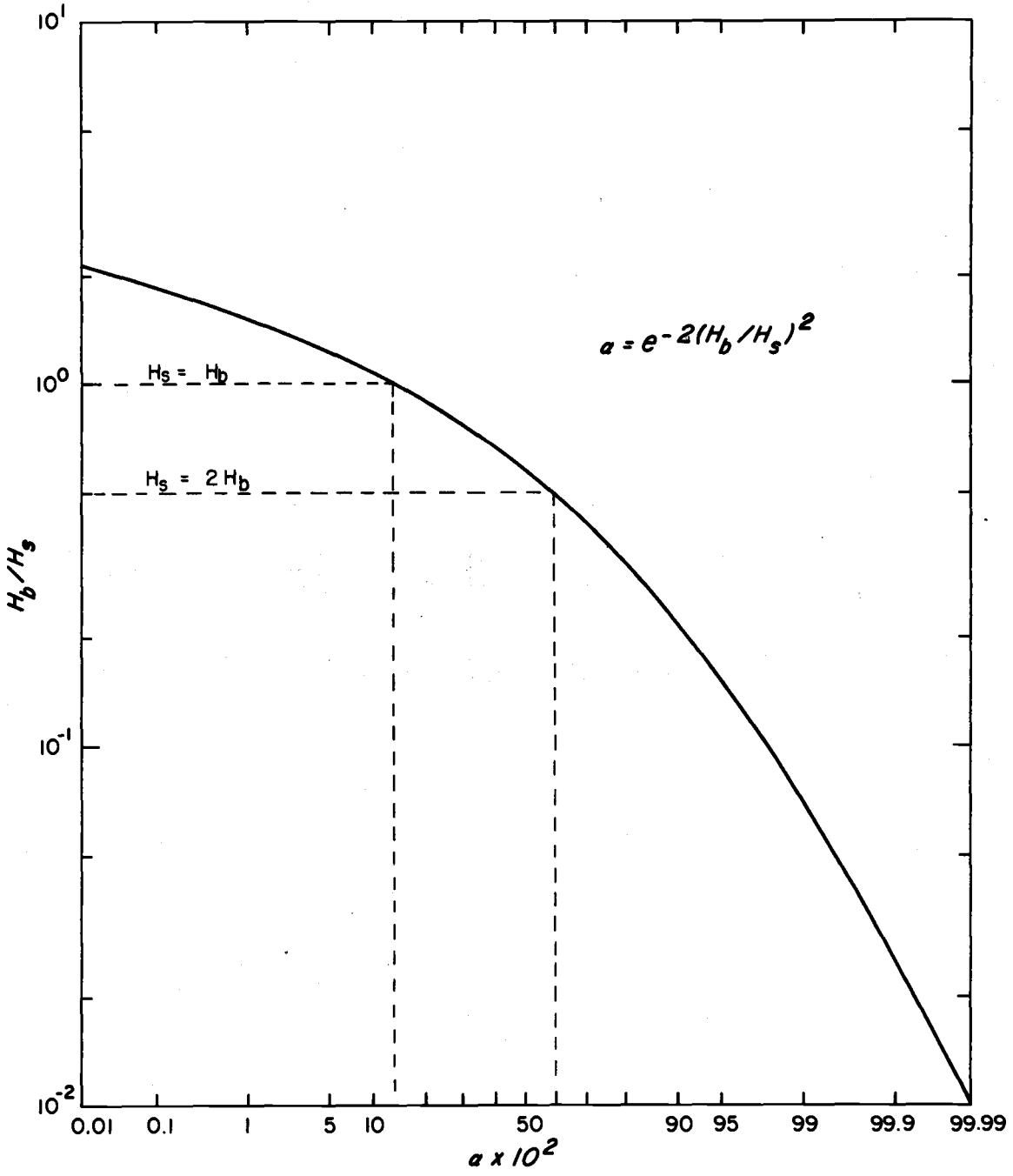

Figure 31. Hazard index α (%) as a function of the ratio of breaking height ($T = \bar{T}_o$) to significant height (at depth d, current U).

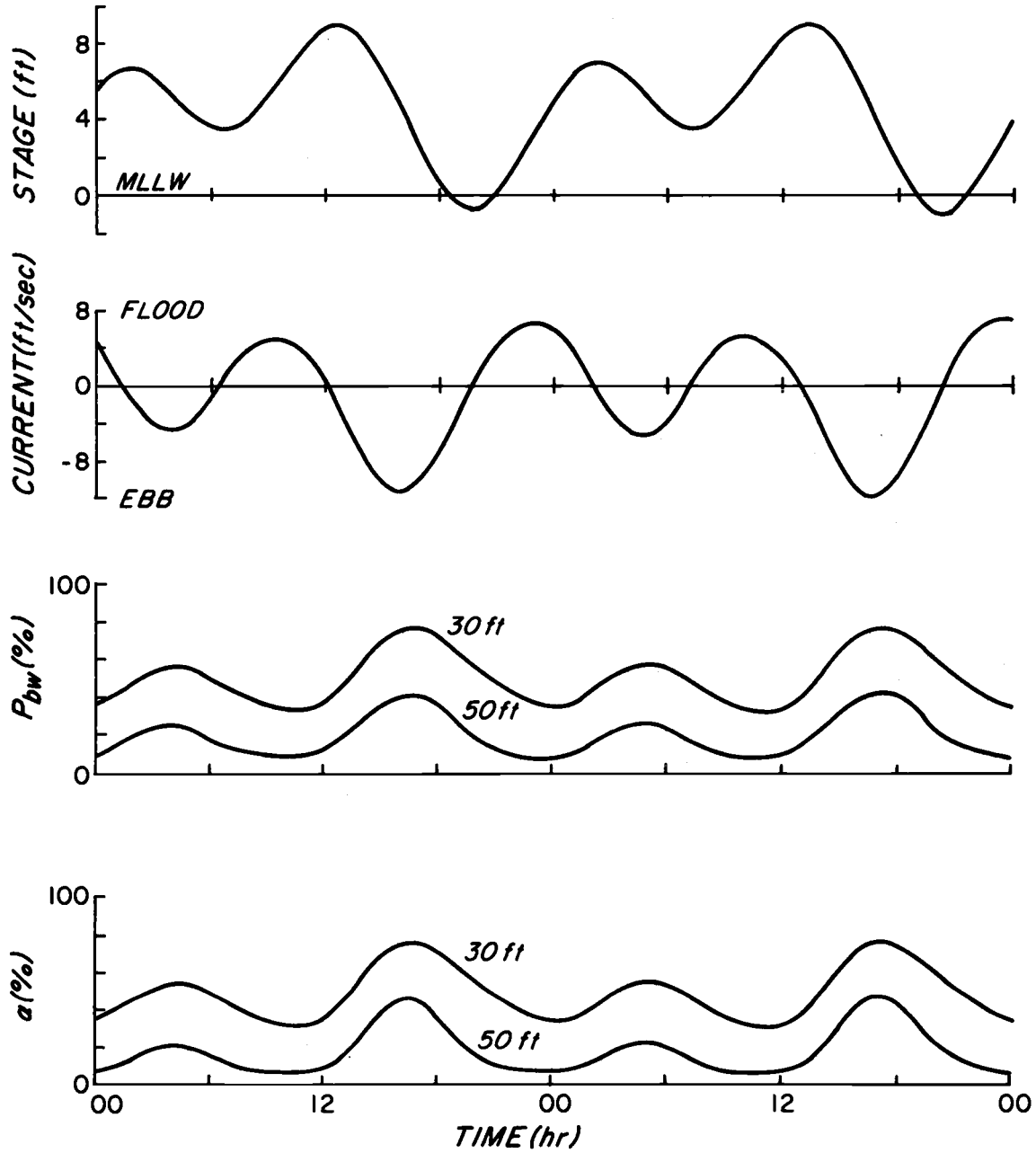

Figure 32. Tide stage and current (Columbia River entrance), probability of breaking (P_{bw}), and hazard index (α) over two diurnal tidal cycles; shown for bathymetric depths of 30 and 50 feet. Significant height and average period in deep slack water are 40 feet and 11 seconds.

height and average zero upcrossing period in deep slack water were kept constant at 40 feet and 11 seconds. Total depth is taken as the sum of the bathymetric depth (MLLW) and tide stage (MLLW). The hazard index α is computed as described previously, with the transformed significant height.

The index α follows P_{bw} quite closely at both depths. At the 50 foot depth α is slightly higher at the peak ebb, and slightly lower at the peak flood. The maxima of P_{bw} and α occur about one hour after the maximum ebb currents, due to decreasing tide stage. However the influence of tide stage variations is smaller than that of changes in tidal current and bathymetric depth. The latter two are about equal in their effect and induce variations of 30-40% in P_{bw} and α.

Summary

The breaking index (H_b/T^2) has been generalized to include the effects of current as well as depth. That is, $H_b/T^2 = \nu(d/T^2, U/T)$. For ocean swell at depths typical of river entrances (up to 50 feet), ν is only weakly dependent on the swell periods, and more strongly affected by water depth.

Assuming that wave heights and periods are statistically independent and distributed according to a Rayleigh function, an expression was derived for the probability of breaking waves in deep slack water, P_{bw}. The arguments used were extended to the case of arbitrary depth and current, using the function $\nu(d/T^2, U/T)$ and a truncated Rayleigh distribution for wave periods (when the mean current opposes the waves).

The probability that swell of a given period ($\geq$ 8 seconds) break at river entrances is strongly dependent on the r.m.s. wave height, the current and water depth, but only weakly dependent on the swell period (due to the behavior of the breaking index, ν).

It was noted that, when the significant wave height and average wave period are large (typical of high swell conditions), the probability that any wave breaks is very nearly equal to the probability that swell with the average period break (at river entrances). The latter probability depends on the steepness of waves in deep water and on the relative depth and relative current at the river mouth, but does not depend on the statistical distribution of wave periods. This function (given by equation [7-41]) is therefore ideally suited as an index of bar hazard during winter storm conditions.

VIII. SYNTHESIS

Introduction

It is the aim of this chapter to illustrate the combined use of the deep water semi-automated forecast method and the hazard index, α (Chapter VII). Three high-swell situations affecting the Columbia River were selected from the 1971-1972 winter as examples. Each was "hindcast" by the semi-automated deep water method developed in Chapter IV. The hindcasts are equivalent to forecasts in which the forecaster has six-hourly surface pressure analyses and "perfect" (correct) prognoses to a distance of 2000 nautical miles from the Columbia River. The hazard index (α) was computed from the hindcast heights and periods as outlined at the end of Chapter VII. Wave heights from visual observations and the seismometer at Newport are used as verification, as well as the bar closure periods at the Columbia River. Results are interpreted with the aid of information on time of day, tide stage, wind, amount of cross swell, and breaker observations at the South Jetty of the Columbia River.

The Data

The output from the hindcasts consists of six-hourly significant height and average zero upcrossing period, determined from the hindcast spectrum by theoretical methods (Chapter IV). The hindcast heights and periods were linearly interpolated to hourly values in order to discern tidal effects on the hazard index.

Tide stage and current were estimated by a very simple FORTRAN subroutine which fourier-superimposes the predominant tidal constituents. The twelve largest constituent amplitudes for tide stage at Tongue Point, Oregon, were used along with their constituent frequencies and phases. The ten largest constituent amplitudes for current at Grey's Harbor (with frequencies and phases) were used to compute currents. The latter were modified to conform to a point over the channel nera Jetty "A" at the Columbia River, as shown in "Tidal Current Tables 1971: Pacific Coast of North America and Asia". Hourly values of tide stage (feet) and current (feet per second) were output for the hindcast periods. These computations differed by at most 2% from standard tidal predictions of maxima and minima at the same places.

A bathymetric depth of 40 feet was chosen for computations of the hazard index, α . This is the approximate depth on the north flank of Clatsop Spit, south of the ship channel, where severe breaker conditions are common (Chapter II). The water depth is taken as the sum of the bathymetric depth and the tide stage.

The significant wave height (H_s) at each hourly depth and current was found by applying the amplification factor $\overline{K}$ (from the spectral transformation of Chapter VI) to the hourly (deep water) hindcast height. Then H_s and the (deep water) hindcast average period ($\overline{T}_o$) were used to compute the hazard index of equation (7-40).

Wave heights from Newport, observed visually and by the seismometer (Chapter III), are used for verification of the hindcasts. The wave heights from Newport are always less than the hindcast heights. This tendency was noted in Chapter V, and may be due to a bias in the wind speed inputs for the hindcast. At least part of the discrepancy may be due to the reduction of wave height at the Newport site due to the effects of shoaling and refraction. Unfortunately, the wave observations from the Columbia River Lightship are unreliable, thus Newport (130 nautical miles south of the Columbia River) is the best available source of verification data.

The applicability of Newport wave heights for verification can be seen by comparing them to visual observations of breaker heights at the Columbia River. Breaker heights were estimated daily by Mr. Norm Kujala at the South Jetty during the 1971-1972 winter. The method of observation and treatment of the data are discussed in APPENDIX B. Figure 33 shows time plots of seismometer-inferred significant wave heights at Newport and of breaker heights at the Columbia River. (The seismometer heights which most nearly coincided with the times of the breaker observations were plotted.) The two series seem to be well correlated, especially during October, November and December, 1971. Breaker heights are generally greater than the intermediate-depth Newport wave heights. (This is to be expected from shoaling relationships, solitary wave theory, and the observations of others [Munk, 1949].)

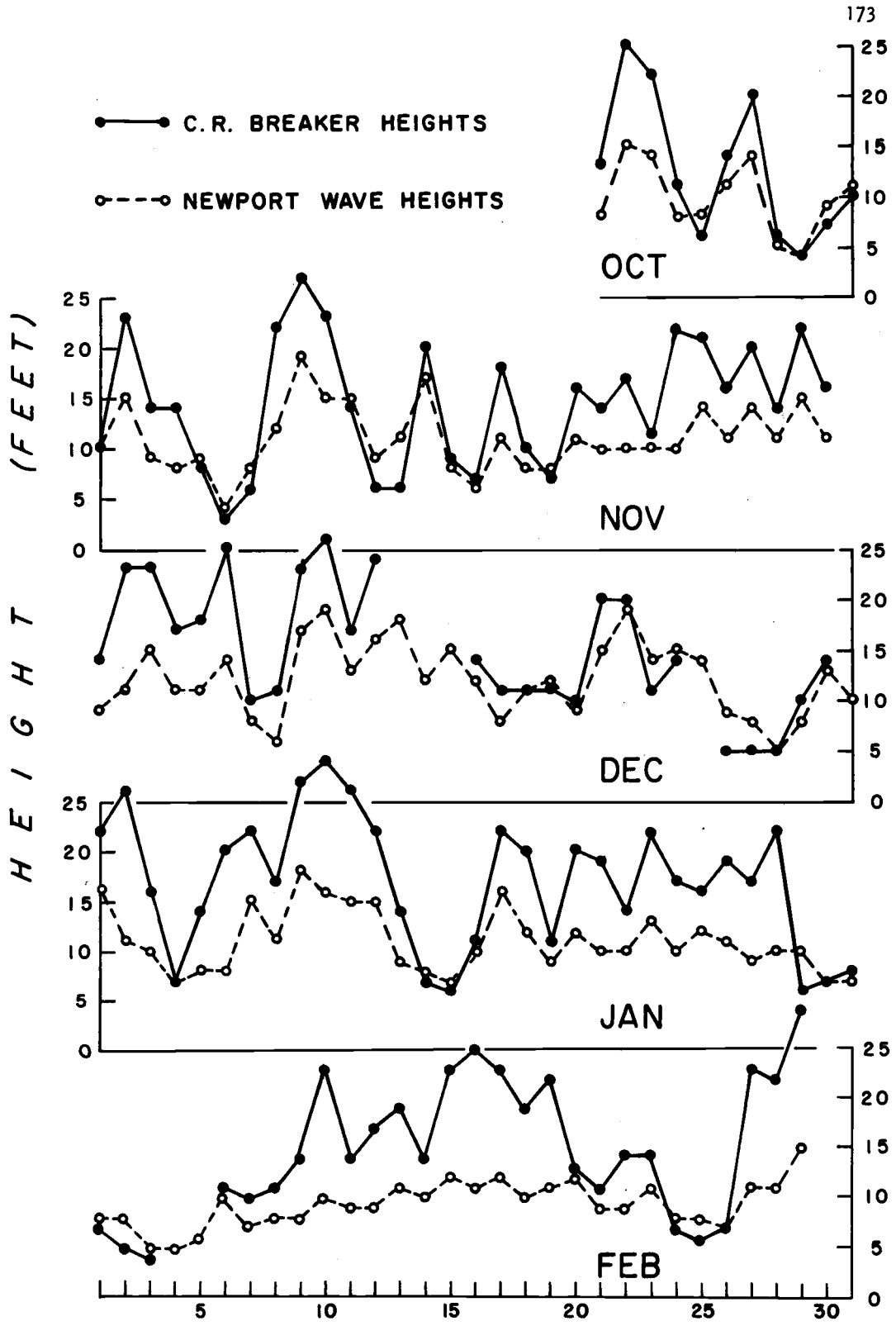

Figure 33. Time plots of daily breaker heights (Columbia River) and seismometer-inferred significant heights (Newport), for the 1971-1972 winter.

Case #1: November 8-10, 1971

At 1600 PST on November 7, 1971, a large stationary cyclone occupied the entire Gulf of Alaska. Thirty-five to fifty knot winds were reported in its southern sector, behind the cold front and aimed at the Oregon-Washington coast, some 500 miles* to the east. Subsequently, this fetch moved somewhat southward and winds of 30 to 40 knots were reported there for the next 24 hours. Meanwhile another fetch developed along the cold front at about 1000 PST, November 8, and stretched southwestward from Vancouver Island for about 1000 miles. Southerly and southwesterly winds were reported along this fetch for the next 30 hours. Shortly before the cold front passed inland at midday on November 9, winds at Newport, Oregon increased abruptly to 50 knots from the south-southwest and continued at 30-35 knots for the next six hours.

Wave heights at Newport exceeded 20 feet seaward of the jetties at flood tide on the evening of November 9 (Figure 34). Hindcast heights reached their maximum of 31 feet somewhat earlier, around midday on November 9.

Westerly swell from the more distant fetch and south-southwesterly seas from the more local fetch apparently arrived nearly simultaneously at the Columbia River on November 9 and 10, indicating a serious cross swell condition.

---

* All reference to distance is in nautical miles.

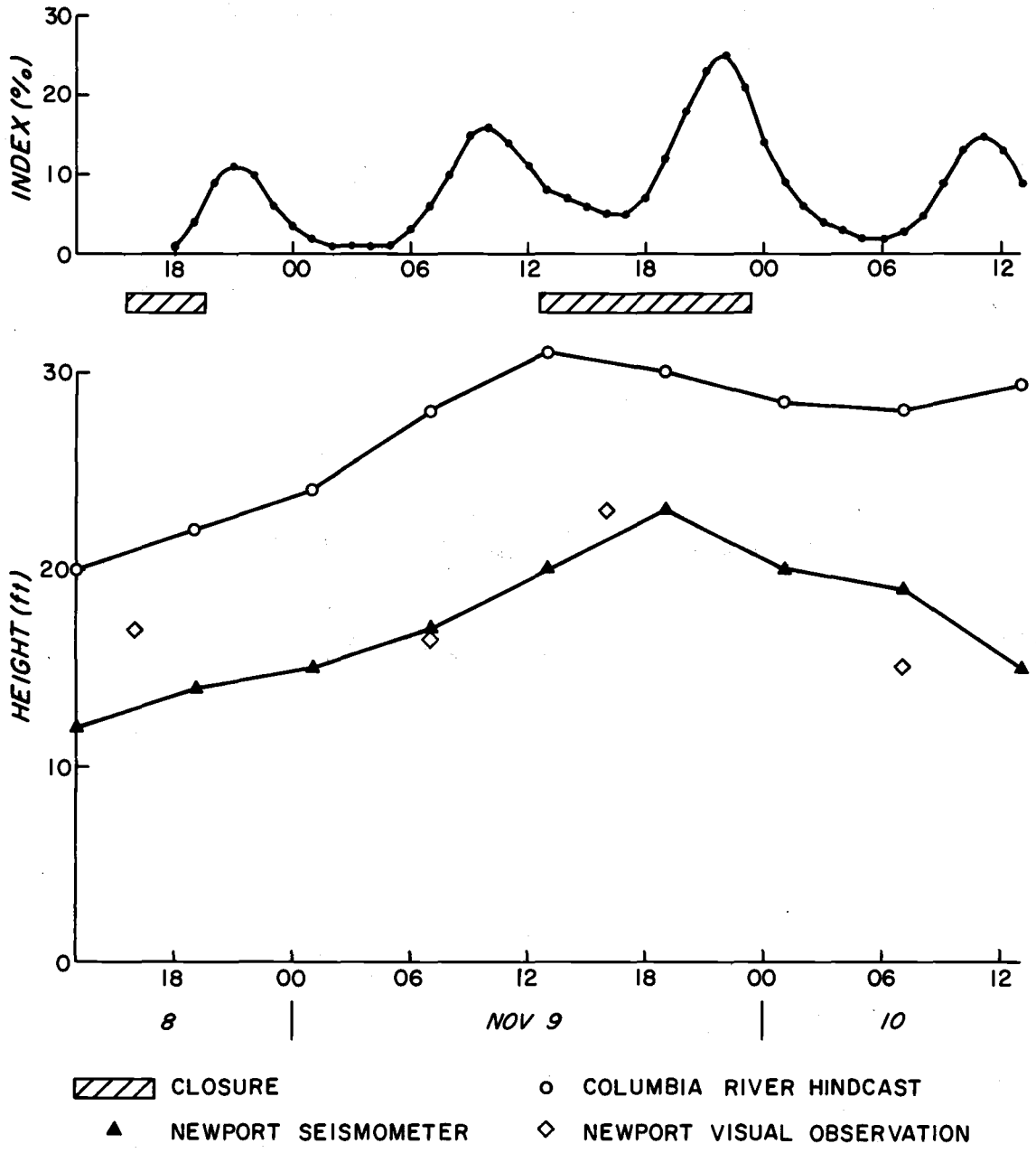

Figure 34. Hindcast hazard index at and deep water significant height off the Columbia River; bar closure periods at the Columbia River; and measured and observed significant heights at Newport (November 8-10, 1971).

The Columbia River bar was closed to ship traffic at 1240 PST, November 9, at the onset of flood tide and remained closed for 11 hours through the succeeding ebb. The closure corresponds closely to the highest observed waves at Newport. The fact that the bar was closed during flood tide and daylight is indicative of very hazardous conditions which transcended the effects of the ebb tide and poor (night) visibility. The decision to close the bar may have been due to the combination of high and increasing waves, intense southerly winds, and the cross swell condition noted previously. Breakers of 27 feet were reported at the South Jetty at the approximate time of closure.

Deep water heights were hindcast at a maximum of 31 feet at the time of closure, resulting in significant (5%) values of the hazard index during flood tide, increasing to 25% on the following ebb. During two previous ebbs the index reached values of 10% and 15%; these may be too high, judging from differences of 10 to 12 feet between hindcast and observed heights during those periods.

A short four-hour bar closure occurred during the afternoon of November 8 at the transition from flood to ebb. There is no clear explanation of this closure from either the observed or hindcast data.

This case is an example of hazardous conditions resulting from the complex interaction of many factors, including high waves, cross swell, and severe local weather.

Case #2: November 28-30, 1971

At 1600 PST on November 27 the cold (south) sector of a low pressure system lay some 400 miles off the coast, with 25-35 knot winds directed eastward at the Columbia river. The disturbance and the fetch moved steadily eastward and somewhat southward over the next 36 hours. The low pressure center crossed the coast at the Columbia River at 2200 PST November 27, while the fetch intercepted the coast to the south. As the system passed inland, high pressures built up behind the low. West-northwesterly winds of 25-40 knots directed at Newport were reported on the northeastern limb of the high pressure cell, some 300 miles off the coasts of Washington and Vancouver Island. This condition continued for about 18 hours. Both fetches affected Newport somewhat more than the Columbia River, with the west-northwesterly fetch following the westerly fetch.

Beginning at 1900 PST, November 28, 15 to 17 foot waves were reported at Newport for the next 24 hours (Figure 35). The hindcast waves reached their maximum height of 21 feet at 1900 PST, November 29. The largest breakers reported at the South Jetty of the Columbia River during the period were 22 feet at midday on November 29.

The Columbia River bar was closed to ship traffic twice on November 29. Both closures occurred during ebb tide, the first for 4½ hours, at night, the second for 8 hours during daylight. During the first closure the hazard index did not exceed 1%, but reached 15% during the

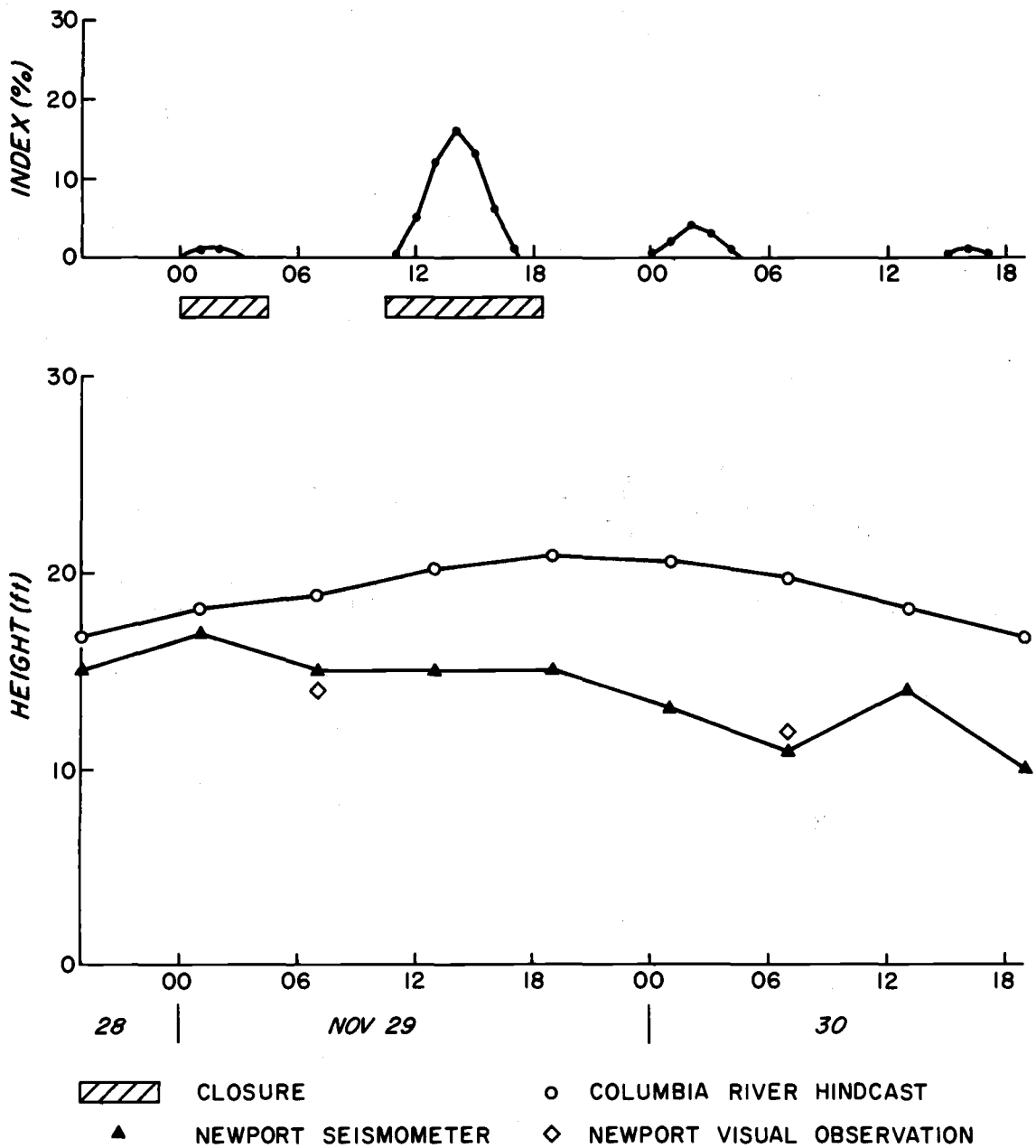

Figure 35. Hindcast hazard index at and deep water significant height off the Columbia River; bar closure periods at the Columbia River; and measured and observed significant heights at Newport (November 28-30, 1971).

second closure. The hazard index appears to correctly indicate that wave conditions were more severe during the second ebb (the second closure was longer in spite of more favorable visibility).

Hazard indices of 4% and 1% were computed for the ebb tides of November 30, but no bar closures occurred. Comparison of hindcast and observed heights suggests that the hindcast may have been too high during this period.

During most of the period a slight cross swell condition existed. Winds at Newport were generally west-southwest to west-northwest at 10 to 20 knots. Thus, overall conditions were not nearly as severe as in the previous example. The conditions illustrated in this case occur quite frequently at the Columbia River, with waves only high enough to cause bar closure during the ebb tide.

Case #3: December 9-10, 1971

At 1000 PST, December 8 a cyclone centered over Anchorage and the Alaskan Panhandle began to intensify. A long and intense fetch was set up with northwesterly winds of 30 to 50 knots directed across the northern portion of the Gulf of Alaska at the Columbia River. Cold air advection over the Gulf from the Alaskan mainland and a developing high center southwest of the fetch seem to have been the principal causes of the development. Wind reports of up to 50 knots continued through 1600 PST, December 9. Thereafter, the winds reduced to 30-35 knots and were directed at the Oregon-California border, further south.

Waves 23 feet high were measured during the evening and night of December 9-10 at Newport (Figure 36). Hindcast arrivals reached their maximum of 31 feet somewhat earlier during the afternoon of December 9. During the morning and afternoon of December 9, hindcast heights were up to 14 feet higher than observed heights at Newport. Breaker heights of 23 and 26 feet were reported at the South Jetty (Columbia River) on the mornings of December 9-10.

On the afternoon of December 9, at flood tide, the Columbia River bar was closed for almost 11 hours. The bar reopened during the subsequent flood and again closed for five hours during ebb tide at about midday of December 10.

The hazard index agrees generally with the closure periods, but no closure was associated with the high index values on the morning of December 9 (ebb tide). This may or may not have been due to excessively high hindcast heights, since the reported breaker heights at the South Jetty were already fairly high (23 feet). In addition, waves from the northern Gulf of Alaska can be expected to arrive somewhat sooner at the Columbia River than at Newport (about 5-6 hours).

High waves and breakers seem to have been the main cause for closure during this period, as winds did not exceed 25 knots (Newport) and there was no cross swell condition indicated. This case is a good illustration of high swell created by storms in the Gulf of Alaska, discussed in Chapter II.

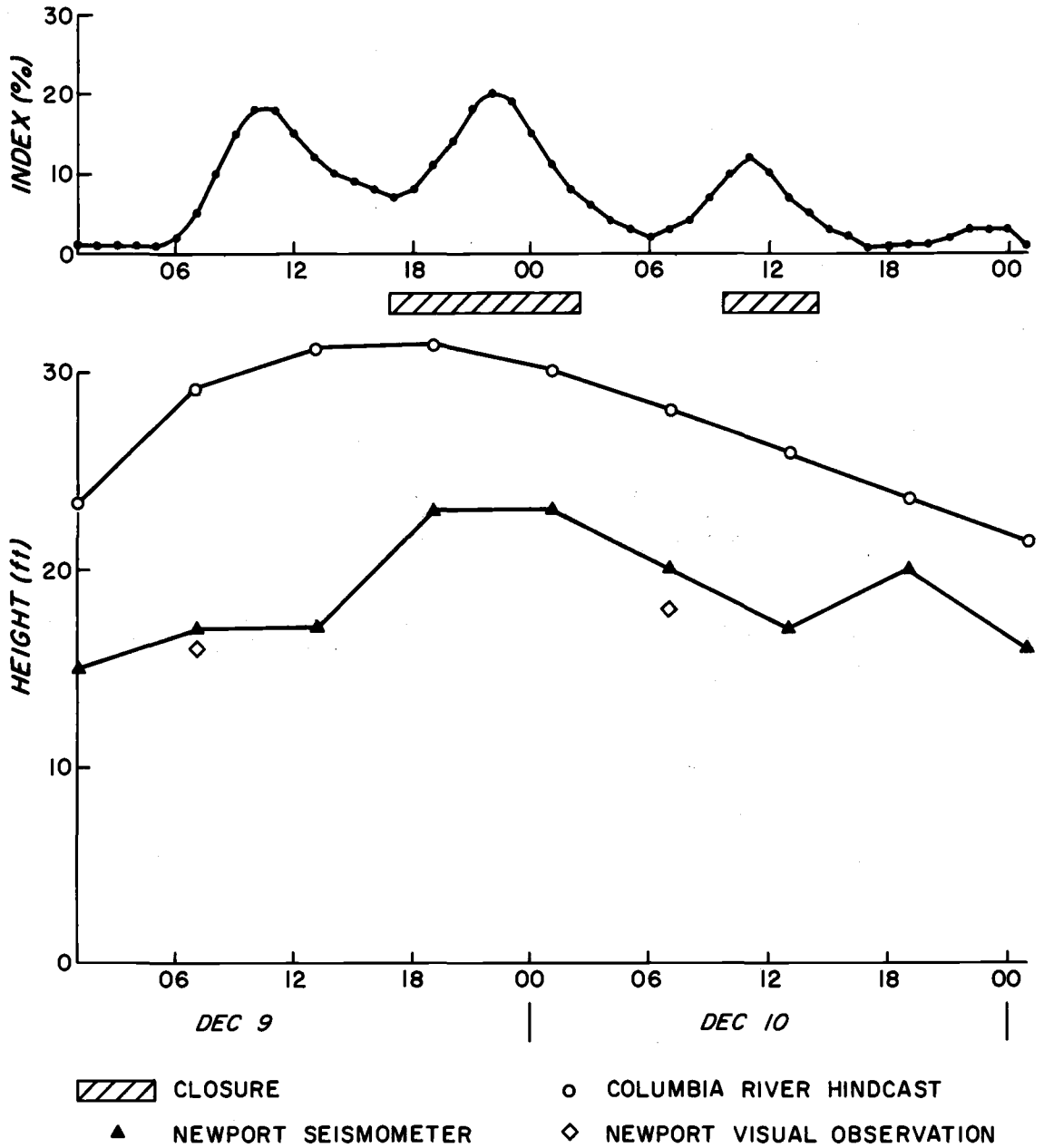

Figure 36. Hindcast hazard index at and deep water significant height off the Columbia River; bar closure periods at the Columbia River; and measured and observed significatn heights at Newport (December 9-10,1971).

Discussion

The combined use of the deep water hindcasts and the hazard index (Chapter VII) was verified by wave observations and bar closures. Where hindcast and observed wave heights agreed well, the hazard index correlated well with the closure periods. Where hindcast heights were considerably higher, moderately high index values at ebb tide were not associated with closure.

Only three cases have been examined in detail here, using hindcasts instead of actual forecasts. They seem to confirm the earlier conclusion that the significant wave height is a critical parameter for forecasting hazardous conditions. To the extent that deep water wave heights can be correctly forecast, the hazard index shows promise as an indicator of navigation hazard at the Columbia River.

IX. SUMMARY, CONCLUSIONS AND RECOMMENDATIONS

Summary and Conclusions

The Columbia River entrance is a large area where shoal zones and strong ebb currents cause waves to increase in height, steepness and frequency of breaking, thus resulting in hazardous navigation conditions for mariners. One of the most critical areas for vessels in bar transit is the outer portion of Clatsop Spit, near buoys six and eight. This area is relatively close to the ship channel, is exposed to offshore waves, and is characterized by rapidly decreasing depths and strong ebb currents. Large swell from winter storms break in this area and in the adjacent ship channel, creating the single greatest hazard for commercial ships.

A computerized, semi-automated method was developed to forecast the significant height and average period of waves in deep water. The method has the following characteristics:

(1) It is a hybrid scheme that combines the spectral principles of Pierson, Neumann and James (1955) with the empirical-theoretical fetch limited spectrum of Liu (1971) and graphical input techniques similar to those suggested by Wilson (1955).

(2) The method eliminates tedious calculations and references to graphs, allowing more time for the careful analysis of fetch histories. It may be applied by persons with relatively little knowledge of wave forecasting principles, but who are familiar with synoptic weather charts.

(3) The method is designed to accept multiple fetches with arbitrary

speeds of movement. Fetch histories may be subdivided to account for sustained changes in wind speed, fetch speed and/or fetch length.

Six-hourly microseism recordings at Newport, obtained during more than four months of the 1971-1972 winter, provide a convenient means of verifying the prediction methods developed in this study. The recordings were unusually noise-free and well correlated with visual observations of waves against a buoy in 50 feet of water offshore. The seismometer at Newport was calibrated to give the approximate significant wave height and average period at the buoy.

The semi-automated method produces wave spectra with characteristics and behavior similar to those of actual spectra. Hindcast significant heights for the 1971-1972 winter at Newport compare well with the heights inferred from the seismometer at Newport. A correlation coefficient of 0.77 was computed for the heights and the visual agreement between time series is particularly good over two to three day intervals. Hindcast and measured average periods had similar means, but a correlation coefficient of only 0.31. This is explained in part by the fact that, unlike significant wave heights, average wave periods depend strongly on the distribution of wave energy with frequency.

Comparison of simulated semi-automated forecasts with manual forecasts by the P-N-J and S-M-B methods suggests that the semi-automated method should give comparable results under operational forecast conditions.

The transformation of wave spectra by shoaling, discussed by

Bretschneider (1963b), was extended to include the effects of currents. A shoaling-current amplification factor for significant height may be found by spectral transformation. The height in water of arbitrary depth and current is the product of the significant height in deep slack water and the amplification factor.

The probability of wave-breaking in water of arbitrary depth and current was derived assuming that the heights and periods-squared of individual waves are independent and statistically distributed according to a Rayleigh function. When the predominant period of high offshore waves is in the range typical of ocean swell (9-14 seconds), the predominant period of breaking waves is also in this range. In such cases the breaking probability is relatively insensitive to the exact form of the wave period distribution.

A function closely related to the probability of breaking swell at the river entrance during high wave conditions was identified and suggested as an index of navigation hazard. The hazard index depends only slightly on the average wave period in deep water but significantly on the mean current, water depth and significant wave height at the river entrance. (The last may be found by multiplying the significant height in deep slack water by the shoaling-current amplification factor.)

The significant wave height and hazard index were hindcast for three two-day periods of high waves at the Columbia River entrance. Occurrences of high hazard index agreed (qualitatively) well with periods of bar closure at the Columbia River. It is concluded that the hazard index is a potentially useful prediction parameter for

hazardous bar conditions, but that it depends strongly on the forecast height in deep water. It is, however, relatively insensitive to errors in the forecast average period, because the breaking heights for swell at river entrances are only weakly dependent on their periods.

Recommendations

Prediction methods were developed for this study with operational usefulness and applicability in mind. However the work was carried out in an academic environment without the benefit of extensive interaction with potential users. The methods should be refined to maximize their efficiency under operational conditions. A program of testing and verification is currently being conducted at the Newport and Portland, Oregon Weather Offices. This study could be expanded to include the hazard index developed here. If the hazard index proves useful, it can, and should, be incorporated into the FORTRAN program currently being used (APPENDIX A).

BIBLIOGRAPHY

Arthur, R. S. 1950. Refraction of shallow water waves: the combined effect of currents and underwater topography. Transactions, American Geophysical Union 31(4):549-554.

Barnes, C. A., A. C. Duxbury and Betty-Ann Morse. 1972. Circulation and selected properties of the Columbia River effluent at sea. In: The Columbia River estuary and adjacent ocean waters -- bioenvironmental studies, ed. by A. T. Pruter and D. L. Anderson, Seattle, University of Washington Press. p. 41-80.

Barber, N. F. and M. J. Tucker. 1962. Wind waves. In: The sea, Vol. 1. ed. by M. N. Hill. New York, Interscience. p. 664-699.

Bowditch, N. 1962. The American practical navigator: an epitome of navigation. U. S. Navy Hydrographic Office Publication No. 9. 1524 pp.

Bretschneider, C. L. 1959. Wave variability and wave spectra for wind-generated gravity waves. Beach Erosion Board Technical Memorandum No. 118, U. S. Army Corps of Engineers. 192 pp.

_____ 1963a. A one-dimensional gravity wave spectrum. In: Ocean wave spectra, Englewood Cliffs, N. J., Prentice-Hall. p. 41-56.

_____ 1963b. Modification of wave spectra on the continental shelf and in the surf zone. Proceedings of the Eighth Conference on Coastal Engineering, Mexico City, ed. by J. W. Johnson. p. 17-33.

Danel, Pierre. 1952. On the limiting clapotis, gravity waves. National Bureau of Standards Circular No. 521. p. 35-38.

Darbyshire, J. 1950. Sea waves and microseisms. Proceedings of the Royal Society of London A 202:439.

_____ 1959. A further investigation of wind generated waves. Deutsche Hydrographische Zeitschrift 12:1-13.

_____ 1962. Microseisms. In: The sea, Vol. 1. ed. by M. N. Hill. New York, Interscience. p. 700-719.

Deacon, G. E. R. 1947. Relation between sea waves and microseisms. Nature 160:419-421.

Dean, R. G. and P. S. Eagleson. 1966. Finite amplitude waves. In: Estuary and coastline hydrodynamics, ed. by A. T. Ippen, New York, McGraw-Hill. p. 93-132.

Dean, R. G. 1970. Stream function wave tables, vol. 1-3. Engineering and Industrial Experiment Station, College of Engineering, University of Florida, Gainesville, Florida.

Draper, L. 1967. The analysis and presentation of wave data - a plea for uniformity. In: Proceedings of the Tenth Conference on Coastal Engineering, Tokyo, Japan, 5-8 September, 1966. Vol. 1. p. 1-11.

Duxbury, A. C. 1967. Currents at the Columbia River Mouth. Photogrammetric Engineering 33(3):305-310.

Goda, Yoshimi. 1970. Numerical experiments on wave statistics with spectral simulations. Report of the Port and Harbour Research Institute 9(3):1-57.

Haubrich, R. A., W. H. Munk and F. E. Snodgrass. 1963. Comparative spectra of microseisms and swell. Bulletin of the Seismological Society of America 53:27-37.

Herbich, J. B. and Lyndell Hales. 1972. The effect of tidal inlet currents on the characteristics and energy propagation of ocean waves. Preprint No. OTC 1618. Offshore Technology Conference, Dallas, Texas. Vol. 2. p. 13-20.

Huang,N.E.,D.T.Chen,C.C.Tung and J.R.Smith. 1972. Interactions between steady non-uniform currents and gravity waves with applications for current measurements. Journal of Physical Oceanography 2(4):420-431.

Hubert, W. E. 1964. Operational forecasts of sea and swell. In: First U. S. Navy Symposium on Military Oceanography, Washington, D. C., U. S. Navy Oceanographic Office. p. 113-124.

Isaacs, J. D. 1948. Discussion of "Refraction of surface waves by currents" by J. W. Johnson. Transactions, American Geophysical Union 29(5):739-741.

Johnson, J. W., M. P. O'Brien and J. D. Isaacs. 1948. Graphical construction of wave refraction diagrams. U. S. Navy Hydrographic Office Publication No. 605. 45 pp.

Kinsman, Blair. 1965. Wind waves. New York, Prentice Hall. 676 pp.

Liu, P. C. 1971. Normalized and equilibrium spectra of wind waves in Lake Michigan. Journal of Physical Oceanography 1:249-257.

Lockett, J. B. 1963. Phenomena affecting improvement of the lower Columbia River estuary and entrance. In: Proceedings of the Eighth Conference on Coastal Engineering, Mexico City, ed. by J. W. Johnson. p. 695-755.

Lockett, J. B. 1967. Sediment transport and diffusion: Columbia River estuary and entrance. Proceedings of the American Society of Civil Engineers. Journal of the Waterways and Harbours Division. Vol. 4. p. 167-175.

Longuet-Higgins, M. S. 1950. A theory of the origin of microseisms. Philosophical Transactions of the Royal Society of London A 243: 1-35.

_____ 1952. On the statistical distribution of the heights of sea waves. Journal of Marine Research 11(3):245-265.

Longuet-Higgins, M. S. and R. W. Stewart. 1961. The changes in amplitude of short gravity waves on steady non-uniform currents. Journal of Fluid Mechanics 10:534-549.

McCowan, J. 1894. On the highest wave of permanent type. Philosophical Magazine 38:1351-1358.

Miche, R. 1944. Mouvements ondulatoires des mers en profondeur constante ou decroissante. Annales des Ponts et Chaussees 25-78; 131-164; 270-292; 369-406.

Michell, J. H. on the highest waves in water. 1893. Philosophical Magazine, Fifth Series 36:430-437.

Munk, W. H. 1949. The solitary wave and its application to surf problems. Annals of the New York Academy of Sciences 51:376-424.

National Marine Consultants. 1961a. Wave statistics for three deep water stations along the Oregon-Washington coast. U. S. Army Corps of Engineers District, Seattle and Portland.

_____ 1961b. Wave statistics for twelve most severe storms affecting three stations off the coast of Washington and Oregon, during the period 1950-1960. U. S. Army Corps of Engineers District, Seattle and Portland.

Neal, V. T. 1972. Physical aspects of the Columbia River and its estuary. In: The Columbia River estuary and adjacent ocean waters -- bioenvironmental studies, ed. by A. T. Pruter and D. L. Anderson, Seattle, University of Washington Press. p. 19-40.

Neumann, Gerhard. 1953. On ocean wave spectra and a new method of forecasting wind generated sea. Beach Erosion Board Technical Memorandum No. 43. U. S. Army Corps of Engineers.

Phillips, O. M. 1958. The equilibrium range in the spectra of wind generated gravity waves. Journal of Fluid Mechanics 4:426-434.

Pierson, W. J., G. Neumann and R. W. James. 1955. Practical methods for observing and forecasting ocean waves. U. S. Navy Hydrographic Office Publication No. 603.

Pierson, W. J. and L. Moskowitz. 1964. A proposed spectral form for fully developed wind seas based on the similarity theory of S. A. Kitaigorodskii. Journal of Geophysical Research 69:5181-5190.

Pore, N. A. and W. S. Richardson. 1969. Second interim report on sea and swell forecasting. Weather Bureau Technical Memorandum TDL-13. 21 pp.

Pore, N. A. 1970. Summary of selected reference material on the oceanographic phenomena of tides, storm surges, waves and breakers. Environmental Sciences Services Administration Technical Memorandum TDL-30. 103 pp.

Rice, S. O. 1944. Mathematical analysis of random noise. In: Selected Papers on Noise and Stochastic Processes, New York, Dover Pub. p. 133-294.

Roll, H. U. and G. Fischer. 1956. Eine kritische bemerkung zum Neumann-spectrum des seeganges. Deutsche Hydrographische Zeitschrift 9:9-14.

Snodgrass, F. E. et al. 1966. Propagation of ocean swell across the Pacific. Philosophical Transactions of the Royal Society of London A. 259:431-497.

Shields, G. C. and G. B. Burdwell. 1970. Western region sea state and surf forecasters' manual. Environmental Sciences Services Administration Manual WBTM WR 51.

Sverdrup, H. V. and W. H. Munk. 1947. Wind, sea and swell: theory of relations for forecasting. U. S. Navy Hydrographic Office Publication No. 601.

Tucker, M. J. 1961. Simple measurement of wave records. In: Proceedings of the Conference on Wave Recording for Civil Engineers, vol. 42, National Institute of Oceanography. p. 231.

Wiegel, R. L. 1964. Oceanographical engineering. Englewood Cliffs, N. J. Prentice-Hall. 532 pp.

Wilson, B. W. 1955. Graphical approach to the forecasting of waves in moving fetches. Beach Erosion Board Technical Memorandum No. 73, U. S. Army Corps of Engineers.

Winston, Jay S. 1954. Aspects of rapid cyclogenesis in the Gulf of Alaska. Tellus 7(4):481-500.

Unna, P. J. H. 1942. Waves and tidal streams. Nature 149:219-220.

U. S. Army Coastal Engineering Research Center. 1966. Shore protection planning and design. Technical Report No. 4, 3rd ed. 204 pp.

Zopf, David. 1972. Inference of near-shore ocean wave characteristics from seismometer data. Submitted to Journal of Geophysical Research in 1972.

APPENDIX

APPENDIX A: DEEP WATER WAVE FORECAST PROGRAM

This appendix documents the FORTRAN program used in the semi-automated deep water wave forecasting method. The major units consist of the main program, FCST, and the principal FORTRAN subroutines, FETCH, LIUSPEC, LINK, DATE and MODAHR. Sample runs were presented in Chapter IV, together with definitions of terms, and detailed discussions of the principles and procedures involved. These will not be repeated here.

Program FCST

The flowchart (Figure 38) and program listing for FCST are found at the end of APPENDIX A. The main functions of FCST are:

(1) to read the input data needed;

(2) to transform input data into units, times, speeds, etc., that are more readily manipulated in computations;

(3) to interact with the user in branching and termination decisions;

(4) to execute the main DO loops which increment computations from one time interval to the next, and from one spectral frequency component to the next;

(5) to integrate forecast spectra and output significant wave height and average period for several time intervals;

(6) to call the principal subroutines.

Input

All input data is read in from a remote terminal in conversation

mode, whereby the user responds to questions written by the program on the teletype. Examples of input conversations are shown in Figures 15 and 17.

Timing

Compilation of FCST and its subroutines requires less than ten seconds of central processor time on the CDC-3300 computer at Oregon State University. Slightly more time is required for average executions involving several fetch histories.

Subroutines and Functions Called

In addition to the principal subroutines already mentioned, FCST also calls TTYIN and TELIO (remote terminal free form input-output subroutines developed for the Oregon State University time-sharing system). Standard FORTRAN functions called by FCST and the principal subroutines include: SQRT, ABS, EXP and ALOG.

Limitations

FCST is not programmed to accept fetches that recede from the forecast point. Angular spreading factors are incorrectly interpolated in such cases. The program should be modified to accept receding fetches if East Coast forecasts are to be made.

The program will incorrectly convert month-day-hour into absolute time for leap years. For leap years, the array elements MON(2,3) through MON(2,12) defined in the DATA statement should each be increased by one.

Principal Subroutines

The FORTRAN listings for the subroutines FETCH, LIUSPEC, LINK, DATE and MODAHR are found at the end of APPENDIX A. Each listing contains an abstract (comment statements) describing its operation.

Call Sequences

```
FETCH (FRQ,DFR1,DREAR1,VF,VR,DUR,TIMCST,TOB,GENDIST,NUM,DFR2,DADS,AS2,
    AS)
LIUSPEC (UU,DD,FRQ,DF,DE)
LINK (UU1,UU2,FRQ,D)
DATE (DATE)
MODAHR (NTIM,NMO,NDA,NHR)
```

Definitions of Parameters Called by Subroutines

parameter	definition
FRQ	frequency (Herz)
DF	band width (Herz)
DE	band energy (feet^2)
UU,UU1,UU2	wind speeds* (see FORTRAN listings)
D,DD,GENDIST	generation distance* (see FORTRAN listings)
DFR1	initial decay distance (from fetch front)
DFR2	final " " " " "
DREAR1	initial distance of fetch rear from forecast point
VF	speed of fetch front
VR	" " " rear

* All speeds are in knots; distances are in nautical miles.

DUR	duration of fetch history (hours)
TIMCST	number of hours after 00 GMT, Jan. 01, that fetch reaches coast
TOB	time from start of fetch to forecast time
NUM	branching parameter for frequency scan
AS2	final angular spreading parameter
DADS	change of angular spreading with distance
AS	interpolated angular spreading factor
DATE	absolute number of hours from 00, Jan. 01
NTIM	" " " " " " " "
NMO	number of months (e.g. June = 6)
NDA	day of a month (1 to 31)
NHR	hour of day (0 to 23)

Comments on Algorithm Methods

LIUSPEC computes the energy in each spectral band according to equations (4-22) through (4-25). LINK solves the equality $S(U_1,D_1,f) = S(U_2,D_2,f)$ for the "effective" generation distance D_2, where $S(U,D,f)$ is the spectral density as a function of wind speed, fetch length (or generation distance) and frequency. This is necessary when energy propagates from one fetch into an adjacent one with greater wind speed, U_2. The equality leads to the equation

$$X_2 = [(U_2/U_1)^4 X_1^{-.888} - .117(fU_2/g)^4 \log(X_2/X_1)]^{-1.125}$$

where $X_1 = gD_1/U_1^2$ (known) and

$X_2 = gD_2/U_2^2$ (D_2 unknown).

The equation is solved iteratively for X_2 using as an initial guess $X_2 = X_1(U_1/U_2)^6$. The iteration usually converges to within ±1% of the correct value in three steps.

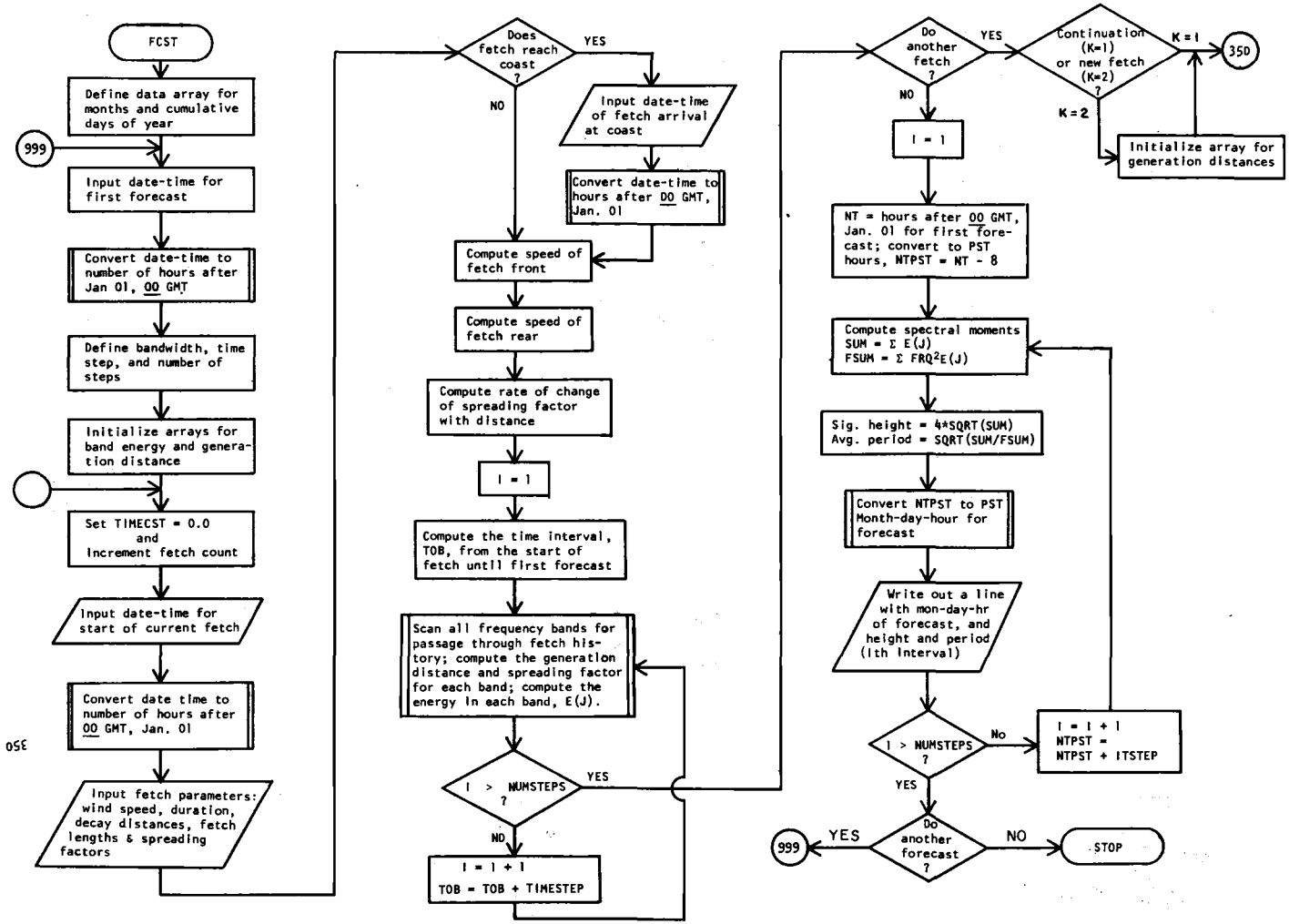

Figure 37. Flowchart for semi-automated forecast program (FCST).

```
C...DEFINE THE COMMON DATA BLOCK FOR MAIN AND SUBROUTS
      DEFINE COMMON
      COMMON/DATA/MON(12,2)
      END

      PROGRAM FCST
      INCLUDE COMMON
C...DEFINE DATA ARRAY FOR MONTHS AND CUMULATIVE DAYS
C   AS OF THE FIRST OF EACH MONTH
      DATA((MON(I,J),I=1,12),J=1,2)=3HJAN,3HFEB,3HMAR,
     23HAPR,3HMAY,3HJUN,3HJUL,3HAUG,3HSEP,3HOCT,3HNOV,
     33HDEC,0,31,59,90,120,151,181,212,243,273,304,334)
      DIMENSION D(25,17), E(25,17)
C...DEFINE RANDKIDIM,TIME STEP,# OF STEPS
C...ASK FOR TIME THE OF THE FIRST FORECAST
  999 WRITE(61,40)
   40  FORMAT(' WHEN IS OUR FIRST FORECAST FOR?')
C...CONVERT INPUT MONTH-DAY-HOUR TO ABSOLUTE NUMBER OF
C   HOURS COUNTING FROM 00 HOURS(MT) ON JAN 01 (SAME YEAR)
      CALL DATE(TI)
      DF=.01
      TIMESTEP=6.
      ITSTEP=1/TIMESTEP
C...INITIALIZE THE FETCH NUMBER
C...INCREMENT TIME FOR NEXT FORECAST INTERVAL
      NUMSTEPS=5
      NFTCH=0
C...SET K=2 (IMPLIES A NEW FETCH)
      K=2
C...INITIALIZE ARRAYS FOR BAND ENERGIES AND GENERATION
C   DISTANCES.
      DO 15 I=1,NUMSTEPS
      DO 15 J=1,17
   15 D(I,J)=E(I,J)=0.0
C...SET TIME FETCH REACHES COAST TO ZERO--NOT TO BE CHANGED
C   UNLESS  THE FORECASTER SPECIFIES THAT FETCH REACHES
C   COAST--THEN TIMCST=TIME OF FETCH ARRIVAL.
  350 TIMCST=0.0
      NFTCH=NFTCH+1
      WRITE(61,51) NFTCH
C...ASK FOR TIME FETCH NUMBER "NFTCH" STARTED.
   51  FORMAT(' TIME FETCH # ',I1,' STARTED:')
C...ASK FOR FETCH HISTORY INPUT DATA (WIND SPEED,DURATION,
C   INITIAL AND FINAL DECAY DISTANCES,FETCH LENGTHS,AND
C   ANGULAR SPREADING FACTORS).
      CALL DATE(TI)
      U=TTYIN(4H WIN,4HD SP,4HEED ,4H=    )
      IF(K.EQ.2) U1=U
      DUR=TTYIN(4H DUR,4HATIO,4HN (H,4HOURS,4H) = )
      DFR1=TTYIN(4H INI,4HTIAL,4H DEC,4HAY D,4HISTA,4HNCE ,
     24H=    )
      DFR2=TTYIN(4H FIN,4HAL D,4HECAY,4H DIS,4HTANC,
     34HE = )
      FL1=TTYIN(4H INI,4HTIAL,4H FET,4HCH L,4HENGT,
     44H = )
      FL2=TTYIN(4H FIN,4HAL F,4HETCH,4H LEN,4HGTH ,
     54H=    )
      AS1=TTYIN(4H INI,4HTIAL,4H SPR,4HEADI,4HNG F,
     64HACTO,4HR = )
      AS2=TTYIN(4H FIN,4HAL S,4HPREA,4HDING,4H FAC,
     74HTOR ,4H=    )
C...IF FETCH REACHES COAST, ASK WHEN
      IF(DFR1.GT.0..AND.DFR2.EQ.0.) 939,941
  939 NTIM=TT+DUR
      CALL MODAHR(NTIM,NMN,NDAY,NHR)
      WRITE(61,54) NHR,MON(NMN,1),NDAY
   54  FORMAT(' DOES FETCH REACH COAST BEFORE ',I2,'Z ',
     1A3,1X,I2)
      L=TELIO(8HK(YES/NO))
      IF(L.EQ.1) 940,941
  940 WRITE(61,55)
   55  FORMAT(' WHEN ?')
      CALL DATE(TIMCST)
C...FIND VELOCITIES OF FETCH FRONT(VF)AND REAR(VF2).
  941 VR=((DFR1+FL1)-(DFR2+FL2))/DUR
      IF(TIMCST.EQ.0.0)21,22
   21  VF=(DFR1-DFR2)/DUR
      GO TO 23
   22  TIMCST=TIMCST-TT
      VF=DFR1/TIMCST
C...FIND INITIAL DISTANCE OF FETCH REAR, THEN CHANGE IN
C   SPRDING FACTOR FROM INITIAL REAR TO FINAL FRONT DIVIDED
C   BY SEPARATION OF SAME.
   23  DREAR1=DFR1+FL1
      DADS=(AS2-AS1)/(DREAR1-DFR2)
C...FIND OBSERVATION TIME FOR FIRST FORECAST
      TOB=TI-TT
C...INITIATE TIME LOOP
      DO 200 I=1,NUMSTEPS
C...INITIATE FREQUENCY LOOP
      DO 100 J=1,17
      FJ=J
      FRQ=FJ*.01+.03
C...FIND GENERATION DISTANCE AND SPRDING FACTOR
C   FOR THE J-TH FREQUENCY BAND.
      CALL FETCH(FRQ,DFR1,DREAR1,VF,VR,DUR,TIMCST,TOB,GENDIST,NUM
     1,DFR2,DADS,AS2,AS)
C...NUM=1: PROPAGATION LINE DIDN'T PENETRATE POLYGON--
C          INCREMENT FREQUENCY.
      IF(NUM.EQ.1)GO TO 100
C...NUM=2: FREQUENCY SCAN COMPLETED--INCREMENT TIME.
      IF(NUM.EQ.2)GOTO 199
C...GO TO 75 FOR NEW FTCH,3076 FOR CONTINUATION
      IF(K.EQ.2)75,76
   75  D(I,J)=GENDIST
      GO TO 77
C...IF WIND INCREASES IN CONTINUATION FTCH,FIND GEN-DIST.
C   NEEDED TO GENERATE THE INCOMING ENERGY AT NEW WIND SPEED
   76  IF(U.GT.U1) CALL LINK(U1,U,FRQ,D(I,J))
      D(I,J)=D(I,J)+GENDIST
C...COMPUTE GENERATED BAND ENERGY LEAVING CURRENT FETCH
   77  CALL LIUSPEC(U,D(I,J),FRQ,DF,DE)
C...APPLY ANG.SPREADING FACTOR AND COMPUTE FINAL ENERGY
      IF(K.EQ.2)78,79
   78  E(I,J)=AS*DE+E(I,J)
      GO TO 100
   79  ASDE=AS*DE
      IF(E(I,J).GT.ASDE)GO TO 100
      E(I,J)=ASDE
  100 CONTINUE
  199 TOB=TOB+TIMESTEP
  200 CONTINUE
C ANOTHER FETCH? IF SO, A NEW ONE(2) OR CONTINUATION(1)?
      N=TELIO(8HINPUT AN,8HOTHER FE,8HTCH(YES/,8HNO)  ?  )
      IF(N.EQ.2)301,300
  300 K=TTYIN(4HCONT,4HINUA,4HTION,4H OF ,4HPREV,4HIOUS,
     14H FET,4HCH (,4H1) 0,4HR NE,4HW FE,4HTCH ,4H(2) ,
     24H? : )
      IF(K.EQ.1) 58,59
   58  U1=U
      GO TO 350
C...NEW FETCH: INITIALIZE GENERATION DISTANCE ARRAY,
   59  DO 60 M=1,NUMSTEPS
      DO 60 N=1,17
   60  D(M,N)=0.0
      GOTO350
C...WRITE OUT THE FORECAST TABLE
  301 WRITE(61,44)
   44  FORMAT(//' MONTH  DAY  HOUR(PST)  SIG.HGT.  PERIOD(S)')
      NT=TI
      NTPST=NT-8
      DO 500 I=1,NUMSTEPS
      SUM=0.0
      FSUM=0.0
C...COMUTE ZEROTH & 2ND SPECTRAL MOMENTS (SUM & FSUM),
      DO 400 J=1,17
      SUM=SUM+E(I,J)
      FJ=J
      FRQ=FJ*.01+.03
      FSUM=FSUM+E(I,J)*FRQ**2
  400 CONTINUE
C...COMPUTE SIG HEIGHT AND AVERAGE PERIOD.
      PER=SQRT(SUM/FSUM)
      HS=4.0*SQRT(SUM)
C...CONVERT ABSOLUTE PST HOURS TO PST MON-DAY-HR.
      CALL MODAHR(NTPST,NMO,NDA,NHR)
      WRITE(61,850)MON(NMO,1),NDA,NHR,HS,PER
  850 FORMAT(2X,A3,I6,I7,8X,F4.1,6X,F4.1)
      NTPST=NTPST+ITSTEP
  500 CONTINUE
      LEND=TELIO(8HWANT TO ,8HDO ANOTH,8HER FOREC,8HAST ?   )
      IF(LEND.EQ.1) GO TO 999
      STOP
      END
```

```
      SUBROUTINE FETCH(FRQ,D1,D2,VF1,VF2,TD,TIMCST,TOB,GENDIST,NUM
     1,DFR2,DADS,AS2,AS)
C...THIS SUBROUTINE DETERMINES THE GENERATION DISTANCE AS-
C   SOCIATED WITH THE JTH FREQUENCY AND THE ITH FORECAST IN-
C   TERVAL. IT FINDS THE TIMES AT WHICH THE PROPAGATION LINE
C   INTERSECTS THE FETCH HISTORY, T1 AND T2. THE DIFFERENCE,
C   DRTN=ABS(T1-T2), IS THE TIME SPENT BY THE FREQUENCY COM-
C   PONENT UNDER THE INFLUENCE OF THE WIND. FINALLY, THE GENER-
C   ATION DISTANCE IS GENDIST=1.515*DRTN/FRQ. AT THE END OF THE
C   SUBROUTINE THE ANGULAR SPREADING FACTOR FOR THE FREQUENCY
C   COMPONENT IS FOUND FROM (1) THE DECAY DISTANCE FROM THE
C   POINT AT WHICH THE COMPONENT LEAVES THE FETCH, AND (2)
C   THE RATE OF CHANGE OF SPREADING FACTOR WITH DISTANCE,DADS.
      NUM=0
      CG=1.515/FRQ
      DG=CG*TOB
      T1=(D1-DG)/(VF1-CG)
      T2=(D2-DG)/(VF2-CG)
      TP=TD
      IF(TIMCST.NE.0.0)TP=TIMCST
      IF(CG.GT.VF2.AND.T2.GT.TD)100,1
    1 IF(CG.LT.VF1.AND.T1.GT.TP)200,2
    2 IF(CG.GT.VF1.AND.T1.LT.0.0)200,3
    3 IF(CG.LT.VF2.AND.T2.LT.0.0)100,4
    4 IF(TIMCST.NE.0.0.AND.TOB.GE.TIMCST.AND.TOB.LE.TD)50,11
   11 IF(CG.GT.VF2.AND.CG.LT.VF1)12,21
   12 IF(T1.LT.0.0.AND.T2.LT.0.0)13,14
   13 T1=0.0
      T2=TD
      GO TO 80
   14 IF(T1.LT.0.0)15,16
   15 T1=TD
      GO TO 80
   16 IF(T2.LT.0.0)17,80
   17 T2=TD
      GO TO 80
   21 IF(CG.GT.VF1.AND.CG.LT.VF2)22,31
   22 IF(T1.GT.TD.AND.T2.GT.TD)23,24
   23 T1=0.0
      T2=TD
      GO TO 80
   24 IF(T1.GT.TD)25,26
   25 T1=0.0
      GO TO 80
   26 IF(T2.GT.TD)27,80
   27 T2=0.0
      GO TO 80
   31 IF(CG.GT.VF1.AND.CG.GT.VF2)32,41
   32 IF(T1.GT.TD.AND.T2.LT.0.0)33,34
   33 T1=TD
      T2=0.0
      GO TO 80
   34 IF(T2.LT.0.0)35,36
   35 T2=0.0
      GO TO 80
   36 IF(T1.GT.TD)37,80
   37 T1=TD
      GO TO 80
   41 IF(T1.LT.0.0.AND.T2.GT.TD)43,44
   43 T1=0.0
      T2=TD
      GO TO 80
   44 IF(T1.LT.0.0)45,46
   45 T1=0.0
      GO TO 80
   46 IF(T2.GT.TD)47,80
   47 T2=TD
      GO TO 80
   50 IF(T1.LT.TOB.AND.T1.GT.0.0)51,52
   51 T2=TOB
      GO TO 80
   52 IF(T2.LT.TOB.AND.T2.GT.0.0)53,54
   53 T1=TOB
      GO TO 80
   54 T1=TOB
      T2=0.0
   80 DRTN=ABS(T1-T2)
      GENDIST=1.515*DRTN/FRQ
      TTT=T1
      IF(T2.GT.T1) TTT=T2
      DS=CG*(TOB-TTT)-DFR2
      AS=AS2-DADS*DS
      IF(AS.LT..05) AS=.05
      GO TO 300
  100 CONTINUE
      NUM=1
      GO TO 300
  200 CONTINUE
      NUM=2
  300 RETURN
      END
```

```
      SUBROUTINE LIUSPEC(UU,DD,FRQ,DF,DE)
C...LIUSPEC ACCEPTS WIND SPEED (UU,KNOTS), GENERATION DISTANCE
C   (DD,N.MI.), FREQUENCY (FRQ,HZ), AND BANDWIDTH (DF,HZ) AS
C   INPUT. IT CONVERTS SPEEDS AND DISTANCES TO FEET/SEC AND FEET
C   AND DEFINES GRAVITY (G=32). IT COMPUTES THE DIMENSIONLESS
C   FETCH PARAMETER, X=G*D/U**2, THEN FINDS THE SPECTRAL
C   ENERGY IN THE FREQUENCY BAND ACCORDING TO THE FETCH LIMITED
C   SPECTRUM OF LIU (ENERGY=DE).
        IF(DD.LT.1.) GO TO 100
        U=UU*1.67
        D=DD*6000.
        USQ=U**2.
        G=32.
        UG=U/G
        X=G*D/USQ
        F0=1.3/((X**.222)*UG)
        S0=2E-05*USQ*(UG**3.)*(X**.695)
        F4=(F0/FRQ)**4.
        F5=F4*F0/FRQ
        S=3.5*S0*F5*EXP(-1.25*F4)
        DE=S*DF
  100 RETURN
      END

      SUBROUTINE LINK(UU1,UU2,FRQ,D)
C...LINK IS USED WHEN WAVE ENERGY PROPAGATES FROM A FETCH HIS-
C   TORY WITH WIND SPEED U1 INTO AN ADJACENT FETCH HISTORY
C   WITH A GREATER WIND SPEED, U2. THE OBJECT IS TO FIND WHAT
C   GENERATION DISTANCE WOULD HAVE RESULTED IN THE
C   BAND ENERGY OF THE 1ST FETCH IF THE WIND SPEED HAD BEEN
C   U2 THERE INSTEAD OF U1. THIS DISTANCE IS OUTPUT AND LATER
C   ADDED TO THE GENERATION DISTANCE IN THE 2ND FETCH SO THAT
C   THE TOTAL BAND ENERGY CAN BE COMPUTED AT THE NEW WIND
C   SPEED, U2. THE DIMENSIONLESS FETCH PARAMETER CORRESPONDING
C   TO THE OLD GENERATION DISTANCE IS COMPUTED, X1. THE NEW
C   PARAMETER,X2,IS FOUND ITERATIVELY FROM THE CONDITION THAT
C
C            S(X1,U1)=S(X2,U2)
C
C   WHERE S(X,U) = SPECTRAL DENSITY (FTSQ-SEC).
        IF(D.LT.1.) GO TO 100
        D=D*6000.
        G=32.
        U1=UU1*1.67
        U1SQ=U1**2.
        U2=UU2*1.67
        U2SQ=U2**2.
        F4=FRQ**4.
        U2U14=(U2/U1)**4.
        U2G4=(U2/G)**4.
        X1=G*D/U1SQ
        X2=X1*U1SQ/(U2U14*U2SQ)
        X888=1./(X1**.888)
   99   X22=1./((U2U14*X888-.1165*F4*U2G4*ALOG(X2/X1))**1.125)
        QUOT=ABS((X22-X2)/X2)
        IF(QUOT.LE..01) GO TO 50
        X2=X22
    1   FORMAT(1X,E10.2)
        GO TO 99
   50   D=X22*U2SQ/G
        D=D/6000.
  100 RETURN
      END
```

```
      SUBROUTINE DATE(DATE)
C...THIS SUBROUTINE ASKS THE USER TO INPUT THE MONTH (FIRST
C   THREE LETTERS), DAY AND HOUR FOR SOME DESIRED TIME. IT
C   THEN FINDS THE CORRESPONDING NUMBER OF HOURS FROM 00 GMT
C   ON JAN 01 OF THE SAME YEAR(=DATE). THE ARRAY FOR THE
C   CUMULATIVE DAYS AS OF THE FIRST OF EACH MONTH ("MON")
C   IS SET UP FOR NON-LEAP YEARS.
      INCLUDE COMMON
      WRITE(61,1)
    1 FORMAT(' MONTH:')
      READ(60,2) IMO
    2 FORMAT(A3)
      MDA=TTYIN(4HDAY=)
      NHR=TTYIN(4HHOUR,4H(GMT,4H) = )
      DO 10 I=1,12
      IF(IMO.EQ.MON(I,1)) GO TO 11
   10 CONTINUE
   11 JDAY=MDA+MON(I,2)-1
      DATE=NHR+JDAY*24
      RETURN
      END

      SUBROUTINE MODAHR(NTIM,NMO,NDA,NHR)
C...THIS SUBROUTINE TAKES THE NUMBER OF HOURS AFTER T00 GMT
C   ON JAN 01 (=NTIM) AND CONVERTS IT TO THE MONTH,DAY AND
C   HOUR.
      INCLUDE COMMON
      DO 30 I=1,12
      IP1=I+1
      MA=MON(I,2)
      IF(I.EQ.12) 20,21
   20 MB=366
      GO TO 22
   21 MB=MON(IP1,2)
      JDAY=NTIM/24+1
      NHR=NTIM-(JDAY-1)*24
   22 IF(JDAY.GT.MA.AND.JDAY.LE.MB) GO TO 31
   30 CONTINUE
   31 NDA=JDAY-MON(I,2)
      NMO=I
      RETURN
      END
```

APPENDIX B: OBSERVATIONS OF BREAKER HEIGHTS AT THE COLUMBIA RIVER

Mr. Norm Kujala (Astoria, Oregon) made daily observations of breaker heights at the South Jetty (Columbia River) during the 1971-1972 winter. He observed the breakers south of the jetty from a vantage point on the jetty, somewhat seaward of the shoreline (see Figure 2). When visibility permitted, he observed the swell which broke furthest (seaward) from the observation point (they break in deeper water, therefore are larger and are associated with the locally predominant portion of the wave spectrum). He estimated the apparent height of the breaker crests (H_a) above the still-water level by levelling the crests visually (with binoculars) against the horizon, while noting the approximate height of his eyes above the still-water level. The height estimates were based upon observations of groups of more conspicuous (large), regular swell.

During periods of high swell the largest breakers were often from one to over two miles from the observer. Occasionally, low visibility caused by fog, spray, and/or rain necessitated observation of smaller breakers (closer to shore) without the benefit of a well-defined horizon.

The apparent breaker height, H_a, is greater than the true height of the breaker crest above the still-water level, H_t. The ratio H_t/H_a depends on the observer-to-breaker distance (S_b) relative to the observer-to-horizon distance (S_h):

$$H_t/H_a = 1 - S_b/S_h \qquad \text{(B-1)}$$

(see Figure 38). From Bowditch (1962) the horizon distance is

$$S_h = 6960\ (H_a)^{\frac{1}{2}} \quad , \tag{B-2}$$

where S_h and H_a are in feet. Assuming that solitary wave theory (Munk, 1949) is applicable, the crest-to-trough breaker height, H_b, is

$$H_b = 4/3\ H_t \tag{B-3}$$

and the still-water depth below the breaker is

$$d_b = 1.28\ H_b \quad . \tag{B-4}$$

Combining (B-1), (B-2) and (B-3), one obtains

$$\begin{aligned} H_b &= 4/3\ H_a\ (1 - S_b/S_h) \\ &= 4/3\ H_a\ (1 - f(H_b)/6960\ H_a^{\frac{1}{2}}), \end{aligned} \tag{B-5}$$

where S_b is a function of H_b ($S_b = f[H_b]$) that can be determined from bathymetric charts, predicted tide stage (Z_t) and equation (B-4). Specifically, the bathymetric depth (MLLW) is

$$\begin{aligned} Z_b &= d_b - Z_t \\ &= 1.28\ H_b - Z_t \end{aligned} \tag{B-6}$$

and from bathymetric charts one can find the breaker distance from the observation point as a function of Z_b. Therefore, the true crest-to-trough breaker heights can be inferred from the apparent heights (H_a) by (B-5), (B-6) and the (approximately) known variation of bathymetric depth with distance offshore. This is the procedure that was used to obtain the breaker heights in Figure 33. At the Columbia

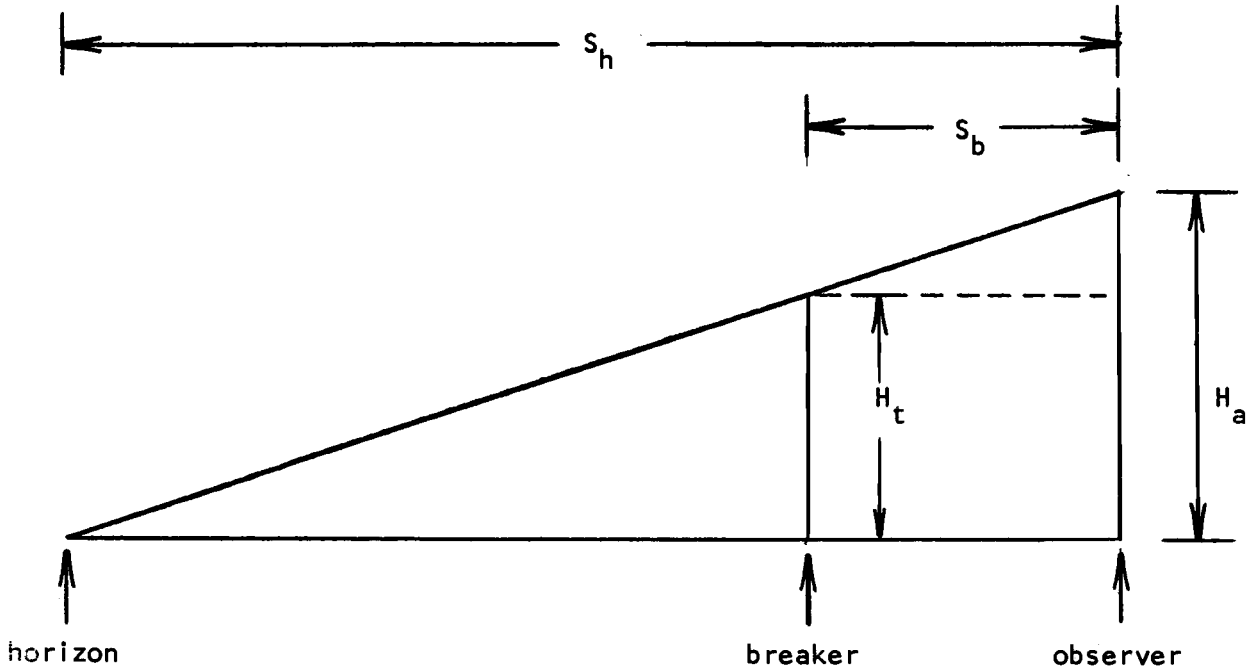

Figure 38. Schematic diagram for determining the relationship between the true and apparent heights of breaker crests above the still-water level (H_t and H_a, respectively). Breaker distance and horizon distance from observer are S_h and S_b, respectively.

River (South Jetty) observation site, neglect of the perspective error (Figure 38) would result in overestimates of about 30%.